



**HAL**  
open science

# Free-flight projectile behaviour : LPV modelling and global sensitivity analysis

Dawid Machala

► **To cite this version:**

Dawid Machala. Free-flight projectile behaviour : LPV modelling and global sensitivity analysis. Automatic. Université de Lorraine, 2019. English. NNT : 2019LORR0165 . tel-02499324

**HAL Id: tel-02499324**

**<https://hal.univ-lorraine.fr/tel-02499324>**

Submitted on 5 Mar 2020

**HAL** is a multi-disciplinary open access archive for the deposit and dissemination of scientific research documents, whether they are published or not. The documents may come from teaching and research institutions in France or abroad, or from public or private research centers.

L'archive ouverte pluridisciplinaire **HAL**, est destinée au dépôt et à la diffusion de documents scientifiques de niveau recherche, publiés ou non, émanant des établissements d'enseignement et de recherche français ou étrangers, des laboratoires publics ou privés.



## AVERTISSEMENT

Ce document est le fruit d'un long travail approuvé par le jury de soutenance et mis à disposition de l'ensemble de la communauté universitaire élargie.

Il est soumis à la propriété intellectuelle de l'auteur. Ceci implique une obligation de citation et de référencement lors de l'utilisation de ce document.

D'autre part, toute contrefaçon, plagiat, reproduction illicite encourt une poursuite pénale.

Contact : [ddoc-theses-contact@univ-lorraine.fr](mailto:ddoc-theses-contact@univ-lorraine.fr)

## LIENS

Code de la Propriété Intellectuelle. articles L 122. 4

Code de la Propriété Intellectuelle. articles L 335.2- L 335.10

[http://www.cfcopies.com/V2/leg/leg\\_droi.php](http://www.cfcopies.com/V2/leg/leg_droi.php)

<http://www.culture.gouv.fr/culture/infos-pratiques/droits/protection.htm>



# Free-Flight Projectile Behaviour

LPV modelling and global sensitivity analysis

Dawid Machala





# Comportement d'un projectile en vol libre : modélisation LPV et analyse de sensibilité

## THÈSE

présentée et soutenue publiquement le 21 novembre 2019

pour l'obtention du

**Doctorat de l'Université de Lorraine**

(mention automatique, traitement du signal et des images)

par

Dawid Mateusz MACHALA

### Composition du jury

<i>Rapporteurs :</i>	Sergei KUCHERENKO	Directeur de recherche - Imperial College London
	Michel BASSET	Professeur - Université de Haute Alsace
<i>Examineur :</i>	Edouard LAROCHE	Professeur - Université de Strasbourg
<i>Directeur :</i>	Marion GILSON	Professeur - Université de Lorraine
<i>Co-directeurs :</i>	Floriane COLLIN	Maître de conférences - Université de Lorraine
	Marie ALBISSER	Chargée de recherche - Institut franco-allemand de recherches de Saint-Louis
	Simona DOBRE	Chargée de recherche - Institut franco-allemand de recherches de Saint-Louis



*En déterminant [...] le chemin des projectiles [...] on a été obligé de faire plusieurs suppositions [...] et lorsqu'ensuite on veut repasser des calculs Mathématiques aux effets Physiques, on trouve bien du déchet sur l'exactitude et sur la précision.*

*Émilie du Châtelet  
Institutions de Physique, chapitre XIX, paragraphe 514, page 394. Paris, 1740*



## Remerciements

Il est impossible d'exprimer avec des mots l'étendue de la chance que j'ai eue en rencontrant tous les collègues qui m'ont accompagné au cours de ma thèse. C'était un grand plaisir et honneur de se trouver entouré d'amis chaleureux et sages. Ces amis, qui ont été une source d'inspiration pendant les moments les plus fructueux de mon travail, mais aussi une source de soutien pendant des jours plus sombres.

Malgré tout, je peux toujours essayer de trouver les bons mots pour remercier chacun d'entre eux.

Tout d'abord, je voudrais remercier mes directrices de thèse : Marion, Floriane, Marie et Simona. Non seulement elles m'ont donné l'opportunité de venir en France pour travailler avec elles, mais elles m'ont aussi encouragé à faire de mon mieux – et le ciel est témoin que resserrer la visse était parfois nécessaire !

Floriane m'a fait décoller dans mon travail sur l'analyse de sensibilité et c'est notamment grâce à elle que la troisième année a été aussi efficace – malgré nos combats féroces contre des théories statistiques très abstraites. Son attitude positive, son talent pédagogique et le fait qu'elle reste toujours zen m'ont permis d'accepter que « petit à petit, on devient moins petit ! »

Marie m'a introduit aux petits détails — néanmoins importants — des descriptions aérodynamiques et des modélisations mathématiques. En tant que chercheuse et gymnaste professionnelle, elle m'a imposé une certaine gymnastique cérébrale pour que je puisse mieux comprendre notre domaine scientifique. Elle a toute ma reconnaissance pour avoir relu bien plus d'une fois le manuscrit en un temps record !

Simona a veillé à ce que je sois bien à l'aise en France dès le début de mon stage — elle m'a offert une tasse à mon arrivée, elle m'a invité à un voyage dans les Vosges avec sa famille, et elle a fait tout ce qui était en son pouvoir pour que la suite de mon doctorat se passe pour le mieux. C'est aussi grâce à sa rigueur scientifique que j'ai développé la mienne.

Je tiens à remercier Marion pour sa compassion maternelle et son vif intérêt pour mon bien-être. Sa porte est toujours restée ouverte pour qu'on puisse discuter ensemble. Elle était toujours présente pour assurer que le travail ne déraile pas et que les buts soient atteignables — et elle n'a pas hésité à modifier les objectifs du doctorat pour qu'il soit possible de finir.

Le doctorat est un voyage dur et parfois sombre, mais tout à fait faisable aussi bien entouré ! :)

Il faut aussi souligner que je suis reconnaissant envers les professeurs Sergei Kucherenko et Michel Basset pour avoir accepté d'être les rapporteurs de ma thèse. Ainsi qu'au professeur Edouard Laroche pour sa participation au jury en qualité d'examinateur. Merci à vous d'avoir consacré de votre temps à mes travaux et d'être venus assister à ma soutenance.

De plus, j'aimerais bien remercier mes amis de Nancy et de Saint-Louis : ceux qui m'ont prêté le vélo, ceux qui m'ont conseillé à acheter des clémentines et m'ont prêté des livres pour les enfants, ceux qui m'ont introduit dans le monde des jeux de société en langue française, ceux qui ont cuit des muffins, ceux avec qui j'ai bu trop des coups, ceux qui m'ont fait visiter l'Allemagne, ceux qui m'ont amené randonner, ceux qui m'ont entraîné au français pendant des pauses-café. Grâce à vous, les lieux de travail sont devenus plus conviviaux et j'ai vécu une des plus belles expériences de ma vie !

I would like to thank Heleen for the hours we've spent on discussing PhD- and life-related

problems—and for her wonderful talent of changing the way I perceive them. Her insights, her sharp sense of humour, and especially her unconditional support have really helped me along the last three years.

I would also like to thank Lucie, whose support, personal coaching, long phone-calls, and great enthusiasm have had a significant impact on my life. I hope that we'll be able to benefit even more from our exchanges during the upcoming years in Prague!

Dziękuję też wreszcie moim polskim przyjaciołom i rodzinie. Mateuszu, Wojtku, Marto, Kubo, Stanisławie, Emeline – ale też Mamo, Tato i Dobrawo – nie wiem, czy dotrwałbym do samego końca tej wielkiej, długiej i czasami przytłaczającej przygody, gdyby nie wasze wsparcie, godziny rozmów telefonicznych i poczucie, że mam dookoła siebie ludzi, którym naprawdę zależy!

# Contents

<b>Nomenclature</b>	<b>ix</b>
<b>Contributions and publications</b>	
<b>Introduction</b>	
<b>Chapter 1</b>	
<b>Nonlinear model of a projectile's behaviour in free-flight experiments</b>	
1.1 Architecture of the studied artillery projectile . . . . .	5
1.2 Test facility . . . . .	6
1.3 Nonlinear model equations . . . . .	7
1.3.1 Reference frames . . . . .	8
1.3.2 State equations . . . . .	9
1.3.3 Measurement equations . . . . .	13
1.4 Conclusions . . . . .	14
<b>Chapter 2</b>	
<b>Quasi-LPV modelling</b>	
2.1 Nonlinear, LPV and quasi-LPV models . . . . .	15
2.1.1 LPV model definition . . . . .	16
2.1.2 Quasi-LPV model definition . . . . .	17
2.2 State of the art of LPV modelling of nonlinear systems . . . . .	17
2.2.1 Jacobian linearisation . . . . .	18
2.2.2 State transformation . . . . .	20
2.2.3 Velocity-based linearisation . . . . .	21
2.2.4 Function substitution . . . . .	21
2.2.5 Analytic function substitution and automatised approaches . . . . .	23
2.2.6 Conclusions . . . . .	24
2.3 Specification for quasi-LPV modelling adapted to application constraints . . . . .	25

2.4	Proposed development of a quasi-LPV model of a projectile . . . . .	28
2.4.1	Alternative nonlinear model representations . . . . .	29
2.4.2	Decomposition of the nonlinear remainder term . . . . .	30
2.4.3	Simulation results . . . . .	32
2.4.4	Conclusions . . . . .	34
2.5	Accuracy and computation time assessment of the models in different reference frames . . . . .	35
2.5.1	Assessment of the fixed-step solvers . . . . .	36
2.5.2	Assessment of the variable-step solvers . . . . .	39
2.5.3	Comparative analysis of the models' trajectories . . . . .	41
2.6	Conclusions . . . . .	43

<p><b>Chapter 3</b>  <b>Global sensitivity analysis of the quasi-LPV model</b></p>
--

3.1	Introduction . . . . .	45
3.2	Theory of global sensitivity analysis . . . . .	46
3.2.1	Analysis of Variance . . . . .	48
3.2.2	Monte Carlo (Sobol'-Saltelli) estimators . . . . .	50
3.3	Application to the quasi-LPV model of a projectile . . . . .	52
3.3.1	Sources of model uncertainty . . . . .	53
3.3.2	Setting up the sensitivity analysis . . . . .	55
3.3.3	Simulation results . . . . .	55
3.4	Conclusions . . . . .	61

<p><b>Conclusions and future research prospects</b></p>
---

<b>Appendix A</b>	<b>Wind reference frame</b>	<b>65</b>
<b>Appendix B</b>	<b>Analytic equivalence of coordinate reference frames</b>	<b>67</b>
	<b>Résumé en français</b>	<b>75</b>
	<b>List of Figures</b>	<b>81</b>
	<b>List of Tables</b>	<b>83</b>
	<b>Bibliography</b>	<b>85</b>

# Nomenclature

## Abbreviations

---

ISL	French-German Research Institute of Saint Louis
ABX	Aerodynamics and eXterior Ballistics
ANOVA	ANalysis Of VAriance
GSA	Global Sensitivity Analysis
LPV	Linear Parameter-Varying
quasi-LPV	quasi-Linear Parameter-Varying
ODE	Ordinary Differential Equation
c.g.	center of gravity
<i>w.r.t.</i>	with respect to

## Physical quantities

---

$a_x, a_y, a_z$	specific force in $x, y, z$ in body axes	$\text{m s}^{-2}$
$a$	speed of sound	$\text{m s}^{-1}$
$A_x, A_y, A_z$	accelerometer signals in $x, y, z$ sensor axes	
$C_x, C_y, C_z$	global force coefficients	
$C_X, C_{N\alpha}, C_{yp\alpha}$	axial force, normal force slope, and Magnus force slope coefficients	
$C_l, C_m, C_n$	global moment coefficients	
$C_D, C_L$	drag and lift coefficients	
$C_{lp}, C_{np\alpha}$	roll damping and Magnus moment slope coefficients	
$C_{m\alpha}, C_{mq}$	pitch moment slope and pitch damping coefficients	
$d$	projectile calibre	m
$\mathbf{F}, \mathbf{F}_A, \mathbf{F}_G$	applied force vector, aerodynamic force vector, gravity force vector	N
$\mathbf{M}, \mathbf{M}_A$	applied moment vector, aerodynamic moment vector	$\text{N m}^{-1}$

## Nomenclature

---

$M$	Mach number	
$g$	gravitational acceleration	$\text{m s}^{-2}$
$G_x, G_y, G_z$	gyroscope signals in $x, y, z$ sensor axes	
$H_x, H_y, H_z$	magnetometer signals in $x, y, z$ sensor axes	
$\mathbf{I}$	inertia matrix	$\text{kg m}^2$
$I_x, I_y, I_z$	longitudinal and transversal moments of inertia	$\text{kg m}^2$
$l$	projectile length	m
$m$	projectile mass	kg
$\rho$	air density	$\text{kg m}^{-3}$
$\bar{q}$	dynamic pressure	$\text{N m}^{-3}$
$S$	surface reference area	$\text{m}^2$
$\mathbf{V}$	translational velocity vector	$\text{m s}^{-1}$
$V$	total velocity, airspeed	$\text{m s}^{-1}$
$u, v, w$	linear velocities in $x, y,$ and $z$ body axis	$\text{m s}^{-1}$
$p, q, r$	roll, pitch, and yaw rates of the projectile	$\text{rad s}^{-1}$
$x_E, y_E, z_E$	c.g. position, expressed <i>w.r.t.</i> Earth reference frame	m
$\alpha, \beta, \alpha_t$	angle of attack, angle of sideslip, total angle of attack	deg
$\boldsymbol{\omega}$	angular velocity vector	$\text{rad s}^{-1}$
$\phi, \theta, \psi$	roll, pitch and yaw angles of the projectile	deg

## Mathematical notations

---

$a$	variable, scalar
$\mathbf{a}, \mathbf{A}$	vector, matrix
$a'$	variable in a non-rolling reference frame
$\sim$	approximation
$\bar{\cdot}$	selected point belonging to signal
$\cdot^T$	matrix transposition
$\dot{x}$	first derivative of $x$
$\frac{df}{dx}$	derivative of $f$ <i>w.r.t.</i> $x$
$\frac{\partial f}{\partial x}$	partial derivative of $f$ <i>w.r.t.</i> $x$

---

$\times$	cross product
$T^{A\bar{A}}$	transformation from coordinate system $\bar{A}$ to $A$
$A, B, C, D$	state, input, output, and feed-through matrix of state-space representation
$x, u, y$	state, input, and output vectors
$t$	time
$E(\cdot)$	expected value
$f(\cdot)$	state function, nonlinear model, nonlinear function
$g(\cdot)$	output function
$h(\cdot)$	remainder term function
$\eta$	trim signal function
$\mu$	mean value
$\sigma$	standard deviation
$O_{x_E, y_E, z_E}$	Earth reference frame axes
$O_{x, y, z}$	body reference frame
$O_{x_W, y_W, z_W}$	wind reference frame
$S_i$	main sensitivity index for $i$ -th uncertain parameter
$S_{T_i}$	total sensitivity index for all terms involving the $i$ -th uncertain parameter
$\Omega_i$	$i$ -th uncertain model parameter
$\Omega, \Omega^1, \Omega^2$	vector of uncertain parameters, its first and second sample
$X_i$	$i$ -th decomposed analytic function of the remainder term
$V(\cdot)$	variance
$\rho$	scheduling variable vector, parameter vector
$p$	exogenous scheduling variable vector, exogenous parameter vector
$z$	scheduling state vector
$w$	non-scheduling state vector
$X, U, Y$	state, input, and output space
$R$	permutation matrix
$\mathbb{R}$	set of real numbers
$n_x, n_u, n_y$	number of state, input and output signals
$n_p$	number of scheduling variables
$n_s$	number of uncertain parameters
$x_i$	$i$ -th sample of uncertain parameter $\Omega$
$g$	weighting function



# Contributions and publications

International journals with peer-review:

- D. Machala, F. Collin, M. Gilson, M. Albisser, S. Dobre. Global Sensitivity Analysis for Modeling the Ballistic Free-Flight Behavior. *AIAA Journal*. *In submission process*.

International conferences with peer review:

- D. Machala, F. Collin, M. Albisser, S. Dobre, M. Gilson. Global Sensitivity Analysis of ballistic free-flight experiments: does the model preserve the behaviour of the system? *9th International Conference on Sensitivity Analysis of Model Output, SAMO 2019*.
- D. Machala, S. Dobre, M. Albisser, F. Collin, M. Gilson. The Analysis of Vehicle's In-Flight Behaviour Using Quasi-LPV and Nonlinear Models. *American Institute of Aeronautics and Astronautics, AIAA SCITECH 2019 Forum*.
- D. Machala, S. Dobre, M. Albisser, F. Collin, M. Gilson. Quasi-LPV modelling of a projectile's behaviour in flight. *18th IFAC Symposium on System Identification, SYSID 2018*, 2018.
- D. Machala, M. Albisser, S. Dobre, F. Collin, M. Gilson. LPV Modelling of the Atmospheric Re-Entry Vehicle in Free Flight. *World Congress of the International Federation of Automatic Control, IFAC2017*, 2017.

International and national workshops:

- D. Machala, M. Albisser, S. Dobre, F. Collin, M. Gilson. LPV model identification of aerodynamic coefficients based on free flight data. *Annual PHD Students Conference IAEM Lorraine, APIL 2018*, Nancy, France, 2018 (poster)
- D. Machala, M. Albisser, S. Dobre, F. Collin, M. Gilson. LPV model identification of aerodynamic coefficients based on free flight data. *27th ERNSI (European Research Network System Identification)*, Lyon, France, 2017 (poster)
- D. Machala, M. Albisser, S. Dobre, F. Collin, M. Gilson. LPV model identification of aerodynamic coefficients based on free flight data. *ISL Scientific Symposium 2018*, Saint-Louis, France, 2018 (poster).



# Introduction

An everlasting trend in the development of artillery ammunition leads towards higher precision and longer range. The above is especially true for long-range projectiles. A prime example of it is the 155mm architecture: developed by Charles de Bange<sup>1</sup> as a general-purpose artillery projectile for the French Army in 1877 [39], it has seen a continuous improvement up till modern day. What followed, was the shift of paradigms in artillery operations. From intensive barrages covering large surfaces of territory, typical for the First and Second World War, the emphasis shifted towards targeting single objects of interest, effectively reducing the collateral damage. This trend is reflected in both the recent and classical examples of long-range munitions (Figure 1), such as the Excalibur, BONUS, Copperhead, or Krasnopol type projectiles that use various guidance and navigation techniques to assure their capability of hitting even a small or moving target [55, 11].

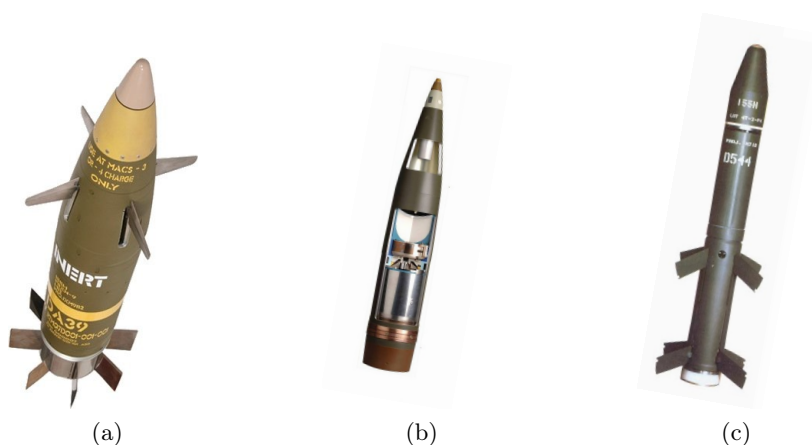


Figure 1: Exemplary long-range artillery architectures: (a) M982 Excalibur, (b) BONUS 155 mm, (c) M712 Copperhead

Introducing a new piece of artillery munition to service is a lengthy process, an important part of which is the assessment of projectile's in-flight behaviour. In mathematical terms, such a behaviour is described by Newton-Euler laws of motion, and depends on a set of aerodynamic coefficients that need to be quantified for each flying vehicle [148]. Inversely, the knowledge of the aerodynamic characteristics allows to predict the trajectory and assess the dynamical behaviour of a projectile. As such, they are necessary for any guidance, navigation or control

---

<sup>1</sup>**Charles Ragon de Bange** (1833–1914) - French military officer and engineer, responsible for the redesign of high-precision artillery systems for the French army in the aftermath of the Franco-Prussian war.

activity, and the research on them remains among the oldest in the field of aerospace. The aerodynamic coefficients can be quantified using several complementary methods, principally divided into the use of Computational Fluid Dynamics simulations (e.g. in [42]), semi-empirical codes (e.g. PRODAS [13] and Missile DATCOM [42]), or wind-tunnel experiments (e.g. in [31, 120]). Their results can be treated as an initial guess of the aerodynamic coefficients, later to be confirmed under real-world experimentation—especially in the form of ballistic free-flight tests. In this context, the *free* flight corresponds to the situation in which the in-flight behaviour of a projectile is not influenced by any external bodies, such as the barrel of a launcher, or the target’s surface.

The aforementioned free-flight experimentation can be considered as a realistic method of aerodynamic characterisation, since the projectile’s in-flight behaviour is observed—and captured live through measurements—under real-flight conditions. Using the obtained data, an identification procedure is applied, resulting in an improved estimate of the aerodynamic coefficients [4, 27, 134]. In Europe alone, there are several ballistic facilities in which the experiments can be performed. Principal examples include the DGA’s Techniques Terrestres facility in Bourges, France [26], Bundeswehr Technical Center for Weapons and Ammunition in Meppen, Germany [33], and the open-range test site in Baldersheim, France, operated by the French-German Research Institute of Saint-Louis (ISL) [1]. The last is considered as a reference in this thesis, and specifics of modelling and analysis presented hereinafter will be adapted to the conditions and constraints imposed by flight conditions and available measurement techniques at the ISL’s facility.

The task of preparing free-flight experiments, identifying a mathematical model of the tested projectile, and preparing it for the use in upcoming guidance and navigation activities poses a plethora of technical and scientific difficulties:

- **Conducting the tests** is feasible only if an initial guess of the aerodynamic characteristics is known, so that the trajectory can be predicted. Moreover, it must be assured that the results will be informative for the purpose of identification. In this context, the domain knowledge helps to predict if, e.g. chosen parameters will be identifiable with the use of available measurement techniques.
- **Identification** of the aerodynamic coefficients must be performed at a wide range of scenarios in order to sufficiently explore the behaviour of a projectile, including the subsonic, transonic and supersonic aerodynamics [4]. The theoretical challenges include the highly nonlinear structure of the model and partially unknown vector of initial state variables that also needs to be identified [1]. The identification task is then influenced by practical constraints, such as high costs of performing free-flight experiments.
- **Guidance and navigation** is usually conducted in the framework of specialised modelling techniques, such as quasi-linear parameter-varying (quasi-LPV) structures that are useful for the design of control loop for projectiles [97, 108]. The process is more difficult for models of general, nonlinear structure. Therefore, if the identified model has a nonlinear structure—as it often has, due to first-principle-model being used—it needs to be modified.

In the context of the aforementioned experimental and practical difficulties associated with free-flight experiments, this thesis concentrates on several of them. Principally, the manuscript discusses the prospects of developing a quasi-LPV model structure that would accurately preserve the nonlinear behaviour of a projectile while being of potential use for future guidance, navigation and control activities. The second aspect of the work is concentrated on investigating

---

the possibilities of enhancing the traditional methods of evaluating the influence and importance of model uncertainties by the use of global sensitivity analysis (GSA).

This thesis proposes a novel approach for an approximations-free quasi-LPV modelling technique and its subsequent use in GSA. The suggested method aims at:

- transforming the nonlinear model equations analytically by changing the projectile's reference frame into a non-rolling one [142],
- applying an algebraic function substitution approach [87] which allows to preserve the nonlinear behaviour of the modelled projectile [130], while representing it in a quasi-LPV form,
- using the obtained quasi-LPV model in a set of Monte Carlo simulations in order to test the influence of uncertain model parameters on its output signals by the means of GSA.

The developments are adapted to the constraints imposed by the experimental nature of free-flight tests. Namely, the projectile's behaviour is observed over a wide range of initial conditions, most of the measurements are indirect, and there is no control input signal. For these reasons, the standard grid-based quasi-LPV linearization is impossible, and the approximations-free approach has proven to be more promising. Moreover, the wide range of experimental conditions limits the amount of physical insights obtainable using local sensitivity analysis, thus motivating the use of GSA.

Additionally, for a spin-stabilised projectile, the reference frame transformation results in a reduction of the computation time needed to calculate trajectory of all its state variables. Therefore, the obtained quasi-LPV model could be considered to be as accurate as the original nonlinear model in describing the projectile's behaviour in flight, but also is sufficiently computationally simple to be directly used in a GSA. This premise is then investigated: in order to assess accuracy of the proposed modelling approach, the analytically-developed quasi-LPV model has been implemented in Matlab and tested numerically through a series of simulations corresponding to free-flight trajectories of an exemplary large-calibre projectile. The obtained trajectories of all state variables were compared with simulations of the original nonlinear model, thus showing their equivalence. Moreover, the quasi-LPV model has proven to be less sensitive to the choice of a numerical solver as well as to be computationally faster, both due to the dependence on a non-rolling reference frame.

Based on the known difficulties in experimental conditions, several model parameters—such as the initial values of state variables and nominal values of aerodynamic coefficients—have been considered as uncertain within known intervals. In such a context, GSA has allowed to gain further insight into the physical behaviour of the quasi-LPV model, and to validate its behaviour as equivalent to the nonlinear one. Additionally, since non-sensitive parameters are non-identifiable, the approach has allowed to determine which parameters of the model can be deemed non-identifiable, either during the whole flight, or during some periods of it. This aspect of work can be considered as a practical approach to gain more insight into the parametric variations within the model.

Organisation of the thesis is as follows.

Chapter 1 presents the nonlinear model of a projectile and its use case. This chapter introduces

the details of the ISL's test site and available measurement methods, specifics of the studied architecture, and of the currently employed nonlinear model. This part will be used as the basis for the subsequent developments in the thesis.

Chapter 2 describes the modelling approach used to develop a quasi-LPV representation of a projectile in flight. In the beginning, state of the art of LPV and quasi-LPV modelling is presented, including the most popular methods and their recent advancements. Afterwards, specifics of spin-stabilised 155mm projectile are presented in the context of LPV and quasi-LPV systems—namely the implications of the lack of controlled input signal, impossibility of point-based linearisation, and the necessity of preserving the nonlinear behaviour of the system—in order to motivate the choice of analytic function substitution as the method applied in the thesis. The remainder of this chapter is focused on the analytic development of a quasi-LPV model in the non-rolling reference frame and its subsequent numerical accuracy assessment.

Chapter 3 is dedicated to GSA of the quasi-LPV model proposed in Chapter 2. Firstly, the bibliographical research on the GSA is presented. It is followed by the set-up of the analysis adapted to the experimental conditions described in Chapter 1. In the sequel, results of GSA and their physical interpretation are presented.

This thesis has been conducted in cooperation with the French-German Research Institute of Saint-Louis and the Centre for Automatic Research of Nancy (CRAN) from Université de Lorraine. The necessary funding has been provided by the Direction Générale de l'Armement (DGA) of the French Ministry of Armed Forces. The research area covered in this thesis lies on the interconnection of interests of these three bodies. The core mission of the ISL is to conduct research and pre-development studies in the fields of defence and security. The ISL's Aerodynamics and eXterior Ballistics (ABX) group, which has initiated the project, deals with investigation of in-flight aerodynamic behaviour of various innovative architectures. CRAN focuses on modelling, identification, and sensitivity analysis of various model structures in their applications. Finally, DGA's field of activity lies in the development and supply of new weapon systems for the French armed forces.

# Chapter 1

## Nonlinear model of a projectile's behaviour in free-flight experiments

*Free-flight experiments allow to quantify the aerodynamic coefficients of a vehicle in flight by means of measurements from various sources. Available data depend on the specifics of a free-flight facility where the experiments are performed, as well as on the projectile's architecture and the embedded sensors integrated within. The details of the projectile architecture analysed in this thesis, and of the ISL's proving ground are described hereafter.*

*The sequel unfolds the specifics of the selected projectile architecture, the notions of free-flight experiments, and the mathematical model currently in use. These details will assist the linear parameter-varying modelling process presented in Chapter 2 and the global sensitivity analysis in Chapter 3.*

### 1.1 Architecture of the studied artillery projectile

Several long-range projectiles are in use in modern military systems. An example of them—that is currently studied at the ISL for its improved control qualities—is the 155 mm artillery. It will be investigated hereinafter.

The projectile has an elongated shape with tapered forebody and afterbody, with a diameter of almost 155 mm and length of 930 mm, as detailed in Figure 1.1. The inner part was originally designed as an area to store explosive payload. The projectile is launched from a rifled gun that induces an initial spin rate, allowing it to be a spin-stabilized vehicle. It is assumed that the projectile is axis-symmetric with the centre of mass located along its axial direction. The projectile is made of non-magnetic materials, so that magnetic sensors can be used without any disturbances.

The nominal physical properties of the studied projectile, such as the diameter  $d$ , length  $l$ , mass  $m$ , reference surface area  $S$ , longitudinal moment of inertia  $I_x$  and transversal moments of inertia  $I_y$ ,  $I_z$ , are summarised in Table 1.1. Those quantities are measured or calculated before the trials, and are considered as constant parameters in the case study.

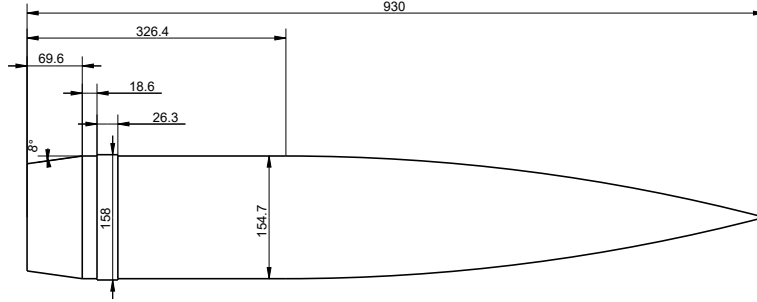


Figure 1.1: Architecture of the 155 mm projectile.

Physical parameters	$d$ (mm)	$l$ (m)	$m$ (kg)	$S$ (m <sup>2</sup> )	$I_x$ (kg m <sup>2</sup> )	$I_y$ (kg m <sup>2</sup> )	$I_z$ (kg m <sup>2</sup> )
Nominal values	155	0.93	45	0.0189	0.15	1.93	1.93

Table 1.1: Physical properties of the studied projectile.

## 1.2 Test facility

The ISL's proving ground located in Baldersheim offers a variety of measurement techniques for obtaining free-flight data necessary for aerodynamic characterisation of projectiles. An exemplary outline of the on-ground devices available for performing the experiments is presented in Figure 1.2. This setting will be considered as a basis for all the upcoming simulations undertaken in the thesis.

Tested projectiles can be launched by means of rifled or smooth-bore powder guns of small (20 mm) to large calibres over a distance up to 1 km. Their initial velocity can be set within the Mach number (representing ratio of the projectile's velocity to the speed of the sound) range of 0.6 to 5.0. In the case of spin-stabilised projectiles, they can be placed in the launcher directly and the rotation is induced by the projectile driving band along the rifled barrel.

The available measurement techniques are twofold, divided into on-ground and on-board sensors. The on-ground devices consist of: a Doppler radar located right after the powder gun that measures the total velocity over the entire flight; and two trajectory trackers, located on equally-distant opposite sides of the fire-line (Figure 1.2) that allow to determine vehicle's position and attitude based on an image processing code [91]. To assure that high speed cameras integrated into the trajectory trackers follow the projectile's position during the entire flight, two sky-screens are located along the fire line. If the vehicle is detected above one of sky-screens, the velocity of the motorised mirrors of trackers is adjusted so that the high-speed camera heads directly at the projectile. Experimental set is triggered by a muzzle-flash detector.

Several embedded sensors can be integrated on-board, depending on the architecture of a projectile and on the experimental conditions. Principally, accelerometers, gyroscopes, and magnetometers are being employed and will be described in the sequel.



Figure 1.2: Example of experimental set-up on the ISL's test site.

There are two possible methods of ending the flight in a safe manner. If the projectile has a sufficiently low terminal velocity, it can be retrieved for future tests by the means of a recovery unit placed at the end of the firing distance. Otherwise, the projectile is launched directly towards the sand bay. In both cases, the impact point can be measured. In the case study, the scenario of tests on large-calibre artillery munition is investigated. For such an architecture, projectiles are not recovered and the data acquisition is performed using telemetry techniques. Hence, the central point of the sand bay is selected as the default target.

### 1.3 Nonlinear model equations

In order to characterise the aerodynamic behaviour of the tested projectile in free flight, a nonlinear first-principles-based model is used. It is described in detail in the following section. This model is known in the literature and will be considered as a reference for the upcoming transformation of its equations into a quasi-LPV structure, which will be presented in Chapter 2.

From the physical point of view, the behaviour of a projectile—or any rigid body in flight—is governed by the Newton-Euler laws of motion. Mathematical model, based on these laws, can be represented as a nonlinear system of first-order ordinary differential equations [148, 119]. This section introduces a model structure adapted to representing the behaviour of a spin-stabilised projectile in free-flight, based on [1]. Its movement is considered with respect to (*w.r.t.*) three different reference frames: Earth, body, and wind. The state and output equations are presented, including the aerodynamic coefficients described as functions of state variables

and model parameters. The nonlinear model presented in this section has been used in previous works at the ISL (e.g. in [4]) and will be considered as a basis for the upcoming quasi-LPV modelling.

### 1.3.1 Reference frames

The projectile equations of motion are defined according to three different orthogonal and right-hand sided axis systems:

- **Earth frame:** the movement is considered *w.r.t.* a selected point on Earth noted as  $O_{x_E, y_E, z_E}$ , where positive  $O_{x_E}$  axis aims at geographic North, positive  $O_{y_E}$  axis aims at geographic East, and positive  $O_{z_E}$  axis is directed towards the centre of the Earth.
- **Body frame:** the movement is considered *w.r.t.* the centre of gravity (c.g.) of the projectile noted as  $O_{x, y, z}$ , and moves along with it. Positive  $O_x$  axis points downrange through the vehicle nose, positive  $O_y$  axis aims horizontally towards right hand side, and positive  $O_z$  points down *w.r.t.* the body. For the projectile,  $O_{xz}$  and  $O_{xy}$  planes are its planes of symmetry. Alternative forms of the body reference frame do exist, namely the body non-rolling and the body non-spinning reference frames [142] that differ by the way the rotations of the projectile are described. They will be introduced in Chapter 2, as they will serve as the basis for quasi-LPV modelling.
- **Wind frame:** the movement is considered *w.r.t.* projectile c.g. noted as  $O_{x_W, y_W, z_W}$ , and is relative to the vehicle trajectory through the air. Positive  $O_{x_W}$  axis is aligned with the velocity vector, positive  $O_{y_W}$  axis aims horizontally towards right hand side, and positive  $O_{z_W}$  points down.

The reference frames are illustrated in Figure 1.3, for a generic example of a fin-stabilised projectile.

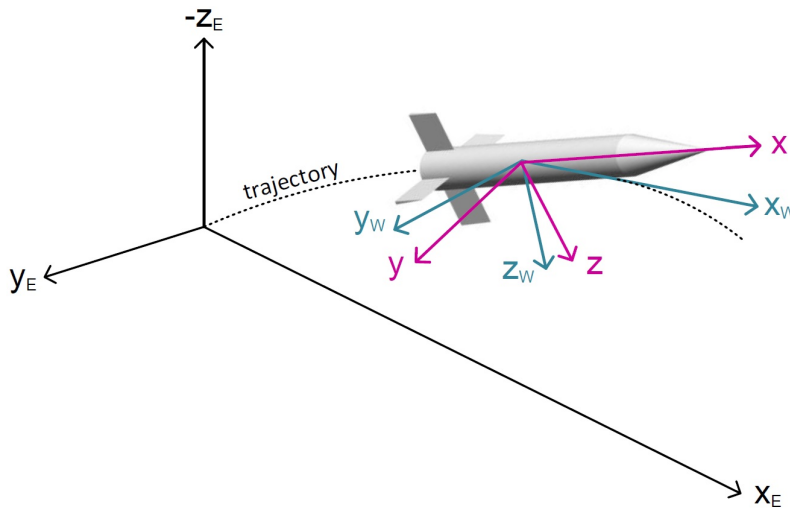


Figure 1.3: Reference frames: Earth, wind and body axes. Reprinted from [4].

### 1.3.2 State equations

The nonlinear model is developed in six degrees of freedom, meaning that the projectile can move and rotate in all three axes in a three dimensional space. The set of state variables can be divided into dynamics' equations, describing the effects of forces and moments acting on a projectile; and into kinematics' equations, tracking the projectile's position and attitude. All the symbols used in the equations correspond to units expressed in the standard *SI* form, fully described in the *Nomenclature*.

#### Dynamic equations

Movement of a rigid body in Earth reference frame is described by Newton's second law of dynamics as:

$$\begin{aligned}\mathbf{F} &= \frac{d}{dt}(m\mathbf{V}), \\ \mathbf{M} &= \frac{d}{dt}(\mathbf{I}\boldsymbol{\omega}).\end{aligned}\tag{1.1}$$

where  $\mathbf{V}$  and  $\boldsymbol{\omega}$  represent translational and angular velocities, respectively,  $m$  and  $I$  are the vehicle mass and inertia matrix,  $\mathbf{F}$  is the applied force and  $\mathbf{M}$  is the moment applied along the centre of gravity. The inertia matrix  $I$ , hereinafter considered to be diagonal, is defined as:

$$\mathbf{I} = \begin{bmatrix} I_x & 0 & 0 \\ 0 & I_y & 0 \\ 0 & 0 & I_z \end{bmatrix},\tag{1.2}$$

where  $I_x$  is the longitudinal moment of inertia, and  $I_y, I_z$  are the transversal moments of inertia.

Equation (1.1) can be represented *w.r.t.* rotating body frame, using the Euler's rotation equation:

$$\begin{aligned}\mathbf{F} &= m\dot{\mathbf{V}} + \boldsymbol{\omega} \times m\mathbf{V}, \\ \mathbf{M} &= \mathbf{I}\dot{\boldsymbol{\omega}} + \boldsymbol{\omega} \times \mathbf{I}\boldsymbol{\omega}.\end{aligned}\tag{1.3}$$

For a three dimensional movement of a projectile, translational velocity is a vector of velocities acting in each of body axes:

$$\mathbf{V} = [u, v, w]^T.\tag{1.4}$$

Those variables are natural candidates for the system states. However, the aerodynamic forces and moments are more often expressed *w.r.t.* the wind reference frame, as functions of  $V$ ,  $\alpha$  and  $\beta$  that represent the total velocity, the angle of attack and the angle of sideslip, respectively. These variables are defined in body axis as:

$$\begin{aligned}V &= |\mathbf{V}| = \sqrt{u^2 + v^2 + w^2}, \\ \alpha &= \arctan\left(\frac{w}{u}\right), \\ \beta &= \arcsin\left(\frac{v}{V}\right).\end{aligned}\tag{1.5}$$

Considering the angular velocity, it can be represented as:

$$\boldsymbol{\omega} = [p, q, r]^T.\tag{1.6}$$

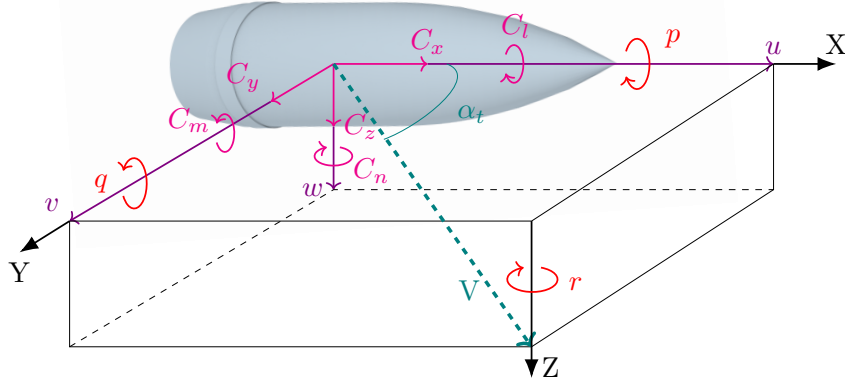


Figure 1.4: Representation of state variables of a spin-stabilised projectile.

In aerospace applications,  $p$ ,  $q$  and  $r$  represent the roll, the pitch and the yaw rates, respectively. The introduced state variables are shown in Figure 1.4.

In order to use equation (1.3) to obtain translational and angular velocities of a vehicle in motion, it is necessary to determine the components of force  $\mathbf{F}$  and moment  $\mathbf{M}$  for the case study of the spin-stabilised projectile. As explained in the previous chapter, in a free-flight test a projectile is launched from a powder gun and has neither thrust on its own nor any means of control. Therefore, only the aerodynamic and gravity forces are influencing the flight trajectory and there is no control input signal to be considered. Gravity can be assumed as uniform and the projectile can be assumed as symmetrical. Hence, there is no gravitational moment acting on the projectile, only the aerodynamic moment. Thus,  $\mathbf{F}$  and  $\mathbf{M}$  can be decomposed as follows:

$$\begin{aligned}\mathbf{F} &= \mathbf{F}_A + \mathbf{F}_G, \\ \mathbf{M} &= \mathbf{M}_A,\end{aligned}\tag{1.7}$$

where  $\mathbf{F}_A$  represent the aerodynamic force,  $\mathbf{F}_G$  is the force of gravity, and  $\mathbf{M}_A$  is the aerodynamic moment.

Force of gravity is defined *w.r.t.* Earth reference frame. However, vehicle flight dynamics are defined *w.r.t.* body reference frame. Therefore, it is required to provide a transformation matrix between those two reference systems. The transformation is usually defined with Euler angles,  $\phi$ ,  $\theta$  and  $\psi$ , representing the projectile roll, pitch and yaw angles, respectively. The transformation matrix  $T^{EB}$  is defined [20] as :

$$T^{EB}(\phi, \theta, \psi) = \begin{bmatrix} \cos \theta \cos \psi & \sin \phi \sin \theta \cos \psi - \sin \psi \cos \phi & \cos \phi \sin \theta \cos \psi + \sin \phi \sin \psi \\ \cos \theta \sin \psi & \sin \phi \sin \theta \sin \psi + \cos \psi \cos \phi & \cos \phi \sin \theta \sin \psi - \sin \phi \cos \psi \\ -\sin \theta & \sin \phi \cos \theta & \cos \phi \cos \theta \end{bmatrix}.\tag{1.8}$$

Using the transformation matrix (1.8), the force of gravity acting on the vehicle in a body coordinate system in equation (1.7) is defined as:

$$\mathbf{F}_G = m \begin{bmatrix} -g \sin \theta \\ g \sin \phi \cos \theta \\ g \cos \phi \cos \theta \end{bmatrix}.\tag{1.9}$$

Aerodynamic forces and moments acting on the vehicle are modelled by dimensionless global aerodynamic force and moment coefficients. Generally, the aerodynamic coefficients are nonlinear functions of translational and rotational velocities and accelerations. Hence, aerodynamic forces and moments of equation (1.7) can be defined in vehicle's body axis frame using global aerodynamic coefficients as:

$$\mathbf{F}_A = \bar{q}S \begin{bmatrix} C_x \\ C_y \\ C_z \end{bmatrix}, \quad (1.10)$$

and

$$\mathbf{M}_A = \bar{q}Sd \begin{bmatrix} C_l \\ C_m \\ C_n \end{bmatrix}, \quad (1.11)$$

where  $\bar{q}$  is the dynamic pressure,  $S$  is the reference surface area, and  $d$  is the projectile calibre. Global aerodynamic force coefficients,  $C_x, C_y, C_z$ , are the axial, side and normal force coefficients, respectively. Global aerodynamic moment coefficients,  $C_l, C_m, C_n$ , are the roll, pitch and yaw moment coefficients, respectively. The global aerodynamic coefficients are illustrated in Fig. 1.4.

The exact description of the aerodynamic coefficients for a selected flying vehicle depends on its predicted operating conditions. For instance, a standard aeroplane in a cruise flight does not experience a significant rolling motion, hence roll-induced effects described by Magnus moment coefficients may be considered negligible. Similarly, the reverse is true for a spin-stabilised projectile, where the effects of its high roll rate have a stabilising influence and are non-negligible [15].

Generally, global aerodynamic coefficients can be represented as functions of state variables and a set of aerodynamic coefficients. They, in turn, can be described using look-up tables, polynomial functions, or spline functions [1]. Herein, these aerodynamic coefficients are functions of two variables: the total angle of attack  $\alpha_t$  and the Mach number  $M$ . They can be defined as:

$$\alpha_t(\alpha, \beta) = \arccos(\cos \alpha \cos \beta), \quad (1.12)$$

and

$$M = \frac{V}{a}, \quad (1.13)$$

where  $a$  is the speed of sound.

Using the state variables defined in (1.4) and (1.6), forces in (1.9) and (1.10) and moments in (1.11), it is possible to define the nonlinear equations of motion by rewriting Euler's equation (1.3), as shown below. To make the equations easier to understand, different colours have been used to mark **states of the system**, **constants**, and the **aerodynamic coefficients**.

*Force equations:*

$$\dot{u} = -rv + qw + \frac{\bar{q}S}{m}C_x - g \sin \theta, \quad (1.14a)$$

$$\dot{v} = +ru - pw + \frac{\bar{q}S}{m}C_y + g \sin \phi \cos \theta, \quad (1.14b)$$

$$\dot{w} = -qu + pv + \frac{\bar{q}S}{m}C_z + g \cos \phi \cos \theta. \quad (1.14c)$$

Moment equations:

$$\dot{p} = \frac{1}{I_x}(\bar{q}SdC_l - qr(I_z - I_y)), \quad (1.15a)$$

$$\dot{q} = \frac{1}{I_y}(\bar{q}SdC_m - pr(I_x - I_z)), \quad (1.15b)$$

$$\dot{r} = \frac{1}{I_z}(\bar{q}SdC_n - pq(I_y - I_x)). \quad (1.15c)$$

This set of force and moment equations constitute the dynamic state equations that describe the behaviour of the projectile subject to forces and moments acting on it.

### Kinematic equations

Rotational kinematic equations are defined by derivatives of Euler angles, and can be defined using angular velocities in (1.6) and the angle transformation matrix in (1.8). After some reformulations, as shown in [20] and [1], the following equations are obtained:

Rotational kinematic equations:

$$\dot{\phi} = p + \tan \theta(q \sin \phi + r \cos \phi), \quad (1.16a)$$

$$\dot{\theta} = q \cos \phi - r \sin \phi, \quad (1.16b)$$

$$\dot{\psi} = \frac{q \sin \phi + r \cos \phi}{\cos \theta}. \quad (1.16c)$$

Concerning the translational kinematics, the projectile velocity in Earth reference frame is a first derivative of its position. Since state variables in (1.4) are defined in body axis system, transformation (1.8) is applied:

$$\begin{bmatrix} \dot{x}_E \\ \dot{y}_E \\ \dot{z}_E \end{bmatrix} = T^{EB}(\phi, \theta, \psi) \begin{bmatrix} u \\ v \\ w \end{bmatrix}. \quad (1.17)$$

Consequently, the following equations are obtained:

Translational kinematic equations:

$$\dot{x}_E = u \cos \theta \cos \psi + v(\sin \phi \sin \theta \cos \psi - \cos \phi \sin \psi) + w(\cos \phi \sin \theta \cos \psi + \sin \phi \sin \psi), \quad (1.18a)$$

$$\dot{y}_E = u \cos \theta \sin \psi + v(\sin \phi \sin \theta \sin \psi + \cos \phi \cos \psi) + w(\cos \phi \sin \theta \sin \psi - \sin \phi \cos \psi), \quad (1.18b)$$

$$\dot{z}_E = -u \sin \theta + v \sin \phi \cos \theta + w \cos \phi \cos \theta. \quad (1.18c)$$

The set of equations (1.14a)-(1.18c) constitutes the nonlinear model that describes the behaviour of a projectile in free flight. It is this model structure which will be transformed into a quasi-LPV model in Chapter 2.

It is worth mentioning, that the nonlinear model is often presented *w.r.t.* the wind reference frame. However, its representation in body reference frame is better adapted for the quasi-LPV modelling approach proposed in this thesis. The superabundance of trigonometric functions and interdependence of state variables render the wind-reference-frame representation difficult to linearise. For this reason, the description in body reference frame will be considered in Chapter 2. For the sake of completeness, the model representation expressed *w.r.t.* the wind reference frame, is presented in Appendix A.

### 1.3.3 Measurement equations

As indicated in the previous chapter, there are several signals that could be considered measurable in the context of free-flight experiments. The following section briefly summarises their equations. For each of the embedded sensors  $j$ , the following parameters have to be known:  $\mathbf{D}_j$ ,  $\mathbf{S}_j$ , and  $\mathbf{offset}_j$ , representing the sensor misalignment matrix, the sensitivity matrix, and the offset vector, respectively.

#### Accelerometers

An accelerometer measures the specific force acting on its axes. The output equations relative to this sensor are as follows [3]:

$$\begin{bmatrix} A_x \\ A_y \\ A_z \end{bmatrix}_B = \mathbf{S}_a \cdot \mathbf{D}_a \cdot \begin{bmatrix} a_x \\ a_y \\ a_z \end{bmatrix}_S + \mathbf{offset}_a, \quad (1.19)$$

where subscripts B and S note body and sensor frame, respectively, and  $[a_x, a_y, a_z]^T$  are the specific force measured at the accelerometer position:

$$\begin{bmatrix} a_x \\ a_y \\ a_z \end{bmatrix} = \begin{bmatrix} a_x^{CG} - (q^2 + r^2) \cdot x_{APCG} + (pq - \dot{r}) \cdot y_{APCG} + (pr + \dot{q}) \cdot z_{APCG} \\ a_y^{CG} + (pq + \dot{r}) \cdot x_{APCG} - (p^2 + r^2) \cdot y_{APCG} + (qr + \dot{p}) \cdot z_{APCG} \\ a_z^{CG} + (pr - \dot{q}) \cdot x_{APCG} + (qr + \dot{p}) \cdot y_{APCG} - (p^2 + q^2) \cdot z_{APCG} \end{bmatrix}, \quad (1.20)$$

and where  $[x_{APCG} \ y_{APCG} \ z_{APCG}]$  represents the position of the accelerometer sensor AP *w.r.t.* the c.g. along the three body-fixed coordinate axes.

#### Magnetometers

A magnetometer measures the projection of Earth's magnetic field on the sensor axes. The measurement equations are as follows [1]:

$$\begin{bmatrix} H_x \\ H_y \\ H_z \end{bmatrix}_B = \mathbf{S}_m \cdot \mathbf{D}_m \cdot \mathbf{T}^{EB} \cdot \begin{bmatrix} H_x^E \\ H_y^E \\ H_z^E \end{bmatrix}_E + \mathbf{offset}_m, \quad (1.21)$$

where  $[H_x^E, H_y^E, H_z^E]^T$  are the Earth's magnetic field values at the experimental test location.

#### Gyroscopes

Gyroscopes allow a direct measurement of the body's rotation rates:

$$\begin{bmatrix} G_x \\ G_y \\ G_z \end{bmatrix}_B = \mathbf{S}_g \cdot \mathbf{D}_g \cdot \begin{bmatrix} p \\ q \\ r \end{bmatrix}_B. \quad (1.22)$$

#### Doppler radar

Doppler radar allows a direct measurement of the vehicle total velocity  $V$ , which results in the following measurement equation [1]:

$$y_V = V = \sqrt{u^2 + v^2 + w^2}. \quad (1.23)$$

## 1.4 Conclusions

The nonlinear model describing the in-flight behaviour of a projectile consists of 12 state equations and 10 output equations, some of them directly dependent on the state variables. The model does not have any input signal, as the projectile is uncontrolled during the flight. The state equations are dependent on 6 global aerodynamic coefficients, which are defined as nonlinear functions of projectile states and model parameters. All of these variables of interest are summarised in Table 1.2.

State variables $\mathbf{x}(t)$		Measurement signals $\mathbf{y}(t)$		Global coefficients	
Dynamic translational	$u, v, w$	Accelerometers	$A_x, A_y, A_z$	Forces	$C_x, C_y, C_z$
Dynamic rotational	$p, q, r$	Magnetometers	$H_x, H_y, H_z$	Moments	$C_l, C_m, C_n$
Kinematic translational	$x_E, y_E, z_E$	Gyroscopes	$G_x, G_y, G_z$		
Kinematic rotational	$\phi, \theta, \psi$	Doppler radar	$V$		

Table 1.2: Summary of state and output variables, and of the global aerodynamic coefficients.

The first-principles-based model described in this chapter has a nonlinear structure. As such, it does accurately represent the behaviour of a projectile in flight and has been used in previous research at the ISL, where the aim has been to use the model to identify the aerodynamic coefficients. Nonetheless, its structure is significantly different to these used in control of projectiles, where a quasi-LPV model structure is often preferred. For these reason, the next chapter addresses the topic of quasi-LPV modelling of the nonlinear model behaviour.

Afterwards, the computational complexity of the model—when it is subject to simulation—will be addressed. Additionally, the nonlinear model depends on several physical properties, such as elements of the initial state vector, that are known only approximately in the context of real-world free flight experiments. An assessment of the influence that this uncertainty has is limited when a local sensitivity analysis is applied, due to the nonlinear structure of the model. Therefore, in Chapter 3 a global sensitivity analysis will be presented, this time on the developed quasi-LPV model.

## Chapter 2

# Quasi-LPV modelling

*The purpose of this part of the project is to develop a linear parameter-varying model that describes a projectile's free-flight behaviour. This chapter introduces the theory of LPV and quasi-LPV models, and the state of the art of the existing modelling techniques. For each approach, its applications and shortcomings are presented. Afterwards, the specifics of the nonlinear model of a projectile in free flight are discussed in order to select the best suited quasi-LPV modelling method. The remainder consists of the transformation of the nonlinear equations into a quasi-LPV structure, followed by a numerical accuracy assessment of both model structures. The research works conducted within the scope of this chapter have resulted in three publications, [71], [72], and [73].*

### 2.1 Nonlinear, LPV and quasi-LPV models

Mathematical modelling based on the laws of physics is an art of compromise: complex nonlinear equations, large number of state variables, and hard-to-achieve experimental conditions can be expected. In aerospace, different research communities have developed various methods to cope with the complexity of the model. In control applications, the usual approach is to use linear parameter varying (LPV) models, which encapsulate the nonlinearities in a quasi-linear structure and allow to use autopilot design methods dedicated for linear systems (see e.g. ([52, 34, 113])). However, in aerodynamic identification applications, a nonlinear model is often employed (e.g. [4, 134]). It remains an interesting research prospect to develop a model structure which would be useful for both the aerodynamic coefficients identification and the subsequent autopilot design. It has been proposed that a quasi-LPV model structure could be used for this purpose [1]. The benefit of such an approach would lay in the ease of utilising quasi-LPV controller design techniques prominent in the works of the ISL in the case where the identified model structure would also be quasi-LPV.

The following chapter is dedicated to the development of a quasi-LPV model of a projectile in flight that could be considered as a middle ground between model structures typical for control and identification.

The model of a projectile's free-flight behaviour obtained thanks to the existing physical equations has a nonlinear continuous-time state-space representation, as shown in the previous chapter. Hence, the scope of this state-of-the-art analysis is limited to the family of nonlinear systems

which can be described in a continuous-time domain using smooth input and output functions  $f$  and  $g$ , respectively. Thus, the nonlinear system subject to quasi-LPV modelling has the following state space form:

$$\mathcal{M} : \begin{cases} \dot{\mathbf{x}}(t) = f(\mathbf{x}(t), \mathbf{u}(t)) \\ \mathbf{y}(t) = g(\mathbf{x}(t), \mathbf{u}(t)) \end{cases}, \quad (2.1)$$

where  $\mathbf{u} \in \mathbb{U}$ ,  $\mathbf{x} \in \mathbb{X}$ ,  $\mathbf{y} \in \mathbb{Y}$  are system inputs, states, and output signals, respectively, and  $\mathbb{U}, \mathbb{Y}, \mathbb{X} \subseteq \mathbb{R}$ .

The underlying idea behind LPV and quasi-LPV models is to represent the nonlinear behaviour of the system in a form similar to linear model, while preserving its accuracy [130]. The historically first attempt in this direction has been the *gain scheduling* approach: a nonlinear model is linearised around a set of operating points into a number of linear, locally valid models; these local models are then interpolated based on current operating conditions [66]. Gain scheduling has been initially used in aerospace research, and has led to the development of the first surface-to-air missiles: Nike Ajax [81], and Talos [84], and aircraft autopilots. It has been also used in non-aerospace applications, such as in automotive engine-fuel control [97].

However, the gain scheduling approach has significant disadvantages. Firstly, the linear models are valid only in close proximity to linearization points. Thus, they—in general—do not preserve the nonlinear system behaviour, especially its transient dynamics. Secondly, it was impossible to assure global stability of a designed controller [130]. As such, gain scheduling can be considered as a heuristic method which—while being successfully employed in a number of applications—does not provide neither the theoretical guarantees of the model behaviour being equivalent to the original, nonlinear one [66], nor stability of a controller developed on it [130]. These two limitations have sparked the research works aiming at improving the theoretical background of gain scheduling in the 1990s.

### 2.1.1 LPV model definition

The first theoretical approach to enhance gain-scheduling with stability assurances arose with the works of Rugh, Shamma and Athans [96, 110]. Their approach has been centred around the premise that the nonlinear equations of a system can be rewritten in a linear form, with all nonlinearities dependent on set of auxiliary measurable variables, called *scheduling parameters*. Thus, the equations become *linear*, but *vary* dependent on selected model *parameters*. Hence, the new class of models bears the name *linear parameter-varying*. An LPV representation of a  $n$ -th order system (2.1) is defined as:

$$\mathcal{M}_{LPV} : \begin{cases} \dot{\mathbf{x}}(t) = \mathbf{A}(\mathbf{p}(t)) \mathbf{x}(t) + \mathbf{B}(\mathbf{p}(t)) \mathbf{u}(t) \\ \mathbf{y}(t) = \mathbf{C}(\mathbf{p}(t)) \mathbf{x}(t) + \mathbf{D}(\mathbf{p}(t)) \mathbf{u}(t) \end{cases}, \quad (2.2)$$

where  $\mathbf{u} \in \mathbb{R}^{n_u}$ ,  $\mathbf{y} \in \mathbb{R}^{n_y}$ ,  $\mathbf{x} \in \mathbb{R}^{n_x}$ .  $\mathbf{A}$ ,  $\mathbf{B}$ ,  $\mathbf{C}$  and  $\mathbf{D}$  are state matrices of dimensions  $n_x \times n_x$ ,  $n_x \times n_u$ ,  $n_y \times n_x$ ,  $n_y \times n_u$ , respectively. The scheduling parameters vector  $\mathbf{p} \in \mathbb{R}^{n_p}$  is comprised of the measurable variables which are exogenous to the system, i.e. they are not states of the system.

LPV formulation of the system equations has some practical benefits. Principally, it bridges the gap between nonlinear and linear systems theory: it enables the use of  $H_{inf}$ ,  $H_2$ , and  $\mu$ -*synthesis* [12, 44] controller design methods with sufficient stability guarantees [130]. Benefits

for system identification are not immediate, but it is possible to use tools such as maximum likelihood [62], bilinear analysis or set memberships calculation methods [105, 14].

### 2.1.2 Quasi-LPV model definition

Since 1990s, further development of LPV systems has been conducted which allowed to include non-exogenous parameters—such as state variables—into the scheduling parameters. In practice, nonlinearities often appear in the system through some of its states [44, 97, 113]—in which case the scheduling vector  $\boldsymbol{p}$  cannot consist of exogenous variables only. For example, dynamical properties of the aircraft change with its velocity, being one of the system states. This new class of models is called *quasi-LPV*.

The state vector  $\boldsymbol{x}(t)$  can be decomposed into vector of scheduling states  $\boldsymbol{z}(t)$  and non-scheduling states  $\boldsymbol{w}(t)$  as follows:

$$\boldsymbol{x}(t) = \begin{bmatrix} \boldsymbol{z}(t) \\ \boldsymbol{w}(t) \end{bmatrix}. \quad (2.3)$$

Consequently, the scheduling vector  $\boldsymbol{\rho}(t)$  may consist of both scheduling states  $\boldsymbol{z}(t)$  and exogenous parameters  $\boldsymbol{p}(t)$ :

$$\boldsymbol{\rho}(t) = \begin{bmatrix} \boldsymbol{z}(t) \\ \boldsymbol{p}(t) \end{bmatrix}. \quad (2.4)$$

Thus, the continuous-time quasi linear parameter-varying state-space representation of a  $n$ -th order system (2.1) can be described by:

$$\begin{bmatrix} \dot{\boldsymbol{z}}(t) \\ \dot{\boldsymbol{w}}(t) \\ \boldsymbol{y}(t) \end{bmatrix} = \begin{bmatrix} \mathbf{A}_{11}(\boldsymbol{\rho}(t)) & \mathbf{A}_{12}(\boldsymbol{\rho}(t)) & \mathbf{B}_1(\boldsymbol{\rho}(t)) \\ \mathbf{A}_{21}(\boldsymbol{\rho}(t)) & \mathbf{A}_{22}(\boldsymbol{\rho}(t)) & \mathbf{B}_2(\boldsymbol{\rho}(t)) \\ \mathbf{C}_1(\boldsymbol{\rho}(t)) & \mathbf{C}_2(\boldsymbol{\rho}(t)) & \mathbf{D}(\boldsymbol{\rho}(t)) \end{bmatrix} \begin{bmatrix} \boldsymbol{z}(t) \\ \boldsymbol{w}(t) \\ \boldsymbol{u}(t) \end{bmatrix}, \quad (2.5)$$

or, by writing it in a standard quasi-LPV form:

$$\mathcal{M}_{quasi-LPV} : \begin{cases} \dot{\boldsymbol{x}}(t) = \mathbf{A}(\boldsymbol{\rho}(t)) \boldsymbol{x}(t) + \mathbf{B}(\boldsymbol{\rho}(t)) \boldsymbol{u}(t) \\ \boldsymbol{y}(t) = \mathbf{C}(\boldsymbol{\rho}(t)) \boldsymbol{x}(t) + \mathbf{D}(\boldsymbol{\rho}(t)) \boldsymbol{u}(t) \end{cases}. \quad (2.6)$$

## 2.2 State of the art of LPV modelling of nonlinear systems

Since the 1990s, the LPV models, usually in the quasi-LPV form, have been used to model movement of missiles [108, 87, 127, 125, 111, 143] and aeroplanes [78, 37, 97, 113, 36], but also specialised jet fighters [58], space probes [17], turbofan engines [94, 43] and rotorcraft dynamics [133]. LPV and quasi-LPV modelling approaches are also popular in non-aerospace applications, such as control of surgical robot [135], modelling of building heat propagation [118], vehicle safety simulation [60], semiconductor thermal monitoring [138], power plant control [54], and many others [44, 105, 97].

Consequently, a great richness of approaches that allow to transform nonlinear system equations into a quasi-LPV form has been developed. Hence, the following section is dedicated to an overview of the methods, so that one of them can be chosen in the sequel for the purpose of modelling the projectile dynamics. This analysis is done on a theoretical level, since comparison of methods is usually performed in a qualitative way. Only a small number of authors have

decided to provide quantitative results of the accuracy analysis of different modelling methods - publications of Reberga [94] and Marcos [78, 77] are one of few tackling the topic.

### 2.2.1 Jacobian linearisation

Jacobian linearisation is the oldest and most common method of obtaining quasi-LPV representation of a nonlinear system, coming directly from *gain scheduling* approach [97]. It can be considered to be the most widely used (quasi)-LPV linearisation technique, with quite a few successful applications [60, 122, 143, 43, 133] and readily available functions in Matlab/Simulink [80].

In order to provide a mathematical background of Jacobian linearisation, let us recall the general structure of the state equation of a nonlinear system, extracted from (2.1):

$$\dot{\mathbf{x}}(t) = f(\mathbf{x}(t), \mathbf{u}(t)). \quad (2.7)$$

Any current state  $\mathbf{x}(t)$  and input  $\mathbf{u}(t)$  of the equation (2.7) can be interpreted as if it was achieved by some time dependent disturbance  $(\delta\mathbf{x}(t), \delta\mathbf{u}(t))$  from a selected constant operating point  $(\bar{\mathbf{x}}, \bar{\mathbf{u}})$ :

$$\mathbf{x}(t) = \delta\mathbf{x}(t) + \bar{\mathbf{x}} \quad (2.8)$$

$$\mathbf{u}(t) = \delta\mathbf{u}(t) + \bar{\mathbf{u}} \quad (2.9)$$

State derivative of (2.8) is, therefore, equal to:

$$\dot{\mathbf{x}}(t) = \frac{d}{dt}\mathbf{x}(t) = \frac{d}{dt}(\delta\mathbf{x}(t) + \bar{\mathbf{x}}) = \delta\dot{\mathbf{x}}(t) \quad (2.10)$$

Substitution of (2.8), (2.9) and (2.10) into the original equation (2.7), yields an equivalent representation in a following form:

$$\delta\dot{\mathbf{x}}(t) = f(\bar{\mathbf{x}} + \delta\mathbf{x}(t), \bar{\mathbf{u}} + \delta\mathbf{u}(t)) \quad (2.11)$$

Resulting system is nonlinear, but now it represents dynamics of the original system (2.7) around a selected operating point  $(\bar{\mathbf{x}}, \bar{\mathbf{u}})$ , which, in general, can be any point of the system trajectory. Rewriting right-hand side of the equation (2.10), using the first-order Taylor series expansion around the selected operating point, yields:

$$f(\bar{\mathbf{x}} + \delta\mathbf{x}(t), \bar{\mathbf{u}} + \delta\mathbf{u}(t)) \approx f(\bar{\mathbf{x}}, \bar{\mathbf{u}}) + \frac{\partial f(\bar{\mathbf{x}}, \bar{\mathbf{u}})}{\partial \mathbf{x}(t)} \delta\mathbf{x}(t) + \frac{\partial f(\bar{\mathbf{x}}, \bar{\mathbf{u}})}{\partial \mathbf{u}(t)} \delta\mathbf{u}(t) \quad (2.12)$$

Hence, behaviour of the nonlinear system (2.7) around  $(\bar{\mathbf{x}}, \bar{\mathbf{u}})$  is approximately equal (i.e. by ignoring higher-order terms of Taylor expansion) to:

$$\delta\dot{\mathbf{x}}(t) \approx f(\bar{\mathbf{x}}, \bar{\mathbf{u}}) + \frac{\partial f(\bar{\mathbf{x}}, \bar{\mathbf{u}})}{\partial \mathbf{x}(t)} \delta\mathbf{x}(t) + \frac{\partial f(\bar{\mathbf{x}}, \bar{\mathbf{u}})}{\partial \mathbf{u}(t)} \delta\mathbf{u}(t) \quad (2.13)$$

where  $\frac{\partial f}{\partial \mathbf{x}}$  and  $\frac{\partial f}{\partial \mathbf{u}}$  are Jacobian matrices of the system. Similar transformation can be applied to the system output equation, resulting in:

$$\mathbf{y}(t) \approx g(\bar{\mathbf{x}}, \bar{\mathbf{u}}) + \frac{\partial g(\bar{\mathbf{x}}, \bar{\mathbf{u}})}{\partial \mathbf{x}(t)} \delta \mathbf{x}(t) + \frac{\partial g(\bar{\mathbf{x}}, \bar{\mathbf{u}})}{\partial \mathbf{u}(t)} \delta \mathbf{u}(t) \quad (2.14)$$

System equations (2.13)-(2.14) are nonlinear, but only because of the presence of the terms  $f(\bar{\mathbf{x}}, \bar{\mathbf{u}})$  and  $g(\bar{\mathbf{x}}, \bar{\mathbf{u}})$  (see, for theoretical reference, [68]).

Hence, in order to linearise the system, the operating point can not be only any point of the trajectory, but also an *equilibrium point* (i.e.  $f(\bar{\mathbf{x}}, \bar{\mathbf{u}}) = 0$ ). By noting Jacobian matrices as  $\mathbf{A}, \mathbf{B}, \mathbf{C}, \mathbf{D}$ , the standard linear time-invariant (LTI) model is derived:

$$\begin{aligned} \delta \dot{\mathbf{x}}(t) &\approx \mathbf{A} \delta \mathbf{x}(t) + \mathbf{B} \delta \mathbf{u}(t) \\ \mathbf{y}(t) &\approx \mathbf{C} \delta \mathbf{x}(t) + \mathbf{D} \delta \mathbf{u}(t) + g(\bar{\mathbf{x}}, \bar{\mathbf{u}}) \end{aligned} \quad (2.15)$$

In order to describe the system behaviour over a large operating range, linearisation around multiple points has to be performed. Thus, the nonlinear system was linearised around  $n \in \mathbb{Z}$  equilibrium points  $(\bar{\mathbf{x}}_i, \bar{\mathbf{u}}_i)$ , where  $i = 1, 2, \dots, n$ .

In order to determine the behaviour of the system around the multiple linearisation points, a weighting function must be used to determine which of the linear models are the most valid at any time instance  $(\mathbf{x}(t), \mathbf{u}(t))$ . Let us introduce set of weighting functions  $\mathbf{g}_i(\boldsymbol{\rho}(t))$ , such that:

- for every  $\boldsymbol{\rho}(t)$  in every time instant:  $\sum_{i=1}^n \mathbf{g}_i(\boldsymbol{\rho}(t)) = 1$
- for every  $\boldsymbol{\rho}_i$ , corresponding to the value of scheduling variables at the  $i$ -th equilibrium point:  $\mathbf{g}_i(\boldsymbol{\rho}_i) = 1$ .

By noting approximation of the state vector  $\mathbf{x}$  with  $\tilde{\mathbf{x}}$ , the (quasi)-LPV model obtained by a Jacobian linearisation becomes:

$$\begin{aligned} \delta \dot{\tilde{\mathbf{x}}}(t) &= \sum_{i=1}^n \mathbf{g}_i(\boldsymbol{\rho}(t)) \mathbf{A}_i \delta \tilde{\mathbf{x}}(t) + \sum_{i=1}^n \mathbf{g}_i(\boldsymbol{\rho}(t)) \mathbf{B}_i \delta \mathbf{u}(t) \\ \mathbf{y}(t) &= \sum_{i=1}^n \mathbf{g}_i(\boldsymbol{\rho}(t)) \mathbf{C}_i \delta \tilde{\mathbf{x}}(t) + \sum_{i=1}^n \mathbf{g}_i(\boldsymbol{\rho}(t)) \mathbf{D}_i \delta \mathbf{u}(t) - \sum_{i=1}^n \mathbf{g}_i(\boldsymbol{\rho}(t)) g(\bar{\mathbf{x}}_i, \bar{\mathbf{u}}_i) \end{aligned} \quad (2.16)$$

Although simple and widely used, the method suffers from many drawbacks. Principally, while the system dynamics are well described at any given operating point [61], the linearised model performs poorly in describing transient dynamics [78, 77]. Subsequently, a linearised system may not preserve stability characteristics of the nonlinear one [130]. Moreover, interpolation by the means of function  $\mathbf{g}$  can lead to altering the behaviour of the system (see as example [122] and [132]).

The Jacobian linearisation is usually considered to be meaningful only around equilibrium points, but there have been some advances to overcome this limitation [53, 83, 116, 18]. For example, Johansen et al. have achieved higher accuracy of a designed controller by using non-equilibrium

models to approximate system local transient behaviour [53]. Their method, however, also suffers from several shortcomings. Firstly, it requires very dense sampling of the transient regions in order to fulfil the slow parameter variation requirement, resulting in increased computational burden [83]. Secondly, behaviour of the system in off-equilibrium area may be highly non-unique. Namely, qualitatively different systems may have similar behaviour around a non-equilibrium point, thus causing problems with interpretation and identification of the global model [116]. Another approach to increase the size of the neighbourhood in which a quasi-LPV model is valid is to select a higher-order of the series expansion [6]. Yet another approach, aiming to increase the validity of the quasi-LPV model in an off-equilibrium area aims to obtain the value of  $f(\bar{x}, \bar{u})$  by the means of a simulation [18].

Nevertheless, Jacobian linearisation is invalid far from equilibrium points, and requires the assumption of slowly varying scheduling variables [130] (an example of a quasi-LPV model behaviour when this assumption is not met is presented in [78]).

## 2.2.2 State transformation

State transformation method was developed by Shamma and Cloutier in the early 1990', as a more robust approach to gain scheduling autopilot design of a missile [111]. It has been appreciated mostly in aerospace domain [125, 115, 123, 77].

Let us assume that the nonlinear system is of such a class, that it is linear *w.r.t.* the input signal  $\mathbf{u}(t)$ , and the nonlinearities come only from the terms dependent on scheduling parameters  $\boldsymbol{\rho}(t)$ :

$$\begin{bmatrix} \dot{z}(t) \\ \dot{\mathbf{w}}(t) \end{bmatrix} = \begin{bmatrix} \mathbf{A}_{11}(\boldsymbol{\rho}(t)) & \mathbf{A}_{12}(\boldsymbol{\rho}(t)) \\ \mathbf{A}_{21}(\boldsymbol{\rho}(t)) & \mathbf{A}_{22}(\boldsymbol{\rho}(t)) \end{bmatrix} \begin{bmatrix} z(t) \\ \mathbf{w}(t) \end{bmatrix} + \begin{bmatrix} \mathbf{B}_1(\boldsymbol{\rho}(t)) \\ \mathbf{B}_2(\boldsymbol{\rho}(t)) \end{bmatrix} \mathbf{u}(t) + \begin{bmatrix} h_1(\boldsymbol{\rho}(t)) \\ h_2(\boldsymbol{\rho}(t)) \end{bmatrix} \quad (2.17)$$

Assuming that there exist functions  $\mathbf{w}_{eq}(\boldsymbol{\rho}(t))$  and  $\mathbf{u}_{eq}(\boldsymbol{\rho}(t))$ , which are continuous, differentiable, and belonging to the system equilibrium manifold (pushing the system into steady state), the following equation is obtained:

$$\begin{bmatrix} 0 \\ 0 \end{bmatrix} = \begin{bmatrix} \mathbf{A}_{11}(\boldsymbol{\rho}(t)) & \mathbf{A}_{12}(\boldsymbol{\rho}(t)) \\ \mathbf{A}_{21}(\boldsymbol{\rho}(t)) & \mathbf{A}_{22}(\boldsymbol{\rho}(t)) \end{bmatrix} \begin{bmatrix} z(t) \\ \mathbf{w}_{eq}(\boldsymbol{\rho}(t)) \end{bmatrix} + \begin{bmatrix} \mathbf{B}_1(\boldsymbol{\rho}(t)) \\ \mathbf{B}_2(\boldsymbol{\rho}(t)) \end{bmatrix} \mathbf{u}_{eq}(\boldsymbol{\rho}(t)) + \begin{bmatrix} h_1(\boldsymbol{\rho}(t)) \\ h_2(\boldsymbol{\rho}(t)) \end{bmatrix} \quad (2.18)$$

System (2.17) can be represented in quasi-LPV form by subtracting (2.18) and rewriting some of the terms (refer to [78]). In result, following formula is obtained:

$$\begin{bmatrix} \dot{z}(t) \\ \dot{\check{\mathbf{w}}}(\boldsymbol{\rho}(t)) \end{bmatrix} = \mathbf{A}(\boldsymbol{\rho}(t)) \begin{bmatrix} z(t) \\ \check{\mathbf{w}}(\boldsymbol{\rho}(t)) \end{bmatrix} + \mathbf{B}(\boldsymbol{\rho}(t)) [\check{\mathbf{u}}(\boldsymbol{\rho}(t))] \quad (2.19)$$

where

$$\begin{aligned} \mathbf{A}(\boldsymbol{\rho}(t)) &= \begin{bmatrix} 0 & \mathbf{A}_{12}(\boldsymbol{\rho}(t)) \\ 0 & \mathbf{A}_{22}(\boldsymbol{\rho}(t)) - \frac{\partial \mathbf{w}_{eq}(\boldsymbol{\rho}(t))}{\partial \mathbf{w}(t)} \mathbf{A}_{12}(\boldsymbol{\rho}(t)) \end{bmatrix} \\ \mathbf{B}(\boldsymbol{\rho}(t)) &= \begin{bmatrix} \mathbf{B}_1(\boldsymbol{\rho}(t)) \\ \mathbf{B}_2(\boldsymbol{\rho}(t)) - \frac{\partial \mathbf{w}_{eq}(\boldsymbol{\rho}(t))}{\partial \mathbf{w}(t)} \mathbf{B}_1(\boldsymbol{\rho}(t)) \end{bmatrix} \\ \dot{\check{\mathbf{w}}}(\boldsymbol{\rho}(t)) &= \dot{\mathbf{w}}(t) - \dot{\mathbf{w}}_{eq}(t) \\ \check{\mathbf{w}}(\boldsymbol{\rho}(t)) &= \mathbf{w}(t) - \mathbf{w}_{eq}(\boldsymbol{\rho}(t)) \\ \check{\mathbf{u}}(\boldsymbol{\rho}(t)) &= \mathbf{u}(t) - \mathbf{u}_{eq}(\boldsymbol{\rho}(t)) \end{aligned} \quad (2.20)$$

The method allows to describe nonlinear dynamics without errors coming from linearisation, provided that  $\mathbf{u}_{eq}(\boldsymbol{\rho}(t))$  and  $\mathbf{w}_{eq}(\boldsymbol{\rho}(t))$  can be found. This assumption is one of the limitations of the state transformation method, as not always can they be found, neither exists a generalised method of obtaining  $\mathbf{w}_{eq}(\boldsymbol{\rho}(t))$  and  $\mathbf{u}_{eq}(\boldsymbol{\rho}(t))$  [130]. Moreover, the number of scheduling states should be equal to the number of control inputs [77] in order to preserve system detectability [78].

State transformation—while being generally more accurate than Jacobian linearisation due to lack of truncation of the higher terms of Taylor series expansion—cannot represent the system behaviour outside of the equilibrium manifold [113]. Moreover, resulting state space representation may be non-minimal [130].

### 2.2.3 Velocity-based linearisation

Velocity-based linearisation of nonlinear system is a method developed by Leith and Leithead in the end on 1990s in a series of publications describing its theoretical background [64, 65, 68]. The technique has lead to the development of a quasi-LPV model of turbofan engine [94] and design of autopilot for an agile missile [67].

First-order Taylor series expansion around an operating point linearises the model only if the operating point is also an equilibrium point. This limitation can be eliminated if the system equations are differentiated, since it results in elimination of the constant term  $f(\bar{\mathbf{x}}, \bar{\mathbf{u}})$ . Resulting model has the form:

$$\begin{aligned}\delta\ddot{\mathbf{x}}(t) &= \frac{\partial f(\bar{\mathbf{x}}, \bar{\mathbf{u}})}{\partial \mathbf{x}(t)} \delta\dot{\mathbf{x}}(t) + \frac{\partial f(\bar{\mathbf{x}}, \bar{\mathbf{u}})}{\partial \mathbf{u}(t)} \delta\dot{\mathbf{u}}(t) \\ \dot{\mathbf{y}}(t) &= \frac{\partial g(\bar{\mathbf{x}}, \bar{\mathbf{u}})}{\partial \mathbf{x}(t)} \delta\dot{\mathbf{x}}(t) + \frac{\partial g(\bar{\mathbf{x}}, \bar{\mathbf{u}})}{\partial \mathbf{u}(t)} \delta\dot{\mathbf{u}}(t)\end{aligned}\tag{2.21}$$

Hence, by considering derivated state, output and input signals instead of the original ones, the linearization can be performed around any operating point  $(\bar{\mathbf{x}}, \bar{\mathbf{u}})$ . A family of locally valid linear models can now be obtained by selecting points representing both equilibrium and transient dynamics of the system, and the quasi-LPV model is derived (see [67]) by interpolating between them.

Main limitation of this method comes from the necessity of obtaining derivatives of states and inputs. Their measurements may not be available in practical realization, inducing inevitable differentiation of existing measurements, thus amplifying the errors and limiting the control and identification perspectives [130]. Moreover, derivation of the off-equilibrium models is possible only if the analytic equations of the nonlinear model are known. If it is not the case, then validity of the (quasi)-LPV model will be limited to surroundings of equilibrium point, as in standard Jacobian linearisation [94].

### 2.2.4 Function substitution

The function substitution method was developed by Tan in 1997 for the class of nonlinear systems with nonlinearities in the control input (recall that this was one of the limitations of state

transformation method) [124]. Similarly to the previous method, it has seen limited use, mostly in aerospace domain, and has been used to design a control loop for F-16 fighter plane [114], and generic missile [125]; as well as in fault detection for Boeing 747 aeroplane [78, 77].

Let us assume that the system is represented by:

$$\begin{bmatrix} \dot{\mathbf{z}}(t) \\ \dot{\mathbf{w}}(t) \end{bmatrix} = \begin{bmatrix} \mathbf{A}_{11}(\boldsymbol{\rho}(t)) & \mathbf{A}_{12}(\boldsymbol{\rho}(t)) \\ \mathbf{A}_{21}(\boldsymbol{\rho}(t)) & \mathbf{A}_{22}(\boldsymbol{\rho}(t)) \end{bmatrix} \begin{bmatrix} \mathbf{z}(t) \\ \mathbf{w}(t) \end{bmatrix} + \begin{bmatrix} \mathbf{B}_1(\boldsymbol{\rho}(t)) \\ \mathbf{B}_2(\boldsymbol{\rho}(t)) \end{bmatrix} \tilde{\mathbf{u}}(\boldsymbol{\rho}(t), \boldsymbol{\delta}(t)) + \begin{bmatrix} h_1(\boldsymbol{\rho}(t)) \\ h_2(\boldsymbol{\rho}(t)) \end{bmatrix} \quad (2.22)$$

where  $\tilde{\mathbf{u}}(\boldsymbol{\rho}(t), \boldsymbol{\delta}(t))$  is now a nonlinear function, which is invertible *w.r.t.*  $\boldsymbol{\delta}(t)$ , being the nonlinear input.

In order to derive an LPV model, equation (2.22) must be reformulated into a form linear *w.r.t.* input. In this sense, a function  $\mathbf{v}$  must be found, such that:

$$\mathbf{v}(\mathbf{z}(t), \mathbf{p}(t), \mathbf{u}(t)) = \mathbf{u}(t) \quad (2.23)$$

Parameter dependent linear input  $\mathbf{u}(t)$  can then be found by using (2.23). With this new input function, the system equation (2.22) becomes:

$$\begin{bmatrix} \dot{\mathbf{z}}(t) \\ \dot{\mathbf{w}}(t) \end{bmatrix} = \begin{bmatrix} \mathbf{A}_{11}(\boldsymbol{\rho}(t)) & \mathbf{A}_{12}(\boldsymbol{\rho}(t)) \\ \mathbf{A}_{21}(\boldsymbol{\rho}(t)) & \mathbf{A}_{22}(\boldsymbol{\rho}(t)) \end{bmatrix} \begin{bmatrix} \mathbf{z}(t) \\ \mathbf{w}(t) \end{bmatrix} + \begin{bmatrix} \mathbf{B}_1(\boldsymbol{\rho}(t)) \\ \mathbf{B}_2(\boldsymbol{\rho}(t)) \end{bmatrix} \mathbf{u}(t) + \begin{bmatrix} h_1(\boldsymbol{\rho}(t)) \\ h_2(\boldsymbol{\rho}(t)) \end{bmatrix} \quad (2.24)$$

This reformulation allows to deal with the nonlinearities in the input. It is useful method for control synthesis, as the controller can be designed *w.r.t.* (2.24), while the actual nonlinear input can be calculated as scheduled, inverse function  $\mathbf{v}(\mathbf{z}(t), \mathbf{p}(t), \mathbf{u}(t)) = \boldsymbol{\delta}(t)$ , and fed back to (2.22).

It is assumed, for simplicity, that there are no exogenous scheduling variables (as in [78]). A single equilibrium point can now be selected, defined by values of scheduling states  $\mathbf{z}_{eq}$ , non-scheduling states  $\mathbf{w}_{eq}$ , and of linear control input  $\mathbf{u}_{eq}$ . The system dynamics around the selected equilibrium point can be defined using trim functions defined as:

$$\boldsymbol{\eta}_z(t) = \mathbf{z}(t) - \mathbf{z}_{eq} \quad (2.25)$$

$$\boldsymbol{\eta}_w(t) = \mathbf{w}(t) - \mathbf{w}_{eq} \quad (2.26)$$

$$\boldsymbol{\eta}_u(t) = \mathbf{u}(t) - \mathbf{u}_{eq} \quad (2.27)$$

Consequently, by substitution of trim functions (2.25)-(2.27), equation (2.24) can be rewritten to represent system dynamics around the equilibrium point:

$$\begin{bmatrix} \dot{\boldsymbol{\eta}}_z(t) \\ \dot{\boldsymbol{\eta}}_w(t) \end{bmatrix} = \begin{bmatrix} \mathbf{A}_{11}(\boldsymbol{\eta}_z(t) + \mathbf{z}_{eq}) & \mathbf{A}_{12}(\boldsymbol{\eta}_z(t) + \mathbf{z}_{eq}) \\ \mathbf{A}_{21}(\boldsymbol{\eta}_z(t) + \mathbf{z}_{eq}) & \mathbf{A}_{22}(\boldsymbol{\eta}_z(t) + \mathbf{z}_{eq}) \end{bmatrix} \begin{bmatrix} \boldsymbol{\eta}_z(t) \\ \boldsymbol{\eta}_w(t) \end{bmatrix} + \begin{bmatrix} \mathbf{B}_1(\boldsymbol{\eta}_z(t) + \mathbf{z}_{eq}) \\ \mathbf{B}_2(\boldsymbol{\eta}_z(t) + \mathbf{z}_{eq}) \end{bmatrix} \boldsymbol{\eta}_u(t) + \mathfrak{F}(\boldsymbol{\eta}_z(t), \mathbf{w}_{eq}, \mathbf{u}_{eq}) \quad (2.28)$$

where:

$$\begin{aligned} \mathfrak{F}(\boldsymbol{\eta}_z(t), \mathbf{w}_{eq}, \mathbf{u}_{eq}) &= \begin{bmatrix} \mathbf{A}_{11}(\boldsymbol{\eta}_z(t) + \mathbf{z}_{eq}) & \mathbf{A}_{12}(\boldsymbol{\eta}_z(t) + \mathbf{z}_{eq}) \\ \mathbf{A}_{21}(\boldsymbol{\eta}_z(t) + \mathbf{z}_{eq}) & \mathbf{A}_{22}(\boldsymbol{\eta}_z(t) + \mathbf{z}_{eq}) \end{bmatrix} \begin{bmatrix} \mathbf{z}_{eq} \\ \mathbf{w}_{eq} \end{bmatrix} + \\ &+ \begin{bmatrix} \mathbf{B}_1(\boldsymbol{\eta}_z(t) + \mathbf{z}_{eq}) \\ \mathbf{B}_2(\boldsymbol{\eta}_z(t) + \mathbf{z}_{eq}) \end{bmatrix} \mathbf{u}_{eq} + \begin{bmatrix} h_1(\boldsymbol{\eta}_z(t) + \mathbf{z}_{eq}) \\ h_2(\boldsymbol{\eta}_z(t) + \mathbf{z}_{eq}) \end{bmatrix} \end{aligned} \quad (2.29)$$

Hence, such a system representation is obtained, that the only source of nonlinearities in (2.28) is the nonlinear function  $\mathfrak{F}(\boldsymbol{\eta}_z(t), \mathbf{w}_{eq}, \mathbf{u}_{eq})$ . Such a function can be, with some approximations, decomposed into set of functions  $f(z)$ , each linear *w.r.t.* one of scheduling variables from the scheduling state vector  $\boldsymbol{\eta}_z(t)$ . The task of decomposition is not unique, hence a method of minimization of the approximation error over the entire state space envelope must be used [130]. The final step using this approach is to *substitute* the functions  $f(z)$  into (2.28) as follows:

$$\begin{bmatrix} \dot{\mathbf{z}}(t) \\ \dot{\mathbf{w}}(t) \end{bmatrix} = \begin{bmatrix} \mathbf{A}_{11}(\mathbf{z}(t) + \mathbf{f}_1(\mathbf{z}(t))) & \mathbf{A}_{12}(\mathbf{z}(t)) \\ \mathbf{A}_{21}(\mathbf{z}(t) + \mathbf{f}_2(\mathbf{z}(t))) & \mathbf{A}_{22}(\mathbf{z}(t)) \end{bmatrix} \begin{bmatrix} \mathbf{z}(t) - \mathbf{z}_{eq} \\ \mathbf{w}(t) - \mathbf{w}_{eq} \end{bmatrix} + \begin{bmatrix} \mathbf{B}_1(\boldsymbol{\rho}(t)) \\ \mathbf{B}_2(\boldsymbol{\rho}(t)) \end{bmatrix} (\mathbf{u}(t) - \mathbf{u}_{eq}) \quad (2.30)$$

The above formulation can be considered as a quasi-LPV form.

The function substitution method has the advantage of requiring only one equilibrium point in order to derive an LPV model, but resulting dynamics may vary depending on the selected equilibrium point [130]. Another advantage comes from the fact that resulting LPV model may accurately describe nonlinear system dynamics outside of the equilibrium manifold, hence overcoming the limitation of state transformation and Jacobian linearisation methods [114]. However, a significant disadvantage is that accuracy of the previous two methods can be much greater in close proximity to equilibrium points [78].

### 2.2.5 Analytic function substitution and automatised approaches

Further development of LPV modelling over 2000s has led to formulating methods of automatized LPV model generation for models described by analytic functions. Because of the high complexity of these algorithms, only a brief overview will be presented herein.

In 2006, Kwiatkowski has proposed a method of transforming the nonlinear equations in a quasi-LPV model by performing all possible combinations of nonlinear terms and comparing complexity of resulting representations [59]. By applying symbolic solver, the first equation of the nonlinear system (2.1) is decomposed row by row (each row corresponds to one state variable) in such a way, that every row  $i$  (out of  $n$  rows in total) is decomposed into  $n_i$  irreducible additive terms:

$$[f(\mathbf{x}, \mathbf{u})]_i = \sum_{j=1}^{n_i} f_{ij}(\mathbf{x}, \mathbf{u}) \quad (2.31)$$

Afterwards, every summand  $f_{ij}$  is factorized and assigned into matrix  $\mathbf{A}$  or  $\mathbf{B}$  and associated with a scheduling variable [59]. Both matrices are then calculated as an linear combination of terms dependent on scheduling variables. The same procedure is applied to the output equation (2.1). Resulting quasi-LPV representation of nonlinear system is affine. The algorithm can produce a high number of possible LPV models, so a method for selecting the less complex one is required. Unfortunately, no formal method is proposed in the original paper. In 2009, the research team of Donida et al. has proposed a methodology for transforming nonlinear dynamics into an LPV representation, using MODELICA software environment [30]. Nonlinear equations of the system are formulated as first-order differential equations that can consist of some unknown parameters. The transformation into LPV is based on triangulation of the nonlinear differential equations and solving them recursively until a set of linear system equations is found. All remaining nonlinear terms and unknown parameters are treated as scheduling variables of an LPV model. Resulting

LPV representation is based on linear factorial transformation. However, it is impossible to predetermine which variables will be treated as scheduling variables [130].

The grid-based methods mentioned up to now do not address some of the important design steps. For instance, it is unknown how many local models are required to sufficiently represent the dynamics of the nonlinear system, or what is the best way of selecting scheduling states. Since grid-based LPV representation is non-unique [66], different realizations may offer different accuracy and computational complexity [59], or even diverse behaviours [130]. It is not possible to directly reformulate the nonlinear system as an LPV model, but rather to over-bound it (i.e. every solution to the nonlinear system is also a solution to the LPV system, but not *vice versa*). In other words, there are operating points and state trajectories existing in the LPV system, but not in the original nonlinear one [66].

In the late 2000s, Tóth has developed a mathematical framework of assuring equal behaviour of LPV and original nonlinear system [131]. In his work, LPV system is developed using an algorithm similar to Kwiatkowski's [59], but in so-called *kernel form*. The behavioural approach of Tóth aims at representing the nonlinear model equations in the following summand form:

$$\dot{\mathbf{x}}(t) = f(\mathbf{x}, \mathbf{u}) = \sum_{j=1}^{n_i} f_{ij}(\mathbf{x}, \mathbf{u}) \quad (2.32)$$

Afterwards, similarly as for the Kwiatkowski algorithm [59], every summand  $f_{ij}$  is factorized and assigned—if possible—into matrix  $\mathbf{A}$  or  $\mathbf{B}$ . Such an assignment might be non-unique and different representations might result in different complexity of the quasi-LPV model [130]. The resulting analytic form resembles the function substitution approach shown in (2.24), with the difference that now the remainder term consists of  $n_h$  summands which could not be directly assigned to state matrices:

$$\begin{bmatrix} \dot{\mathbf{z}}(t) \\ \dot{\mathbf{w}}(t) \end{bmatrix} = \begin{bmatrix} A_{11}(\boldsymbol{\rho}(t)) & A_{12}(\boldsymbol{\rho}(t)) \\ A_{21}(\boldsymbol{\rho}(t)) & A_{22}(\boldsymbol{\rho}(t)) \end{bmatrix} \begin{bmatrix} \mathbf{z}(t) \\ \mathbf{w}(t) \end{bmatrix} + \begin{bmatrix} B_1(\boldsymbol{\rho}(t)) \\ B_2(\boldsymbol{\rho}(t)) \end{bmatrix} \mathbf{u}(t) + \begin{bmatrix} \sum_{j=1}^{n_h} h_{1j}(\mathbf{x}, \mathbf{u}) \\ \sum_{j=1}^{n_h} h_{2j}(\mathbf{x}, \mathbf{u}) \end{bmatrix} \quad (2.33)$$

There exists no generalised approach to assign the remainder summands to state matrices in such a way, that the behaviour of the nonlinear model will be preserved. Tóth proposes a number of simple tricks, such as multiplication and division of the summand terms by one of the non-zero scheduling variables, so that they can be assigned to  $\mathbf{A}$  or  $\mathbf{B}$  matrix [130]. In the domain of aerospace, this analytic function substitution approach has been used for instance by Pfifer [87]. However, Pfifer has additionally proposed to assume a number of restrictions on the flight conditions of the modelled projectile, effectively simplifying some of the remaining summands. Resulting model would not preserve the nonlinear behaviour in the Tóth sense.

## 2.2.6 Conclusions

In this section, an overview of the LPV modelling techniques has been presented. Available methods usually assume existence of equilibrium points as a prerequisite for the analysis. Additional

requirements regarding scheduling variables include necessity of them to be directly measurable in real time, to be sufficiently slowly varying, and that number of them is small.

Standard Jacobian linearisation method is sufficiently accurate in representing the nonlinear system in most applications, which is proved by a large number of real world implementations for a variety of systems. State transformation method may be used to increase accuracy of the LPV system around equilibrium points. Function substitution may be used if the number of equilibrium points is small, if there are large variations in input signal, or if the system's transient dynamics are significantly influencing the trajectory. Those methods assume that the nonlinear system is for majority of time in close proximity to its equilibrium points.

Alternatively, if the nonlinear system has mostly off-equilibrium behaviour, velocity-based method and modified Jacobian linearisation method may be used. However, only a small number of real world applications is available in the topic.

Behavioural analysis can be performed to assure that nonlinear system is accurately represented by the LPV model, but, because of the high computational burden, it is especially important that there is a small number of scheduling variables in the model.

The aforementioned methods have their underlying assumptions and use cases. The next section of this chapter will position the existing nonlinear model presented in Chapter 1 and the constraints imposed by the application, *w.r.t.* the quasi-LPV modelling methods known in the literature. This part will be followed by the development of a quasi-LPV model and its subsequent numerical analysis.

## 2.3 Specification for quasi-LPV modelling adapted to application constraints

A plethora of quasi-LPV modelling methods exists in the literature. They differ by their underlying assumptions, and thus should be chosen carefully *w.r.t.* modelling constraints of each application. For example, the standard Jacobian linearisation method requires that several, potentially densely packed, equilibrium points are found in the operating state-space of the model. Inherently, the underlying assumption is that it is possible to trim the model at a manifold of points, which might not always be the case.

There are several peculiarities of the nonlinear model in the context of its application—modelling spin-stabilised projectile subject to free-flight experiments—that have to be discussed in order to select the most-appropriate quasi-LPV modelling technique. They are as follows:

- **Lack of input signals.**

The model of a projectile in free flight lacks an input signal. As such, the projectile cannot be trimmed, thus limiting the range of existing equilibrium points in the state space. This has several implications. Firstly, there is no input-dependent manifold of equilibrium points, which severely limits the practicality of grid-based methods, such as Jacobian linearisation method or state transformation. Secondly, even if input-independent equilibrium points are sought for, there exist no set of state values during a typical flat-fire flight during which the model would be at equilibrium for all of its states (as for

instance its altitude would indefinitely reduce due to the influence of gravity). Hence, even the function substitution approach—which requires only one equilibrium point—can be deemed unsuitable.

- **Indirect measurements.**

In accordance with the literature, it is required to select some of the state variables as the scheduling signals of the quasi-LPV model. Furthermore, these signals should be measurable and available at a given time instant [130]. However, the latter requirement might be difficult to fulfil in the case of embedded measurements that are available in the case study of a spin-stabilised projectile.

As it was underlined in Chapter 1, the nonlinear model of a projectile in free-flight consists of 12 state variables and 9 embedded sensor signals. The measurement signals come from the embedded accelerometers, magnetometers, and gyroscopes. However, the magnetometers and accelerometers do not directly measure any of the state variables, but rather the effects of specific forces and projections of Earth’s magnetic field, respectively. Only the gyroscopes offer a direct measurement of rotational velocities of the projectile, hence offering a measurement of state variables that could potentially be used as scheduling variables.

Moreover, the variables considered most frequently in the aerospace literature as good candidates for scheduling signals, i.e. the linear velocities [109, 86, 127, 79], are not directly measured. Although there are applications in which the accelerometer measurements are used to calculate the incidence angles, e.g. [87, 63, 19], such an estimation is possible only in specific conditions (e.g. under assumption of a low angle of attack). In the present case, only the total velocity  $V$  is measured—by the Doppler radar.

Magnetometer signals are related to attitude of projectile and this relation is taken advantage of in several applications [145, 128, 33].

To summarise, out of the available embedded sensors, only the gyroscopes provide a direct measurement of at least some of the state variables, as their signals correspond to variations of the angular velocities of the projectile. Additionally, the Doppler radar offers the measurement of total velocity.

- **Wide space of parameter variations**

The physical nonlinear model of a projectile’s in-flight behaviour is characterised by inter-state coupling and trigonometric relations that appear in most of the state equations. When the projectile is subject to free-flight experiments, it is tested under a wide range of initial flight conditions, in a process that aims to sufficiently explore its nonlinear behaviour. It is, therefore, important to preserve the nonlinear behaviour of a projectile over a wide range of flight conditions.

However, in typical aerospace-oriented quasi-LPV modelling, a usual solution is to significantly simplify the nonlinear model. Usually, it is done through decoupling the nonlinear model into so-called longitudinal and lateral-directional modes [113], assuming a small incidence angle of the projectile [38], or analysing only the high-frequency effects of the forces and moments [87, 125].

These assumptions are not always appropriate. For example, a fast-spinning projectile’s motion cannot be decoupled, it can be subject to wide variations of incidence angles, and the low frequency effects of a gravitational pull are important for a longer range firing.

Therefore, the third difficulty of quasi-LPV modelling in this case study lies in the necessity of preserving the behaviour of the nonlinear model, which renders the usual simplification assumptions impractical.

- **Existence of exogenous scheduling variables**

The choice of LPV or quasi-LPV model structure depends on the existence of potential exogenous variables in the model. As can be seen, the nonlinear model equations (1.14)-(1.16) consist of several sources of uncertainties. These stem from:

- multiplication of state variables, especially in the form of coupling between linear and angular velocities,
- trigonometric relations in which especially the Euler angles are involved,
- nonlinear nature of aerodynamic forces and moments that mostly depend on the total angle of attack  $\alpha_t$  and the total velocity  $V$  of the projectile.

Hence, the linear and angular velocities, as well as the Euler angles, introduce nonlinearity to the model structure. All of these variables are also state variables of the nonlinear model, hence the sought-for model structure is rather quasi-LPV than LPV. The only exogenous variables that could be used as scheduling variables are  $V$  and  $\alpha_t$ .

Such a conclusion is also in line with the literature on the subject. Especially the total velocity, angular velocities and Euler angles are often used as scheduling variables for projectiles, as in [109, 87, 127], so that the resulting models are quasi-LPV.

- **High accuracy constraints**

The principal use of the nonlinear model (1.14)-(1.16) in the previous research has been oriented towards identification of various flying architectures [28, 4, 1]. The underlying idea for the development of a quasi-LPV model is to accurately represent the behaviour of the existing nonlinear model.

Hence, the family of LPV modelling techniques that aim at simplification and/or point-based linearisation of the nonlinear model dynamics and be deemed ill-adapted for the task of preserving the nonlinear behaviour. The above includes methods such as Jacobian linearisation, state transformation, velocity-based linearisation, the standard function substitution approach, and the behavioural kernel-based analysis of Tóth. The aforementioned methods constitute the majority of existing LPV modelling techniques.

The only methods that could preserve the behaviour of the model are the methods that aim at analytic transformation of the nonlinear equations into a quasi-LPV form. Such an approach is formalised by the *analytic function substitution approach*, and its examples can be seen in the works of Pfifer [87]. Consequently, it has been chosen as the approach to be used in the thesis.

The analysed projectile is equipped with three types of sensors: gyroscopes, magnetometers, and accelerometers. Additionally, the in-flight measurements are supplemented by an on-ground Doppler radar. The gyroscopes measure angular velocities of the projectile, thus  $p, q, r$  are considered as known. Accelerometer's signal correspond to the specific force acting on the projectile, which in turn is influenced by vehicle's linear and angular velocities. Combined with gyroscope measurements, it is possible to obtain measurements of at least some of the linear velocities (see e.g. [85], [19]).

In the following, the linear velocity  $u$  is considered to be measurable. The magnetometers measure a projection of the Earth's magnetic field on the sensor axes, which allows to obtain the values of the roll angle  $\phi$  [1], and—in combination with accelerometers—the pitch angle  $\theta$  [16]. The Doppler radar measures the total velocity  $V$  of the projectile. Moreover, the initial position, corresponding to the gun placement, is known.

Consequently, 6 out of 12 state variables in the variable-roll frame, i.e.  $u, p, q, r, \phi, \theta$  can be considered to be measurable. Furthermore, the total velocity  $V$  is considered as an exogenous scheduling variable.

## 2.4 Proposed development of a quasi-LPV model of a projectile

Based on the above-mentioned considerations, it is proposed in this thesis to apply the analytic function substitution approach to quasi-LPV modelling. Therefore, the nonlinear model equations have to be developed into the following form:

$$\dot{\mathbf{x}} = \mathbf{A}(\mathbf{x}_1, \boldsymbol{\rho})\mathbf{x} + \mathbf{B}(\mathbf{x}_1, \boldsymbol{\rho})\mathbf{u} + h(\mathbf{x}_1, \boldsymbol{\rho}) \quad (2.34)$$

where  $\mathbf{x}_1$  and  $\boldsymbol{\rho}$  are the scheduling states and exogenous scheduling signals, respectively. The nonlinear function  $h$  is the remainder term. The remainder term has to be decomposed into a form linear *w.r.t.*  $\mathbf{x}_1$ , such as:

$$h(\mathbf{x}_1, \boldsymbol{\rho}) = \mathbf{A}_1(\mathbf{x}_1, \boldsymbol{\rho})\mathbf{x} \quad (2.35)$$

so that it can be substituted into the state matrix  $\mathbf{A}$ . Consequently, a quasi-LPV model can be obtained. Including the fact of lack of input signal, it should have the following form:

$$\dot{\mathbf{x}} = [\mathbf{A}(\mathbf{x}_1, \boldsymbol{\rho}) + \mathbf{A}_1(\mathbf{x}_1, \boldsymbol{\rho})]\mathbf{x} \quad (2.36)$$

As can be concluded by looking on the force equations in the body reference frame (1.14a)-(1.14c) and wind reference frame (A.2a)-(A.2c), the latter introduces much more trigonometric nonlinearity to the model equations. If the wind reference frame was used, the scheduling vector would need to consist of all the Euler angles and of the total velocity  $V$ , angle of attack  $\alpha$  and the angle of sideslip  $\beta$ . On the other hand, the body reference frame representation offers a better starting point, as the effects of coupling between the angular and linear velocities are separated from the effects of the nonlinear forces of aerodynamics and gravity. Moreover, since the angular velocities are directly measured by gyroscopes, it can be concluded that the coupled part can be easily separated into scheduling signals (i.e. gyroscope signals) and the linear velocities.

When the moment equations (1.15a)-(1.15c) are taken into account, it can be concluded that again, the nonlinearity comes from the effects of nonlinear aerodynamic effects, and from the coupling between velocities.

The kinematic equations, both for the attitude (1.16a)-(1.16c) and the position (1.18a)-(1.18c), introduce significant trigonometric nonlinearities to the model. This nonlinearity needs to be dealt with. An interesting possibility to reduce it would be to change the description in which the attitude is described (e.g. into a quaternions-based representation [140]) or to change a reference frame in which the dynamics of the projectile are described (e.g. into a non-rolling representation [141]). The latter option might bring significant computational benefits for the case of a spin-stabilised projectiles [142]. Therefore, it will be considered in the sequel.

### 2.4.1 Alternative nonlinear model representations

The historical motivation to use a non-rolling frame has been to overcome the drawback of time-consuming simulations for spin-stabilized projectiles [7]. Indeed, the computation time depends on the highest natural frequency of a system. In the case of spinning projectiles, it corresponds to the roll angle  $\phi$  variations, which are removed in the non-rolling reference frame [142]. More recently, this frame has been also applied in modelling of dual-spin projectiles [21].

The roll angle equation for a reference frame rigidly bounded to the centre of gravity position is as follows:

$$\dot{\phi}_F = p_F + q_F \sin \phi_F \tan \theta_F + r_F \cos \phi_F \tan \theta_F \quad (2.37)$$

where subscript  $\cdot_F$  indicates a variable associated with the reference frame (e.g. rotation angle of the frame, not a rotation angle of a projectile expressed *w.r.t.* the frame). The non-rolling frame is defined *w.r.t.* a fixed horizontal plane, i.e.  $\dot{\phi}_F = \phi_F = 0$ . Hence, (2.37) leads to:

$$p_F = -r' \tan \theta' \quad (2.38)$$

where the superscript  $\cdot'$  indicates a variable expressed *w.r.t.* the non-rolling frame. Thanks to (2.38), the model equations (1.14)-(1.18) become:

*Translational dynamics*

$$\begin{bmatrix} \dot{u}' \\ \dot{v}' \\ \dot{w}' \end{bmatrix} = \begin{bmatrix} 0 & -r' & q' \\ r' & 0 & r' \tan \theta' \\ -q' & -r' \tan \theta' & 0 \end{bmatrix} \begin{bmatrix} u' \\ v' \\ w' \end{bmatrix} + \frac{\bar{q}S}{m} \begin{bmatrix} C_x \\ C_y \\ C_z \end{bmatrix} + g \begin{bmatrix} -\sin \theta \\ 0 \\ \cos \theta \end{bmatrix} \quad (2.39)$$

*Attitude dynamics*

$$\begin{bmatrix} \dot{p}' \\ \dot{q}' \\ \dot{r}' \end{bmatrix} = \begin{bmatrix} q' r' \frac{I_z - I_y}{I_x} \\ -(\frac{I_x}{I_y} p' + r' \tan \theta') r' \\ (\frac{I_x}{I_z} p' + r' \tan \theta') q' \end{bmatrix} + \bar{q} S d \begin{bmatrix} C_l \\ C_m \\ C_n \end{bmatrix} \quad (2.40)$$

*Translational kinematics*

$$\begin{bmatrix} \dot{x}'_E \\ \dot{y}'_E \\ \dot{z}'_E \end{bmatrix} \begin{bmatrix} \cos \theta' \cos \psi' & -\sin \psi' & \sin \theta' \cos \psi' \\ \cos \theta' \sin \psi' & \cos \psi' & \sin \theta' \sin \psi' \\ -\sin \theta' & 0 & \cos \theta' \end{bmatrix} \begin{bmatrix} u' \\ v' \\ w' \end{bmatrix} \quad (2.41)$$

*Attitude kinematics*

$$\begin{bmatrix} \dot{\theta}' \\ \dot{\psi}' \end{bmatrix} = \begin{bmatrix} 1 & 0 \\ 0 & \cos^{-1} \theta' \end{bmatrix} \begin{bmatrix} q' \\ r' \end{bmatrix} \quad (2.42)$$

The roll angle can be calculated *a posteriori* [142] as:

$$\dot{\phi}' = p' + \psi' \sin \theta' \quad (2.43)$$

or

$$\phi(t) = \int_0^t p'(\tau) + r'(\tau) \tan \theta(\tau) d\tau. \quad (2.44)$$

This new model representation, expressed in a non-rolling reference frame, is analytically equivalent to the original, variable-roll reference frame. The analytic development supporting the claim of frames' equivalence is presented in Appendix B.

Additionally, the signals measured in the variable-roll frame can be transformed to the non-rolling frame through (2.45)-(2.46).

The nonlinear model equations (2.39)-(2.42) are already in a quasi-LPV form, with the exception of forces and moments. Consequently, the forces and moments equations are considered to be the remainder term.

Linear and angular velocities depend on the selected frame, and can be transformed from one frame to another [32] through the following relations:

$$\begin{bmatrix} u' \\ v' \\ w' \end{bmatrix} = \begin{bmatrix} 1 & 0 & 0 \\ 0 & \cos \phi & -\sin \phi \\ 0 & \sin \phi & \cos \phi \end{bmatrix} \begin{bmatrix} u \\ v \\ w \end{bmatrix} \quad (2.45)$$

$$\begin{bmatrix} p' \\ q' \\ r' \end{bmatrix} = \begin{bmatrix} 1 & 0 & 0 \\ 0 & \cos \phi & -\sin \phi \\ 0 & \sin \phi & \cos \phi \end{bmatrix} \begin{bmatrix} p \\ q \\ r \end{bmatrix} \quad (2.46)$$

The Euler angles and positions are equivalent regardless of the selected frame. The signals measured in the variable-roll frame can be transformed to the non-rolling frame through the inverse of (2.45)-(2.46).

## 2.4.2 Decomposition of the nonlinear remainder term

The suggested decomposition approach is based on algebraic transformations, as in [125, 87, 92]. Alternatively, a numerical decomposition could be applied, [113], but the physical insight into the nonlinearity would be reduced.

Firstly, the global force coefficients  $C_y, C_z$  can be expressed as coefficients of the normal force slope  $C_{N\alpha}$  and Magnus force slope  $C_{yp\alpha}$ . Similarly, the global aerodynamic moment coefficients  $C_l, C_m, C_n$  can be developed into the following coefficients: roll damping  $C_{lp}$ , pitch moment coefficient slope  $C_{m\alpha}$ , pitch damping  $C_{mq}$ , and Magnus moment coefficient slope  $C_{np\alpha}$  [1]. Consequently, the linear and angular velocities appear in the equations through multiplication, which can be used in the decomposition of the remainder term:

$$\begin{aligned} C_x &= -C_X(u, V) \\ C_y &= -C_{N\alpha}(V) \frac{v}{V} + \frac{d}{2V} C_{yp\alpha}(V) \frac{w}{V} p \\ C_z &= -C_{N\alpha}(V) \frac{w}{V} - \frac{d}{2V} C_{yp\alpha}(V) \frac{v}{V} p \\ C_l &= \frac{d}{2V} C_{lp}(V) p \\ C_m &= C_{m\alpha}(V) \frac{w}{V} + \frac{d}{2V} C_{mq}(V) q + \frac{d}{2V} C_{np\alpha}(V) \frac{v}{V} p \\ C_n &= -C_{m\alpha}(V) \frac{v}{V} + \frac{d}{2V} C_{mq}(V) r + \frac{d}{2V} C_{np\alpha}(V) \frac{w}{V} p \end{aligned} \quad (2.47)$$

The nonlinear remainder term then has the following form, described through auxiliary functions

$X_1, \dots, X_7$ :

$$\begin{aligned}
 \frac{\bar{q}S}{m}C_x - gs\theta &= X_1(u, V, z'_E) - g(z'_E)s\theta' \\
 \frac{\bar{q}S}{m}C_y &= X_2(V, z'_E)w'p' + X_3(V, z'_E)v' \\
 \frac{\bar{q}S}{m}C_z + gc\theta &= -X_2(V, z'_E)v'p' + X_3(V, z'_E)w' + g(z'_E)c\theta' \\
 \frac{\bar{q}Sd}{I_x}C_l &= X_4(V, z'_E)p' \\
 \frac{\bar{q}Sd}{I_t}C_m &= X_5(V, z'_E)w' + X_6(V, z'_E)q' + X_7(V', z'_E)v'p' \\
 \frac{\bar{q}Sd}{I_t}C_n &= -X_5(V, z'_E)v' + X_6(V, z'_E)r' + X_7(V, z'_E)w'p'
 \end{aligned} \tag{2.48}$$

where:

$$\begin{aligned}
 X_1(u, V, z_E) &= -0.5m^{-1}\rho(z'_E)V^2SC_X(u, V) \\
 X_2(V, z_E) &= 0.25m^{-1}\rho(z'_E)SdC_{yp\alpha}(V) \\
 X_3(V, z_E) &= -0.5m^{-1}\rho(z'_E)VSC_{N\alpha}(V) \\
 X_4(V, z_E) &= 0.25\rho(z'_E)Vd^2C_{lp}(V) \\
 X_5(V, z_E) &= 0.5\rho(z'_E)VdC_{m\alpha}(V) \\
 X_6(V, z_E) &= 0.25\rho(z'_E)Vd^2C_{mq}(V) \\
 X_7(V, z_E) &= 0.25\rho(z'_E)d^2C_{np\alpha}(V).
 \end{aligned}$$

where  $C_X$  depends on both  $u$  and  $V$ , due to  $s^2\alpha_t = (1 - \frac{u^2}{V^2})$ . Additionally, based on (2.45) and fully developed in Appendix B, the following equivalences can be stated:  $\alpha_t = \alpha'_t$  and  $V = V'$ .

Only  $X_1$  and the gravity components are not in a form multiplied by a measurable state variable. Hence, they need to be assigned to be decomposed arbitrarily, by multiplication and division by any measurable signal. In case of a spin-stabilized projectile, the spin rate  $p$  is such a signal. By integrating the spin rate in the decomposition, the following decomposition of  $X_1$  may be obtained:

$$X_1(u, V, z_E) = X_1(u, V, z_E) \cdot \frac{1}{p} \cdot p \tag{2.49}$$

The gravity terms may be treated in the same way. However, in ballistic free-flight testing, the pitch angle  $\theta$  can be assumed to be close to zero (assuming a flat-fire trajectory). Using the small angle approximation, i.e.  $s\theta \approx \theta$ ,  $\tan \theta \approx \theta$ ,  $c\theta \approx 1$ , it can be decomposed *w.r.t.*  $\theta$ .

Finally, it can be noted that  $x_E$  and  $y_E$  are decoupled from the rest of state equations, i.e. no state variable depends on their evolution. Thus, they have been removed from the state matrix.

Consequently, all the nonlinear remainder terms have been developed to a form which either depends on the measurable variables, or can be directly assigned to non-measurable state variable, or—as in case of  $\theta$ —can be simplified in a flat-fire scenario. As a result, the quasi-LPV model of the following form has been obtained:

$$\dot{\mathbf{x}}' = \mathbf{A}(u', V, p', q', r', \theta, \psi, z'_E)\mathbf{x}' \tag{2.50}$$

with the full matrix  $\mathbf{A}$  presented in (2.51), as:

$$\mathbf{A} = \begin{bmatrix} 0 & -r' & q' & \frac{X_1 - g \sin \theta'}{p'} & 0 & 0 & 0 & 0 & 0 \\ r' & X_3(V, z'_E) & r' \tan \theta' + X_2(V, z'_E)p' & 0 & 0 & 0 & 0 & 0 & 0 \\ -q' & -r' \tan \theta' - X_2 p' & X_3 & \frac{g \cos \theta}{p'} & 0 & 0 & 0 & 0 & 0 \\ 0 & 0 & 0 & X_4 & 0 & 0 & 0 & 0 & 0 \\ 0 & X_7 p' & X_5 & -\frac{I_x}{I_t} r' - \frac{r' r' \tan \theta}{p} & X_6 & 0 & 0 & 0 & 0 \\ 0 & -X_5 & X_7 p' & \frac{I_x}{I_t} q' + \frac{q' r' \tan \theta}{p} & 0 & X_6 & 0 & 0 & 0 \\ 0 & 0 & 0 & 0 & 0 & 1 & 0 & 0 & 0 \\ 0 & 0 & 0 & 0 & 0 & 0 & \cos^{-1} \theta & 0 & 0 \\ \cos \theta \cos \psi & -\sin \psi & \sin \theta \cos \psi & 0 & 0 & 0 & 0 & 0 & 0 \\ \cos \theta \sin \psi & \cos \psi & \sin \theta \sin \psi & 0 & 0 & 0 & 0 & 0 & 0 \\ -\sin \theta & 0 & \cos \theta & 0 & 0 & 0 & 0 & 0 & 0 \end{bmatrix} \quad (2.51)$$

The proposed development is valid for describing the model dynamics, using the state matrix  $\mathbf{A}$ . Should the control input be added to the model, it would necessitate an appropriate treatment of matrix  $\mathbf{B}$  as well.

### 2.4.3 Simulation results

The proposed quasi-LPV model, developed analytically in the previous section, has to be tested through a series of comparability simulations in order to assess its accuracy *w.r.t.* the existing nonlinear model. For such a comparison to be indicative, it would need to be performed for the same initial conditions, using the same numerical solver, and *w.r.t.* the same reference frame (variable-roll or non-rolling).

Considering that the original knowledge-based model—considered herein as a reference—describes the motion of a projectile in a variable-roll reference frame, the quasi-LPV model simulations will be transformed into a variable-roll reference frame as well. The inverse of (2.45)-(2.46) can be used to transform the evolution of state variables.

There are several ways in which errors in the development of the quasi-LPV model would manifest themselves in the aforementioned testing set-up:

- The transformation between the reference frames is sensitive to erroneous roll angle  $\phi$ , since this variable is directly used in (2.45)-(2.46). Therefore, assuring its accurate evolution is of paramount importance.
- The aerodynamic forces and moments depend directly on the evolution of the dynamic state variables, *i.e.* the linear and angular velocities. Therefore, their evolution also need to be compared for both models.
- An inaccurate description of the aerodynamic coefficients would result in increasingly incorrect forces and moments, thus diverging over time from the ones obtained in the simulation of the nonlinear model. Therefore, the time evolution of the aerodynamic coefficients has to be compared for both models.

In order to perform simulations, a set of conditions corresponding to the flight conditions at

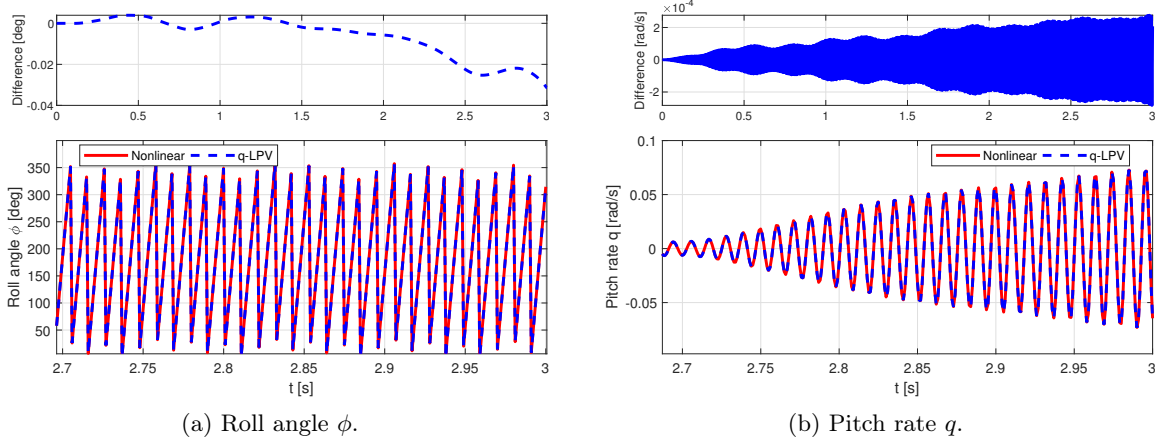


Figure 2.1: Evolution of exemplary state variables as calculated in both reference frames.

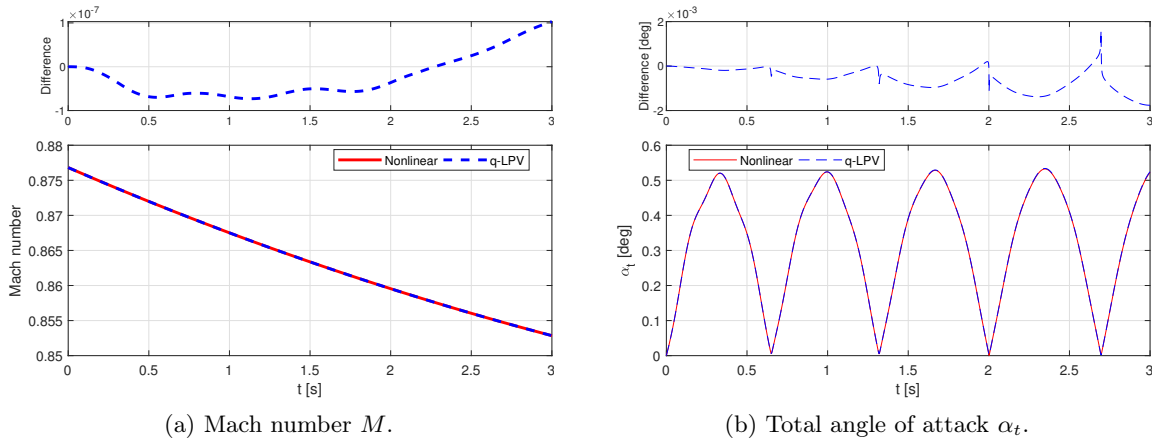


Figure 2.2: Evolution of the aerodynamic variables.

the ISL's open-range test site in Baldersheim has been chosen. The initial Mach number has been set up to a variation range from 0.88 to 1.77, with the initial spin rate from 608 to 1217 rad/s. Simulations are conducted for a flat-fire scenario: the initial velocity vector is almost parallel to the Earth's surface. The polynomial descriptions of the aerodynamic coefficients for such experimental conditions are known, and were used in both models' descriptions. For both model, an implementation of their state equations in Matlab is used.

Exemplary results of the simulations are summarised in:

- Fig. 2.1a and Fig. 2.1b showing the evolution of the roll angle  $\phi$  and an exemplary angular velocity  $q$ , respectively. Error of the  $\phi$  angle remained small for the tested scenarios (less than 0.1 deg difference between models). Consequently, the measurable signals could be accurately transformed between the frames. It is exemplified by the pitch rate evolution: the error is three orders of magnitude smaller than the signal. Due to high frequency of both signals and for the sake of brevity, only last 0.3 s of signals' evolution are portrayed.

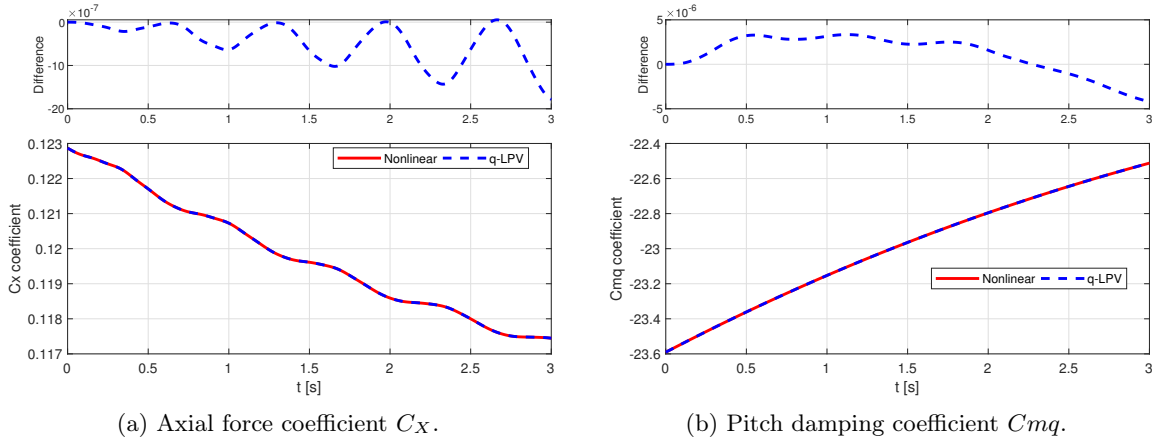


Figure 2.3: Evolution of the exemplary aerodynamic coefficients.

- Fig. 2.2a and 2.2b displaying the evolution of Mach number  $M$  and the total angle of attack  $\alpha_t$ , respectively. The polynomial descriptions of the coefficients in (2.47) are functions of  $M$  and  $\alpha_t$ . For both reference frames, these variables are in good alignment: the errors are increasing over time, but their magnitude is of two orders smaller than the signals.
- Fig. 2.3a and Fig. 2.3b, showing the trajectory of the axial force coefficient  $C_X$ , and the pitch damping coefficient  $C_{mq}$ , respectively. Good alignment of  $\phi$ ,  $\alpha_t$  and  $M$  has resulted in accurate calculations of the aerodynamic coefficients. Behaviour of the error is the same as previously: slowly increasing, but of small magnitude.

Additionally, the expected computation time reduction has indeed been observed. For the initial spin rate  $p_0 = 608$  rad/s, the simulation lasted 15s in the variable-roll frame, and 0.8s in non-rolling frame.

It has to be noted that even though the simulations were performed for the same initial conditions and the same reference variable-roll reference frame, some discrepancy can be observed. For the tested case, as shown in Fig. 2.1a, the error of the roll angle  $\phi$  has reached the value of 0.1 deg. Such an error, although appearing small in magnitude for the flat small-range trajectory, is nonetheless worrying. Without the proper understanding of its sources, it could potentially compromise the accuracy of longer range simulations.

#### 2.4.4 Conclusions

In this section, a quasi-LPV model of a projectile in free flight has been proposed. The chosen approach exploits the established practices in quasi-LPV modelling: the function substitution [125, 87] that allows to analyse the projectile's behaviour even for a non-equilibrium flight [78]; and the reference frame transformation [7, 142] that reduces the computational complexity of the system for the case of spin-stabilised ammunition. The resulting quasi-LPV model is computationally more efficient, is analytically equivalent to the nonlinear model without any additional approximations assumed, and resembles the control-oriented quasi-LPV model presented by [109].

However, a comparison of simulations of the nonlinear and quasi-LPV models has shown non-

negligible differences in their obtained state trajectories. Such differences are especially problematic in the case of long-range simulations, since the simulated results could diverge from the real trajectory over time.

Considering that the two models predicted only a slightly different trajectory—when initiated with the same set of initial state vector and the same aerodynamic coefficients description—it is predicted that the differences stem from an inappropriate selection of a numerical solver of the ordinary differential equations (*ODE*). Indeed, while analytic derivations of the model equations in various reference frames are known for decades [7, 8, 144], the influence of *ODE* solver selection on the accuracy of the non-rolling model’s state trajectory has not been thoroughly studied in published sources.

The following section will address the problem of selecting a numerical solver apt to calculating longer range trajectories accurately.

## 2.5 Accuracy and computation time assessment of the models in different reference frames

The objective of the following section lies in the evaluation of how much do the reference frame transformation and the numerical solver selection influence the accuracy of a trajectory simulation.

Accuracy of a numerical solution to a system of *ODE*-s can be evaluated through a comparison with an analytic solution, if the latter is known. It is not usually the case for six-degrees-of-freedom Newton-Euler models of flight dynamics: for them an analytic solution can be found only by imposing additional constraints, e.g. restricting the analysis to a grid of equilibrium points, as it is done for airplane models [20, 112]. However, imposing such a restriction would be impractical since the end goal of the project is to develop a quasi-LPV model structure that would accurately preserve the nonlinear behaviour of a projectile for a wide range of flight conditions.

An alternative approach, proposed in the present work, consists of applying a numerical solver with—impractically strict—accuracy constraints. Then its solution is considered as a reference and used to evaluate which of existing numerical solvers with less strict constraints provide a comparable accuracy. The analysis is conducted within the Matlab software that contains a pre-implemented set of *ode* solvers [112] that can be used in the last step.

Numerical solvers consist of fixed- and variable-step categories. The latter is applicable to stiff problems, has a shorter computation time and better convergence properties [5], for which reasons it is embedded in Matlab [112]. The fixed-step category, on the other hand, can be slower in solving an *ODE* due to inability to modify the time-step, albeit offer a direct control over the solver’s order and sampling time, allowing to easily observe convergence of a solution. Hence, in order to find a reference solution, it is decided to apply a fixed-step *ODE* solver with a high order and high sampling frequency. Such a solution can be then used in assessment of much faster variable-step solvers, so that the most accurate solver can be selected. The approach is represented in the ideogram in Fig. 2.4.

It is important to assess if solutions converge and are stable, prior to declaring one of them as a reference solution. They can be evaluated by varying the solver’s order and sampling time.

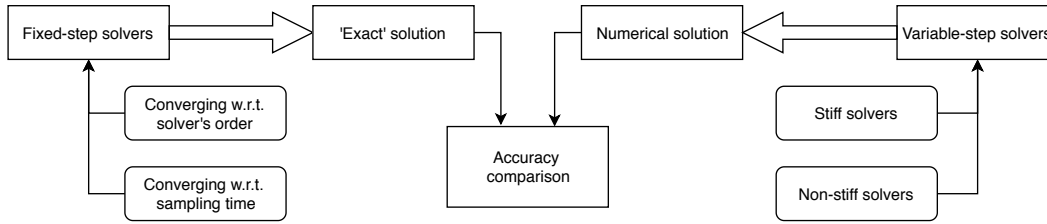


Figure 2.4: Comparison of exact and numerical solutions

Herein, it is proposed to find an 'exact' (as in Fig. 2.4) solution using the following approach:

1. Obtain a number of numerical solutions using fixed-step solver for a range of solver's orders and sampling times, in such a way, that the solutions are expected to be stable and accurate, e.g. by arbitrarily specifying the maximum step size [45, 48].
2. Test if the solutions converge with an increasing solver order.
3. Test if the solutions converge with an increasing sampling.
4. If the solutions are stable and converging, select the solution obtained with the highest order and highest sampling time, as the 'exact' one.

Such a procedure allows to find a solution that can be considered as a reference, albeit is heavily computationally expensive. This computational cost motivates the search for a much faster variable-step solver that produces the most similar results.

The evaluation will be performed on the two models:

- the nonlinear one in a variable-roll reference frame, similar to these usually used in simulations for the purpose of free-flight experiments [4],
- the proposed quasi-LPV one in a non-rolling frame, resembling these used in control [109].

The test scenario applied in the analysis corresponds to a parabolic flight trajectory. The set of initial values is as follows:  $u_0 = 700 \text{ m/s}$ ,  $p_0 = 1420 \text{ rad/s}$ ,  $\theta_0 = 15 \text{ deg}$ ,  $\psi_0 = 0 \text{ deg}$ . The remainder initial state variables are set to zero. Such an initial elevation angle and velocity would result in a flight lasting approximately 30 s in real life.

### 2.5.1 Assessment of the fixed-step solvers

#### Solution of the nonlinear model

Firstly, the influence of the solver's order is investigated. The sampling time has been fixed to  $20 \mu\text{s}$ . This selection is motivated by the highest frequency of the model *i.e.* the roll angle evolution, which has a period of approximately  $5 \text{ ms}$ —it is of two orders of magnitude larger than the sampling time, allowing to obtain an accurate solution. Fixed-step solvers with orders ranging from one to five have been applied.

An exemplary figure from the convergence analysis is presented in Fig. 2.5. The figure portrays the trajectory of  $q$  for each solver order and the differences between them—as calculated *w.r.t.* the highest-order solution. It can be observed that for each increase in solver’s order, the difference between the solutions obtained for the given order and the highest tested order is decreasing, which suggests that the results are converging. The trajectories are noted as *ode2–ode5*, and *ode1* is not shown, since the solution was unstable. The solution calculated for the fifth-order solver (*i.e.* Runge-Kutta method) differs only by approximately  $2e-8$  from the fourth-order solution, *i.e.* the magnitude of the difference is  $10^8$  smaller than the magnitude of the pitch rate signal.

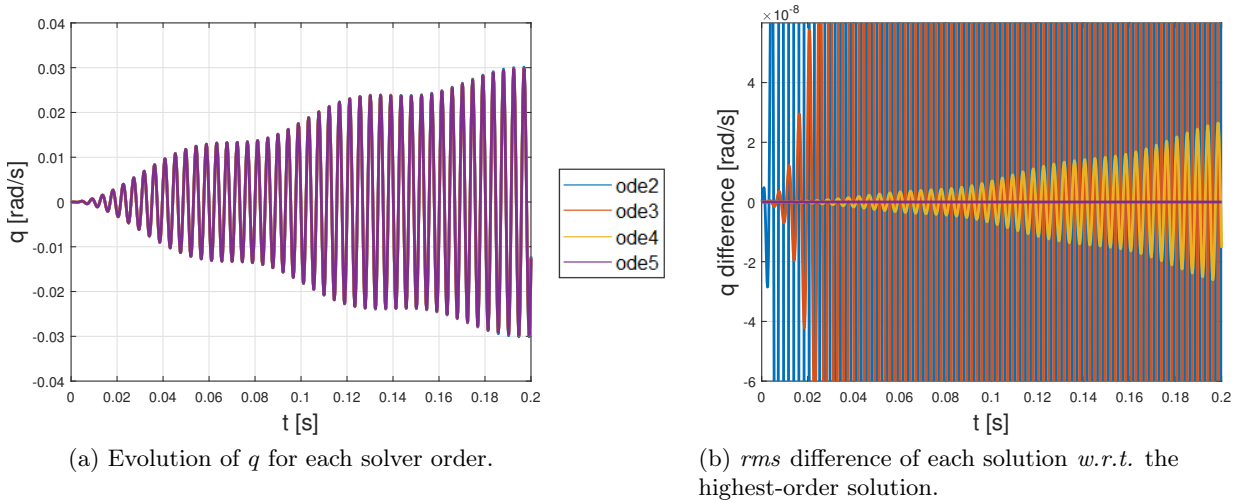


Figure 2.5: Convergence of a numerical solution for the nonlinear model on the example of the pitch rate  $q$ : the first 0.2s are shown.

The convergence of solutions can become even more visible when analyzing the root mean square (*rms*) differences. For this reason, Fig. 2.6.a) presents *rms* differences calculated *w.r.t.* the highest-order solution for three exemplary state variables:  $y_E, \theta$ , and  $\psi$ . For the analyzed flight scenario, these variables reach values from the range of  $y_E \in (0, 6.5) m$ ,  $\theta \in (-25, 15) deg$ , and  $\psi \in (0, 2) deg$ . The magnitude of *rms* differences between the reference solution and the lower-order solutions is decreasing ten- to thousandfold with each increase in solver’s order.

Therefore, with an increase of the order, the solution gets more stable and converges more easily. Moreover, the solution for the fifth-order differs only negligibly from the fourth-order solution, hence the fifth-order can be considered as a sufficiently accurate.

Secondly, the influence of the sampling time has been investigated. A solver’s order equal to five, considered in the prequel as sufficiently accurate, has been used for all the tests. The sampling time ranged from 20 to 100  $\mu s$ . Fig. 2.6.b) presents the *rms* differences between simulations for the increasing sampling frequency. It can be seen that the *rms* decreases ten- to hundredfold for a twofold increase in sampling frequency, hence the solutions can be considered as converging for a decreasing sampling time.

Therefore, the solutions converge and become more stable *w.r.t.* the solver’s order and sampling time, while the differences between solutions become negligibly small. Hence, the solution obtained for the highest order and the most dense sampling, *i.e.* the fifth-order solution for 20  $\mu s$

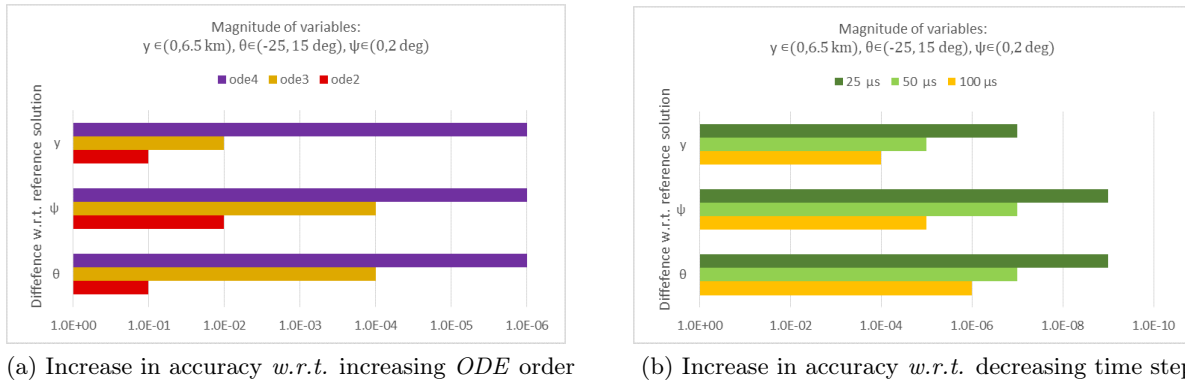


Figure 2.6: The *rms* difference *w.r.t.* solution of the fifth-order solver with 20  $\mu s$ : convergence with increasing solver's order and sampling time

sampling is considered as a reference for the future analysis.

### Solution of the quasi-LPV model

Numerical analysis of the quasi-LPV model in the non-rolling frame has been performed using the same procedure as for the nonlinear model in the variable-roll reference frame. Due to slower system's dynamics (the equations are decoupled from the fast-varying roll angle [142]), the sampling time of 300  $\mu s$  has been sufficient to obtain a stable solution, even for the first-order solver.

The exemplary results showing the influence of the solver's order are presented in Fig. 2.7 and 2.8. Figure 2.7 presents the *rms* of the difference between the solution obtained for each solver order *w.r.t.* the solution obtained for the highest order. It can be seen that the *rms* difference decreases thousandfold with each increase in solver's order. Moreover, the differences are smaller than for the case of variable-roll model. Such effect stems from slower system dynamics. It can also be observed for the example of the pitch rate  $q$  in Fig. 2.8, whose variations are slower than in Fig. 2.5.

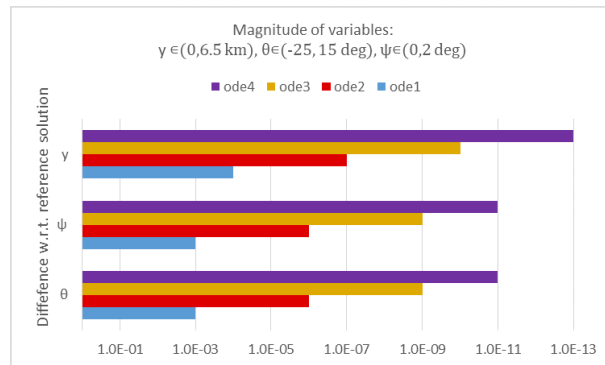


Figure 2.7: Root mean square difference *w.r.t.* solution of the fifth-order solver with 300  $\mu s$ : the solutions converge with increasing solver's order

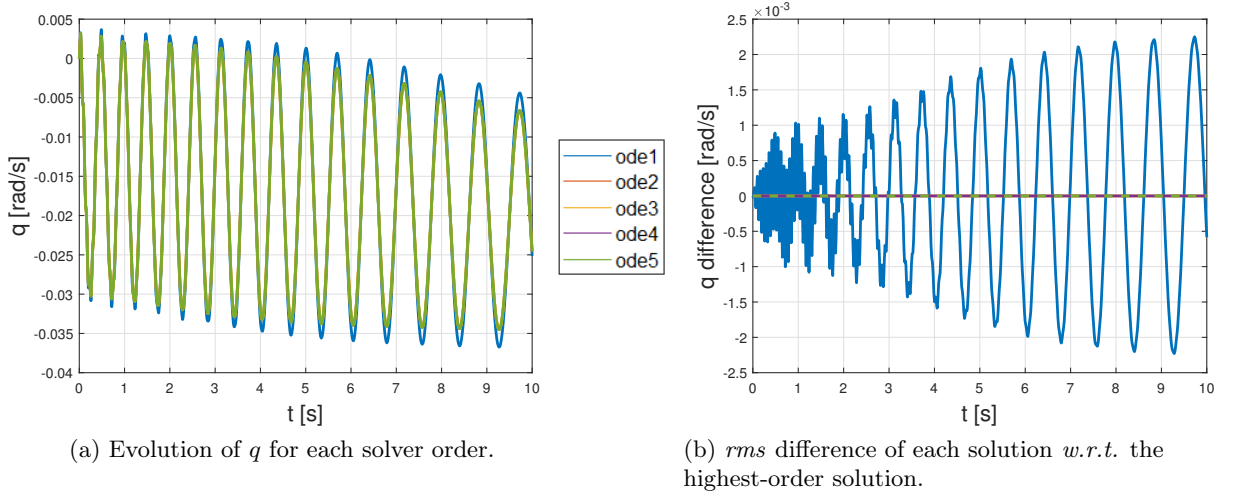


Figure 2.8: Convergence of a numerical solution for the quasi-LPV model on the example of the pitch rate  $q$

## Summary

Using fixed-step solvers, stability and convergence of solutions of the two models has been assessed and their reference solutions have been obtained. Additionally, it can be observed that for the same initial conditions and solver's order, the non-rolling frame results are of higher accuracy than the variable-roll ones.

The duration of a simulation is significantly reduced by the change of model's structure, as can be seen in Table 2.1. The fixed-step simulation of a 100-seconds-long lasts approximately 50 minutes for the nonlinear model, and approximately 3 minutes for the quasi-LPV model. The difference in time stems from different sampling used in each *ODE* settings.

Model structure	Computation time
Nonlinear (variable-roll)	50 minutes
Quasi-LPV (non-rolling)	3 minutes

Table 2.1: Duration of a simulation: non-rolling model structure influences the computation time.

### 2.5.2 Assessment of the variable-step solvers

In the previous section, a numerical solution considered as a reference has been found for both models. However, the reference solutions are computationally expensive to obtain due to strict order and sampling-time constraints. In order to reduce the computational complexity, it is proposed to analyse the variable-step solvers in this section. Their solutions are easier to compute due to varying time step. Their accuracy is assessed *w.r.t.* the reference solutions, as shown in Fig. 2.4.

The variable-step *ODE* solvers available in Matlab, including the ones adapted for non-stiff problems like the Runge-Kutta based *ode23* and *ode45* or the Adams-Bashforth-Moulton based *ode113*, and the ones adapted for stiff problems, such as the variable-step-variable-order *ode15s* [112] are used in the following tests.

### Nonlinear model analysis

The reference solution to the nonlinear model obtained in the previous section allows to assess accuracy of the variable-step solvers. The same set of initial state values is used.

As can be seen based on the results summary presented in Table 2.2, the selection of a solver influences the accuracy and computation time significantly. The solver adapted to stiff problems, *ode15s*, achieves the lowest accuracy of all the solvers in the case of kinematic variables, such as position  $y_E$  and attitude angles  $\theta, \psi$ . Over a long-distance simulation, such discrepancy can have a significant effect on the accuracy of predicted trajectory. On the other hand, the *ode45* solver has allowed to obtain the highest accuracy for all the state variables, while requiring less than 6 minutes (as compared to 50 minutes of calculating the reference solution) to compute the trajectory.

Solver	Computation time	<i>rms</i> error <i>w.r.t.</i> the reference solution				
		u[m/s]	q[rad/s]	$\theta$ [deg]	$\psi$ [deg]	$y_E$ [m]
<i>ode45</i>	5min 34s	e-04	e-04	e-05	e-05	e-03
<i>ode23</i>	20min 37s	e-04	e-04	e-04	e-04	e-02
<i>ode113</i>	1min 35s	e-04	e-04	e-04	e-04	e-03
<i>ode15s</i>	1min 49s	e-03	e-04	e-03	e-03	e-01

Table 2.2: Variable-roll reference frame: order of magnitude of the *rms* difference between the reference solution and variable-step simulations' results of the nonlinear model

### Quasi-LPV model analysis

The reference solution to the quasi-LPV model in the non-rolling frame obtained in the previous section allows to assess accuracy of the variable-step solutions.

Solver	Computation time	<i>rms</i> error <i>w.r.t.</i> the reference solution				
		u[m/s]	q[rad/s]	$\theta$ [deg]	$\psi$ [deg]	$y_E$ [m]
<i>ode45</i>	5s	e-04	e-06	e-05	e-05	e-05
<i>ode23</i>	9s	e-04	e-06	e-05	e-05	e-05
<i>ode113</i>	8s	e-04	e-06	e-05	e-05	e-05
<i>ode15s</i>	4s	e-04	e-06	e-05	e-05	e-05

Table 2.3: Non-rolling reference frame: order of magnitude of the *rms* difference between the reference solution and variable-step simulations' results of the quasi-LPV model

Similarly as in the previous case, the variable-step solvers available in Matlab have been tested, and the results are summarized in Table 2.3. Since the roll angle is decoupled, the problem is less stiff and less computationally expensive. It can be observed that all the variable-step solvers have

similar accuracy, and all the solvers offer higher accuracy and shorter computation time than in the case of the nonlinear model. Consequently, it can be argued that the model represented in a non-rolling reference frame is numerically more stable. Among the tested solvers, *ode45* and *ode15s* have the lowest computation time. Therefore, it is recommended to use them in the non-rolling frame simulations. The simulation lasts 4 to 5 seconds, which is shorter than the duration of the flight in real world.

## Summary

Using variable-step solvers embedded in Matlab, the numerical solutions have been obtained for both the nonlinear and quasi-LPV models. As predicted, the approach is less computationally expensive than using fixed-step solver, albeit for the price of being more errors-prone. Based on the results presented in Tables 2.2 and 2.3, it is concluded that the most accurate *ODE* solver is *ode45*, which for both models allows to obtain a solution similar to the reference one.

### 2.5.3 Comparative analysis of the models' trajectories

The previous section shows how to obtain accurate solutions using the fixed-step and variable-step solvers for both reference frames. The analytic derivation presented in [7, 8] suggests that the variable-roll and non-rolling reference frame can be considered as equivalent to each other: the results obtained in either of the frames can be converted to the other one using the transformation matrices (2.45)-(2.46) or their inverse. In order to test these premises on numerical grounds, an additional long-range simulation has been performed.

The non-zero initial conditions correspond to  $u_0 = 798.4 \text{ m/s}$ ,  $p_0 = 1619 \text{ rad/s}$ ,  $\theta_0 = 63 \text{ deg}$ , and  $\psi_0 = -0.046 \text{ deg}$ . Resulting parabolic flight over the distance of 20 km lasts approximately 100 seconds, therefore the numerical discrepancies should become visible over such a long trajectory.

Firstly, to emphasize the importance of the selection of an appropriate *ODE* solver, a variable-step solution has been calculated for both models using *ode15s*—since such a selection could be made based on the suspected stiff nature of the nonlinear model. However, as seen in Table 2.2, it is the least accurate solver in practice. The results of such a simulation are presented on an example of the total angle of attack evolution in Fig. 2.9. Indeed, the difference between reference frames reaches up to one degree at the end of the flight, and the two trajectories diverge.

However, the difference can be reduced, using the procedure described in the two previous sections. A reference solution for each frame is found using the fifth-order fixed-step *ODE* solver, with the sampling time equal to  $20 \mu\text{s}$ . Two exemplary variables, the total angle of attack  $\alpha_t$  and the total velocity  $V$ , are plotted in Fig. 2.10 for comparison, as they should be equal in both frames. Indeed, the maximum difference between the reference solutions for both frames is lower than  $2 \mu\text{deg}$  and  $1 \mu\text{m/s}$ , respectively, which is more accurate than available measurement techniques. Hence, the reference solutions are equivalent, as predicted by analytic developments.

In the next step, the variable-step solvers have been applied. Accordingly with the results presented in Tables 2.2 and 2.3, solver *ode45* has been used. The resulting trajectories of  $\alpha_t$  and  $V$  are presented in Fig. 2.11. The maximum difference between the variable-step solvers remains smaller than  $0.01 \text{ deg}$  and  $0.01 \text{ m s}^{-1}$ , respectively. Such a difference, albeit higher than in the

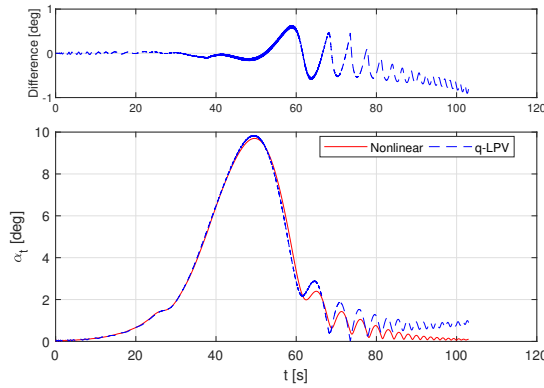


Figure 2.9: Consequences of poor selection of the *ODE* solvers: difference in  $\alpha_t$  evolution for long-range trajectory

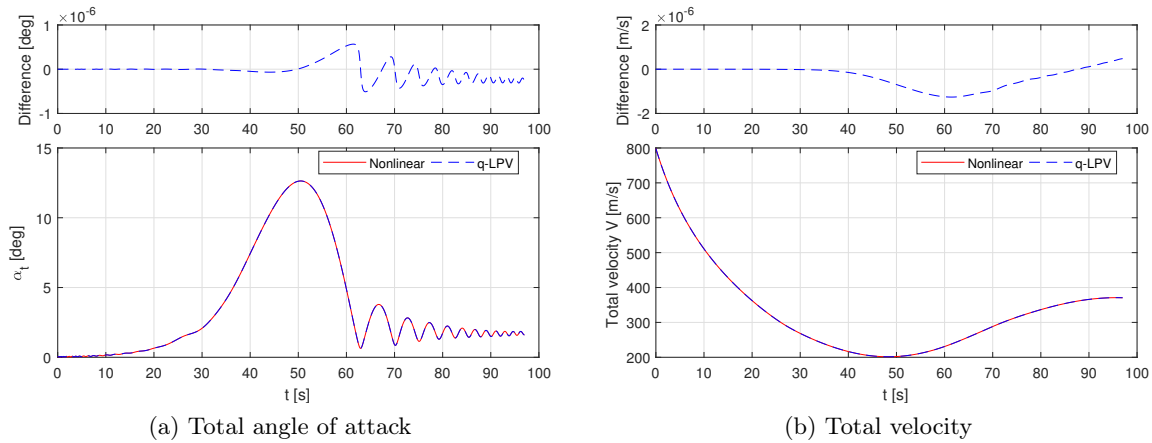


Figure 2.10: Comparison of fixed-step solutions in both frames

case of fixed-step simulations, can still be considered acceptable compared to magnitude of the signals.

Finally, the final-step error for selected state variables, calculated *w.r.t.* the reference solution for each solver, is presented in Table 2.4. If compared, the state variables obtained using fixed-step solver differ in the range of orders of magnitude between e-04 and e-07; which corresponds to the accuracy presented in Fig. 2.6. Should a higher accuracy be required, simulation with *ODE* of orders six or above would have to be used.

Additionally, it can be seen that accuracy of the simulation obtained with variable-step solvers is significantly higher for the case of the non-rolling reference frame: when compared to the variable-roll frame simulation, the state variables are at least 100 times more accurate. It can be concluded that simulating the trajectory in the non-rolling frame first, and transforming the results to the variable-roll frame afterwards, is in fact both faster and more accurate than simulating them only in the variable-roll frame.

Consequently, the non-rolling frame can be considered as an accurate alternative for the rolling-

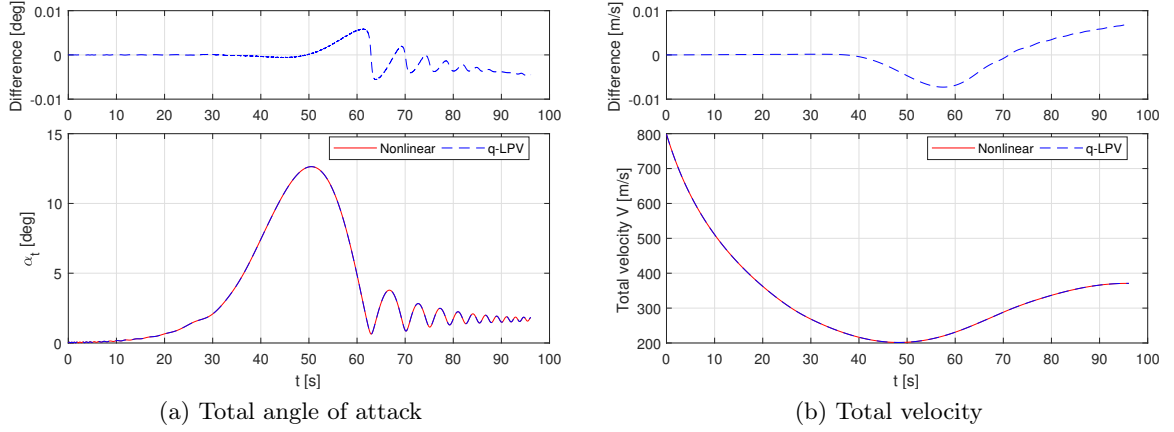


Figure 2.11: Comparison of variable-step solutions in both frames

State	Unit	Range	Final step difference <i>w.r.t.</i> the reference solution		
			fixed-step non-rolling	variable-step variable-roll	variable-step non-rolling
$u$	m/s	400–800	e-07	e-03	e-06
$p$	rad/s	1100–1700	e-07	e-03	e-06
$\phi$	deg	0–360	e-04	e-01	e-04
$\theta$	deg	$\pm 70$	e-07	e-04	e-08
$\psi$	deg	0–16	e-06	e-04	e-07
$x_E$	m	0–20000	e-05	1.02	e-05
$y_E$	m	0–1000	e-04	-3.75	e-06
$z_E$	m	0–12000	e-05	-0.61	e-05

Table 2.4: Range of variation of state variables and the order of magnitude of the final-step difference *w.r.t.* the reference solution

frame simulations. The benefits are the higher robustness to numerical solver errors and faster computation.

## 2.6 Conclusions

This chapter investigates the prospects of using a reference frame transformation in developing a quasi-LPV model of a projectile’s in-flight behaviour. The analysis have been dedicated to an example of a spin-stabilised large calibre projectile. Firstly, the projectile’s equation of motion have been transformed into a non-rolling reference frame, which has simplified the model equations and reduced computation time. Secondly, the quasi-LPV model has been obtained using the analytic function substitution method.

Two models of vehicle’s in-flight behaviour: the nonlinear, developed in a variable-roll reference frame, and a proposed quasi-LPV, developed in a non-rolling reference frame have been then compared in simulations. Their numerical accuracy has been studied, principally *w.r.t.* the selection of an ordinary differential equations solver. Both models were initialised with conditions

corresponding to these of real-world long-range ballistic experiments. A numerical solution close to the exact one has been obtained for both models by applying a fixed-step numerical solver with a high order and high sampling frequency. Such a method is computationally expensive but allows to obtain accurate results. Afterwards, the much faster variable step solvers have been applied on the models. Their accuracy has been analyzed *w.r.t.* the fixed-step solver's solution, considered as a reference. It is shown that while it is possible to obtain a numerical solution for both representations, the quasi-LPV model in the non-rolling reference frame offers a solution with higher accuracy, better convergence properties, and shorter computation time.

The proposed quasi-LPV model of a projectile depends on a set of parameters—such as the initial state vector and the values of aerodynamic coefficients—that can be considered as uncertain. Their uncertainty stems from the realistic nature of the free-flight experiments, and will manifest itself in uncertain measurements. An assessment of this uncertainty—and different sources of it—can lead to better understanding of the quasi-LPV model. Of particular interest are the implications of the analysis of the output signals on identifiability of model parameters. As such, the next chapter will be dedicated to sensitivity analysis of the proposed model.

## Chapter 3

# Global sensitivity analysis of the quasi-LPV model

*The quasi-LPV model proposed in the previous chapter depends on a set of parameters that—due to the realistic application of free flight experimentation—can be considered as known only approximately. This uncertainty is especially critical in the case of the elements of initial state vector and the values of aerodynamic coefficients, as they have a direct influence on the trajectory of flight. An assessment of this uncertainty—and different sources of it—can lead a to better understanding of the quasi-LPV model of a projectile in-flight behaviour. This will in turn aid the future safety studies, aiming to evaluate the maximum dispersion of projectiles-in-flight at a given distance, necessary before free-flight experiments. A tool that can be used to address the aforementioned issue is the sensitivity analysis. Therefore, the current chapter presents the theory of sensitivity analysis and its application to the proposed quasi-LPV model. The obtained results allow to detect non-identifiability of some of the model parameters and have lead to two publications,[69] and [70].*

### 3.1 Introduction

Free-flight tests pose several technical and scientific difficulties. It must be assured that the projectile will land in a dedicated safe zone, even though some of the initial state variables are unknown. Similarly, it must be assured that the identified model structure will resemble the ones used for guidance and navigation tasks—principally in a quasi-LPV form—even though the physical model is nonlinear. Moreover, due to the fact that the experiments are performed in real-flight conditions, several sources of uncertainty are introduced to model parameters. For instance, initial state vector will differ from its nominal value due to stochastic effects induced by interior ballistics [15]. Similarly, an initial guess of the aerodynamic coefficients, based on similar architectures in the literature, will likely be imprecise. These uncertainties influence the model dynamics, and thus propagate through the model into its output signals.

The influence that the uncertain model parameters have on the model output can be evaluated by the means of sensitivity analysis [100]. Such a knowledge offers the possibility of assessing the influence of parameter uncertainties on the model behaviour [102, 50, 22]. When assessed,

the 'least' influential parameters can be set to a nominal value, since they do not significantly influence the model dynamics, whereas the identification and modelling efforts can be concentrated on the most influential parameters. The methods of sensitivity analysis can be divided into local and global techniques. The local methods evaluate the uncertain parameters' influence around nominal operating points [102], primarily using one-at-a-time sampling and differential analysis [41]. However, they fail to characterize the behaviour of the model far from the selected nominal condition, and—in the case of one-at-the-time sampling—explore only a limited area of the state-space [100]. The global methods aim to explore the full space of uncertain model parameters. There are several methods allowing to assess the global sensitivity of the model. Principally the variance-based analysis using so-called Sobol' indices (also called Analysis of Variance, ANOVA) [100, 117] is used to determine both the individual influence of each parameter and their interactions [100, 95].

In aerospace applications, sensitivity analysis is usually conducted using local sensitivity analysis, as in [129, 137, 147, 25, 74, 2]. Only a few works deal with global sensitivity analysis (GSA). Among them, the prominent applications include the works of Huan et al. [47] who used a surrogate modelling approach to identify the most influential parameters in scramjet combustor simulations. Wei et al. [139] used a modified Monte-Carlo approach to calculate sensitivity indices in order to minimize the variance of model output for a wing-structure model. Jiang et al. [51] have employed GSA in order to guide a design process of an aircraft by assessing which model parameters influence the most its final acquisition cost or maximum time of flight. It is worth noting that the results of a local sensitivity analysis can be misleading or even significantly different than of the global analysis. For example, Hale et al. [40] have shown that local sensitivity analysis might wrongly indicate some of the model parameters as influential; as well as it significantly underestimates the influence of aerodynamic coefficients, since their influence is nonlinear. However, only local sensitivity analysis has been applied in the existing studies of free-flight experiments in the domain of exterior ballistics.

In the context of the aforementioned experimental and practical difficulties associated with free-flight experiments, the following chapter is dedicated to performing GSA of the quasi-LPV model proposed in Chapter 2.

## 3.2 Theory of global sensitivity analysis

When a mathematical model is constructed in order to represent a physical system, it will consist of several parameters, representing various physical quantities. Inherently, these parameters can be known only approximately, either due to an estimation procedure based on noisy measurements, simulation, or even a guesstimate. The way these uncertainties influence the dynamics of the model cannot be directly assessed, but rather deduced based on observations of the model output [100]. Consequently, a question of how to apportion the output uncertainty to its various sources in the form of uncertain model parameters, raises to a high research pertinence.

Sensitivity analysis, over the years, have been developed independently within different domains, such as chemistry, operations research, risk and safety assessment, economics, etc [104, 10, 50, 101, 95, 102, 22]. It may be used to verify the model behaviour, simplify its equations, detect the most influential sources of output uncertainty, or even detect non-identifiability of some of the model parameters [100, 29]. Historically, the first attempts to apply GSA have

been dedicated to linear models. In their context, a possible insight into the importance of various factors, i.e. uncertain parameters, might be obtained using methods such as Pearson correlation coefficients, partial correlation coefficients, regression coefficients, or using derivation-based models [95]. These approaches are indicative only in case of linear models—or nonlinear models for which a number of assumptions can be imposed, such as their monotonicity [95].

Further developments have led to the division of sensitivity analysis methods into local and global approaches. The local methods assess the inputs' influence around nominal operating points [102], primarily using one-at-a-time sampling and differential analysis [41, 104]. However, they fail to characterize the model behaviour far from the selected nominal condition, and—in the case of one-at-the-time sampling—explore only a limited area of the state-space [100]. The global methods aim to explore the full space of model parameters, thus removing the restriction of analysis being valid only for the case of linear or approximately linear models. One of the main conclusions of Saltelli's review is that "both uncertainty and sensitivity analysis should be based on a global exploration of the space of input factors", especially due to the fact that "local/one-at-a-time methods do not adequately represent models with nonlinearities" [104].

In the 1990s, popularity of an idea of using variance-based global sensitivity measures arose. Iman and Hora used variance-based sensitivity measures to assess importance of uncertain parameters in the domain of risk analysis [49]. Independently, Sobol' formalised similar measures as sensitivity indices in the context of high dimension model representations [117]. Two years after Sobol, Wagner [136] proposed analysing global sensitivity of parameters by the use of statistical measures that in the contemporary research correspond to main and total sensitivity indices. These developments have allowed the variance-based methods to become the first that fully formalised GSA.

If the computational complexity of calculating the Sobol' sensitivity indices of all the parameters is prohibitively expensive, the screening methods can be used first: they allow to qualify (but not quantify) the relative importance of parameters [95]. An example of the screening method is the Morris algorithm [82], which uses randomized one-at-a-time sampling to detect inputs with high effects, while not calculating their exact sensitivity indices. Alternatively, scatter plots can be considered amongst the prominent methods of sensitivity analysis, but their utility is limited to cases with a low number of uncertain parameters and low amount of interactions between the parameters [56, 57]. Nonetheless, they can be considered as an initial screening step of sensitivity analysis.

A sensitivity analysis framework selection tree is presented in Figure 3.1. It shows the possible assumptions on the model structure (e.g. linear, monotonic, non-linear) and resulting best-adapted sensitivity analysis methods.

Taking into consideration that the knowledge-based model of a projectile in free flight is neither linear nor monotonic, the approach adapted to performing GSA in this case is the variance-based analysis—principally in the scope of Sobol' framework of Analysis of Variance (ANOVA). Therefore, it will be described in detail in the sequel.

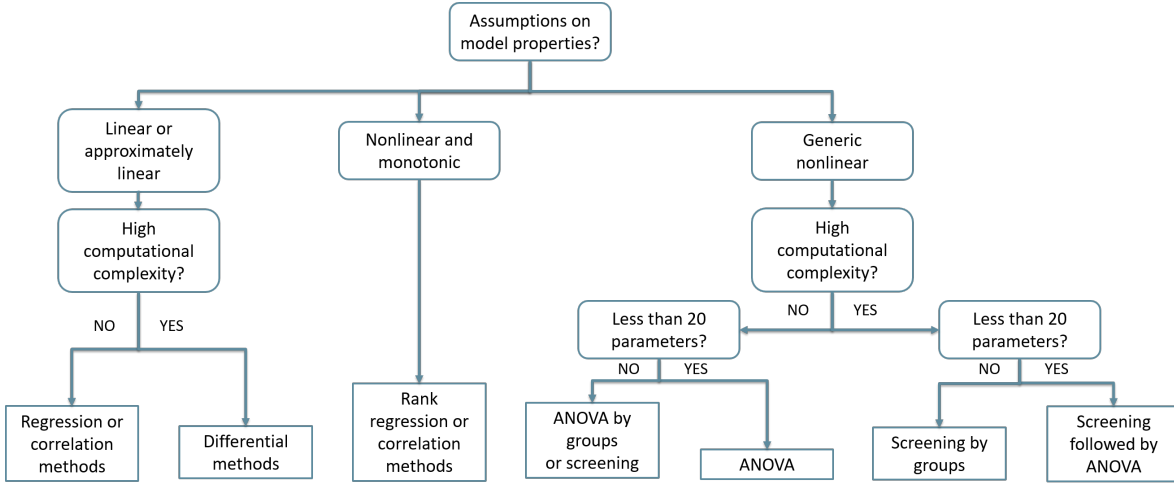


Figure 3.1: A framework selection tree for the sensitivity analysis. Reprinted from [95]

### 3.2.1 Analysis of Variance

Consider the output  $Y \in \mathbb{R}$  of the deterministic model described by a nonlinear function  $g$  of  $s$  parameters  $\Omega_i$ , where  $\boldsymbol{\Omega} \in [0, 1]^s$  and each parameter is itself dependent on *mutually independent* random event  $\chi$ , such that:

$$Y = g(\Omega_1(\chi), \Omega_2(\chi), \Omega_3(\chi), \dots, \Omega_s(\chi)). \quad (3.1)$$

The function  $g(\Omega_1(\chi), \Omega_2(\chi), \Omega_3(\chi), \dots, \Omega_s(\chi))$  can be described in Higher Dimension Model Representation (HDMR) as [117]:

$$g = g_0 + \sum_i g_i(\Omega_i(\chi)) + \sum_i \sum_{i < j} g_{ij}(\Omega_i(\chi), \Omega_j(\chi)) + \dots + g_{12\dots s}(\Omega_1(\chi), \Omega_2(\chi), \dots, \Omega_s(\chi)) \quad (3.2)$$

where:

$$g_0 = E(Y) \quad (3.3)$$

$$g_i = E(Y|\Omega_i(\chi)) - g_0 \quad (3.4)$$

$$g_{ij} = E(Y|\Omega_i(\chi), \Omega_j(\chi)) - g_i - g_j - g_0, \quad (3.5)$$

where  $E(Y)$  corresponds to the expected value of  $Y$  and  $E(Y|\Omega_i(\chi))$  is the conditional expectation of  $Y$  given  $\Omega_i(\chi)$ .

For the sake of simplicity, the  $(\chi)$  notation will be dropped hereinafter. Under a HDMR representation, the variance-based sensitivity indices (or Sobol' indices) can be defined as [117]:

$$S_i = \frac{V(E(Y|\Omega_i))}{V(Y)} \quad , \quad S_{ij} = \frac{V(E(Y|\Omega_i, \Omega_j))}{V(Y)} \quad , \dots \quad (3.6)$$

where  $V(Y)$  is the total variance of  $Y$  and  $V(E(Y|\Omega_i))$  is the conditional variance of  $Y$  given  $\Omega_i$ .

The  $S_i$ 's are called main indices, and indicate how much, on average, the output variance would be reduced if  $X_i$  has been fixed to a constant value. By definition, each  $S_i \in [0, 1]$ , where  $S_i$  close to 1 indicates that  $\Omega_i$  is an influential parameter. The sum of main sensitivity indices offers the following insight into the influence of uncertain parameters on the model:

- $\sum_i S_i = 1$  if the model is additive, indicating that the main sensitivity indices are sufficient to fully describe the model uncertainties.
- $\sum_i S_i < 1$  otherwise, indicating the influence of interactions between model parameters [76].

Main sensitivity indices do not offer full information about dependence of the output on model parameter. Plischke [90] shows an example of a system where main sensitivity index is equal to zero, even though the total influence is non-negligible, as visible even by a scatterplot analysis.

Calculation of higher-order sensitivity indices, e.g.  $S_{ij}$ , although informative, might be computationally expensive. In order to circumvent the problem, the so-called total sensitivity indices [46, 100] can be used:

$$S_{T_i} = \frac{E(V(Y|\Omega_{\sim i}))}{V(Y)} = 1 - \frac{V(E(Y|\Omega_{\sim i}))}{V(Y)}, \quad (3.7)$$

where notation  $\Omega_{\sim i}$  indicates all the elements of  $\Omega$  except for  $\Omega_i$ .

Similarly as in the case of the main sensitivity indices, the sum of all total indices:

- $\sum_i S_{T_i} = 1$  if the model is additive,
- $\sum_i S_{T_i} > 1$  otherwise.

Practically, the sensitivity analysis may proceed by calculating only the main sensitivity indices  $S_i$  and the total sensitivity indices  $S_{T_i}$  [50, 100]. The benefit of performing the variance-based analysis and calculation of Sobol' indices lies in determining both the individual influence of each parameter and their interactions even for the cases for which analytic solution would be difficult or impossible to find. However, a potentially high computational complexity is to be expected [100, 95]. Overall, all the important rules for interpreting the sensitivity indices, *w.r.t.* a selected output signal, are summarized in Table 3.1.

Table 3.1: Rules for interpreting the obtained sensitivity indices.

Observation	Interpretation	Reference
$S_i \approx 1$	The parameter $\Omega_i$ influences directly the output uncertainty.	[100]
$S_i \approx 0$	The parameter $\Omega_i$ does not influence directly the output uncertainty.	[100]
$\sum_i^s S_i \approx 1$	The model is additive, interactions are not present, <i>i.e.</i> $S_{T_i} = S_i$	[76]
$S_{T_i} \approx 1$	The parameter $x_i$ influences (directly or via interactions) the output uncertainty.	[100]
$S_{T_i} \approx 0$	The parameter $x_i$ does not influence the output uncertainty and is non-identifiable.	[100, 29]

Application of HDMR transformation and subsequent calculation of the sensitivity indices, as in (3.6) and (3.7), can be performed analytically. However, it is a problem of increasing complexity that in practice can be applied mostly to simple linear models with few uncertain parameters.

Analysis of complex, nonlinear models is conducted using numerical estimation of the sensitivity indices, typically via Monte Carlo simulations [100].

Alternatively, variance-based GSA can be performed using so-called Fourier Amplitude Sensitivity Test (FAST) or using a meta-modelling approach.

Historically, FAST has been the first method of GSA [100]. The method assigns a test frequency to each unknown input that allows to detect their influence on the model by the means of Fourier decomposition of the output signal [24, 106, 23]. The method is suited to analysis of multiparameter systems, however suffered from a significant limitation: being unable to assess higher-order sensitivity indices [22]. Consequently, its applicability to nonlinear models has been limited. In 1990s, evaluation of higher-order terms has been made possible, (e.g. in [99]) and several methods have been developed for computing the variance-based sensitivity indices in more computationally efficient way, such as the Fourier amplitude sensitivity test [146, 126]. Nonetheless, it remains more complex than in the case of standard Sobol' method [46]. Therefore, it will not be analysed in this thesis.

The metamodelling approach is based on the premise of approximating the model of interest using a set of so-called surrogate (meta-) models, selected in such a way that calculating sensitivity indices would be less computationally expensive than in the case of the original model [93, 9, 121]. A prime example of a surrogate approach is the method of chaos polynomials. It assumes that the model's output signal can be approximated using a family of orthogonal polynomials [9]. The benefit of the method comes from an increased rate of convergence of the sensitivity indices estimators, as compared to the Monte Carlo based estimation [9]. The orthogonality of chaos polynomials can be assured by selecting an appropriate type of polynomials. For instance, Hermite polynomials are orthogonal for parameters that have a normal distribution, and Legendre polynomials are orthogonal if parameters have a uniform distribution [9, 107]. The metamodelling approach, although practical when the computational complexity of the model needs to be reduced, suffers from some limitations. For example, the selection of the order of chaos polynomials used for approximation can pose problems. If the order is too low, it will result in inaccurate sensitivity measures. If the order is too high, it will result in increased computational complexity of the method.

In the present work, the method of Monte Carlo will be used, principally due to its simplicity in implementation, and due to already low computational complexity of the quasi-LPV model developed in a non-rolling reference frame.

### 3.2.2 Monte Carlo (Sobol'-Saltelli) estimators

The sensitivity indices of the HDMR representation proposed by Sobol' [117] require estimating the conditional variances and averages of the parameter's influence on the output. A computationally-efficient method of their estimation has been proposed by Saltelli [98]. Herein, two experiments are performed in order to create sampling matrices **A** and **B**, each containing

$N$  samples of  $s$  parameters:

$$\mathbf{A} = \begin{bmatrix} \Omega_1^{(1)} & \Omega_2^{(1)} & \cdots & \Omega_i^{(1)} & \cdots & \Omega_s^{(1)} \\ \Omega_1^{(2)} & \Omega_2^{(2)} & \cdots & \Omega_i^{(2)} & \cdots & \Omega_s^{(2)} \\ \vdots & \vdots & \vdots & \vdots & \vdots & \vdots \\ \Omega_1^{(N-1)} & \Omega_2^{(N-1)} & \cdots & \Omega_i^{(N-1)} & \cdots & \Omega_s^{(N-1)} \\ \Omega_1^{(N)} & \Omega_2^{(N)} & \cdots & \Omega_i^{(N)} & \cdots & \Omega_s^{(N)} \end{bmatrix} \quad (3.8)$$

and

$$\mathbf{B} = \begin{bmatrix} \Omega_{s+1}^{(1)} & \Omega_{s+2}^{(1)} & \cdots & \Omega_{s+i}^{(1)} & \cdots & \Omega_{2s}^{(1)} \\ \Omega_{s+1}^{(2)} & \Omega_{s+2}^{(2)} & \cdots & \Omega_{s+i}^{(2)} & \cdots & \Omega_{2s}^{(2)} \\ \vdots & \vdots & \vdots & \vdots & \vdots & \vdots \\ \Omega_{s+1}^{(N-1)} & \Omega_{s+2}^{(N-1)} & \cdots & \Omega_{s+i}^{(N-1)} & \cdots & \Omega_{2s}^{(N-1)} \\ \Omega_{s+1}^{(N)} & \Omega_{s+2}^{(N)} & \cdots & \Omega_{s+i}^{(N)} & \cdots & \Omega_{2s}^{(N)} \end{bmatrix}, \quad (3.9)$$

where  $\Omega_i^{(j)}$  denotes the  $j$ -th value of  $i$ -th parameter within an  $N$  elements long sample.

Based on them, matrices  $\mathbf{C}_i$  are created, each containing all columns of matrix  $\mathbf{B}$ , except for the  $i$ th column, which is taken from matrix  $\mathbf{A}$ , such that:

$$\mathbf{C}_i = \begin{bmatrix} \Omega_{s+1}^{(1)} & \Omega_{s+2}^{(1)} & \cdots & \Omega_i^{(1)} & \cdots & \Omega_{2s}^{(1)} \\ \Omega_{s+1}^{(2)} & \Omega_{s+2}^{(2)} & \cdots & \Omega_i^{(2)} & \cdots & \Omega_{2s}^{(2)} \\ \vdots & \vdots & \vdots & \vdots & \vdots & \vdots \\ \Omega_{s+1}^{(N-1)} & \Omega_{s+2}^{(N-1)} & \cdots & \Omega_i^{(N-1)} & \cdots & \Omega_{2s}^{(N-1)} \\ \Omega_{s+1}^{(N)} & \Omega_{s+2}^{(N)} & \cdots & \Omega_i^{(N)} & \cdots & \Omega_{2s}^{(N)} \end{bmatrix} \quad (3.10)$$

In other words, each matrix  $\mathbf{C}_i$  contains a fixed sample of parameter  $\Omega_i$ , whereas all the other parameters are allowed to vary.

Afterwards, the main and total sensitivity indices can be calculated as:

$$S_i = \frac{V(E(Y|\Omega_i))}{V(Y)} = \frac{E(g(\mathbf{A}) \cdot g(\mathbf{C}_i)) - g_0^2}{E(g(\mathbf{A}) \cdot g(\mathbf{A})) - g_0^2} \quad (3.11)$$

and

$$S_{T_i} = 1 - \frac{V(E(Y|\Omega_{\sim i}))}{V(Y)} = 1 - \frac{E(g(\mathbf{B}) \cdot g(\mathbf{C}_i)) - g_0^2}{E(g(\mathbf{A}) \cdot g(\mathbf{A})) - g_0^2}. \quad (3.12)$$

The Monte Carlo simulations method has been over time improved with various techniques to reduce its computational complexity [75, 103, 50]. An example of it is the permutation-based approach proposed by Mara [75]. This approach consists of three steps:

1. A first model response vector  $Y^1 = g(\Omega^1)$  is generated—where the superscript denotes the number of the sample—based on the measurements function  $g$  of the first Sobol' sample  $\Omega^1$ . The sample matrix has a size  $N \times s$ , where  $N$  is the amount of Monte-Carlo samples, and  $s$  is the number of uncertain model parameters.

2. A second sample matrix  $\Omega^2$  is generated based on column-wise permutation of  $\Omega^1$  matrix: each  $i$ -th column (out of  $d$  columns in total) is permuted by a permutation vector  $r_i$ . Hence, noting the permutation matrix as  $R = [r_1, r_2, \dots, r_s]$ , the second sample matrix is obtained as  $\Omega^2 = \Omega^1 \circ R$ . The second model response vector is calculated as  $Y^2 = g(\Omega^2)$ .
3. Main sensitivity indices are calculated for each of  $j$  output signal *w.r.t.* each of  $s$  uncertain parameters, as:

$$\hat{S}_i^j = \frac{(N-1)^{-1} \sum_{k=1}^N (y_{kj}^{r_i} - \hat{\mu}_1^j)(y_{kj}^2 - \hat{\mu}_2^j)}{\hat{\sigma}_1^j \hat{\sigma}_2^j}, \quad (3.13)$$

where  $y_{kj}^{r_i}$  is  $k$ -th element of the  $j$ -th output signal obtained through reordering the  $y_{kj}^1$  according to a column-wise permutation  $r_i$ .

Additionally, the methods of obtaining the sample have to be discussed. In early works, random Monte Carlo sequences have been used; Sobol' indicates that the estimation of sensitivity indices will converge with  $N \rightarrow \infty$  [117]. However, as indicated by Saltelli, the convergence rate can be increased by pseudo Monte Carlo sampling—using low discrepancy samples such as Latin hypercubes or Sobol' sequences—which allows to additionally reduce the computational complexity of the method [100].

### 3.3 Application to the quasi-LPV model of a projectile

Sensitivity analysis answers the question of how can the uncertainty of the model output be apportioned to different sources of uncertainty in the model input [100]. Such a knowledge offers the possibility of assessing the influence of parameter uncertainties on the model behaviour, which can be applied for several purposes [102, 50, 22], two of which are of interest for the present thesis:

- Test the understanding of the model, *e.g.* by testing the coherency between the results and the *a priori* knowledge in the field, in order to confirm the physical behaviour of the simulated model.
- Provide insight into identifiability of the model's parameters, *i.e.* taking advantage of the knowledge that non-influential parameters are also non-identifiable [29]. Therefore, GSA might be used to answer the question if the uncertainty in sensor signals can be apportioned to any of the uncertain parameters - if not, they would be deemed non-identifiable.

In the context of GSA, the general model structure from equation (2.1) has to be extended to allow for stochastic variables to be present in the model. Therefore, we will consider a modified structure  $\mathcal{M}$ , such that:

$$\mathcal{M}_{GSA} : \begin{cases} \dot{\mathbf{x}}(t, \chi) = f(\mathbf{x}(t, \chi), \mathbf{C}(\mathbf{x}(t, \chi), \mathbf{p}_a(\chi))), & \mathbf{x}(0, \chi) = \mathbf{x}_0 \\ \mathbf{y}(t, \chi) = g(\mathbf{x}(t, \chi)), \end{cases} \quad (3.14)$$

where  $\mathbf{y}(t) = [A_x, A_y, A_z, G_y, G_z, H_x, H_y, H_z]^T$  (see 1.19)-(1.22)). The model (3.14) depends on the initial state vector  $\mathbf{x}(0, \chi)$  and on the vector of parameters of aerodynamic coefficients  $\mathbf{p}_a(\chi)$ . These two vectors contain elements that are uncertain and can be considered as random variables. A vector of their uncertain elements is denoted as  $\boldsymbol{\Omega} \in \mathbb{R}^s$ ,  $\boldsymbol{\Omega} = [\Omega_1(\chi), \Omega_2(\chi), \dots, \Omega_s(\chi)]$ , where  $\Omega_1(\chi) \in \mathbb{R}$  and  $\chi$  is an elementary random event. In the sequel, GSA will be applied to the

quasi-LPV model proposed in Chapter 2, hence the function  $f$  corresponds to the matrix  $A$  from equation (2.51).

### 3.3.1 Sources of model uncertainty

When a given model structure is simulated, its trajectory depends on the initial state vector  $\mathbf{x}_0$ ; and on the set of model parameters, such as its aerodynamic coefficient parameters  $\mathbf{p}_a$ , mass, and inertia. In the following subsections, the set of nominal values of the initial state vector and the model parameters will be discussed, together with the possible sources of uncertainty influencing them.

#### Uncertainties of initial state variables

State variables in the model are divided into those describing translational dynamics, attitude dynamics, translational kinematics, and attitude kinematics. Specifics of each influence the model uncertainty in a different way:

- *Translational dynamics.* In the case of free-flight experiments, as carried out at the ISL's open-range test site, the flights are usually performed over a range of flight conditions (e.g. sub-, trans-, and super-sonic regimes) in order to sufficiently explore the projectile flight dynamics [1]. Herein, a selection of four different initial velocities  $u_0$ , ranging from 300 to 600  $\text{m s}^{-1}$  has been chosen as the set of nominal values. Since the projectiles are launched from a rifled-bore powder gun, and each firing varies slightly depending on inaccuracies in powder amount as well as due to internal ballistic effects (such as differences in firing temperature, pressure distribution in-bore, etc) [15], an uncertainty range of  $\pm 1\%$  is assumed. The stochastic effects of internal ballistics on the remaining linear velocities are negligible, therefore  $v_0, w_0$  can be assumed to be zero, without any interval of uncertainty imposed upon them.
- *Attitude dynamics.* In the case of the initial angular rates, the effects of internal ballistics are non-negligible. First of all, the initial roll rate  $p_0$  is a function of initial axial velocity  $u_0$  and the twist rate of the launcher's bore [15]. Herein,  $p_0 = 2.0283 \cdot u_0$  has been assumed, which renders  $p_0$  a linear transformation of  $u_0$ . Since  $u_0$  is already considered as an uncertain parameter, there is no need to assume  $p_0$  as uncertain, since all its uncertainty is already expressed by  $u_0$ . For the initial yaw and pitch rates, the nominal value is  $q_0 = r_0 = 0 \text{ rad s}^{-1}$ . However, their nominal value can be significantly influenced by the stochastic uncertainties stemming from the internal ballistics [15], hence an interval of uncertainty of  $\pm 3 \text{ rad s}^{-1}$  has been assumed on  $q_0$  and  $r_0$ .
- *Translational kinematics.* The initial position of a projectile is equivalent to the position of the launcher. In this case study, it corresponds to  $x_{E_0} = y_{E_0} = 0 \text{ m}$  with the initial altitude of  $z_{E_0} = -1.5 \text{ m}$ , corresponding to the launcher height. Finally, concerning the initial attitude of the projectile, it is dependent on the target location, as the launcher aims to deliver the projectile to its terminal destination, which in this case study corresponds to the centre of a sandbay, located at [1000, 0, -6] m. The negative value of the altitude stems from the definition of the Earth reference frame: positive altitude axis aims towards the center of Earth.

- *Attitude kinematics.* In order to find the initial pitch  $\theta_0$  and yaw  $\psi_0$  angles allowing to hit the target, a least squares estimation has been performed, using a set of fixed nominal values of the remaining state variables, *i.e.* only  $\theta_0, \psi_0$  were estimated. The resulting values have been selected as the nominal values for GSA. An uncertainty interval of  $\pm 0.00049$  rad has been assumed on  $\theta_0$  and  $\psi_0$ . The initial roll angle  $\phi_0$  can be fixed to zero, as it does not influence the trajectory.

All the nominal values of state variables are summarized in Table 3.2, together with their imposed uncertainty intervals. There are four cases in which the model has been investigated, determined by the four initial velocities of the projectile.

Table 3.2: Uncertain initial state variables

State	Nominal value				Uncertainty	Unit
	Scenario A	Scenario B	Scenario C	Scenario D		
$u_0$	300	400	500	600	$\pm 1\%$	$\text{m s}^{-1}$
$q_0$	0	0	0	0	$\pm 3$	$\text{rad s}^{-1}$
$r_0$	0	0	0	0	$\pm 3$	$\text{rad s}^{-1}$
$\theta_0$	0.0602	0.0370	0.0251	0.0188	$\pm 0.00049$	rad
$\psi_0$	-0.0009	-0.0008	-0.0006	-0.0005	$\pm 0.00049$	rad

### Uncertainties of model parameters

Firstly, the axial force coefficient  $C_X$  and normal force coefficient  $C_{N_\alpha}$  have been chosen as the objects of interest for GSA, due to their direct physical links to lift and drag forces acting on a projectile in flight [15]. As a consequence of this physical relationship, it is predicted that their influence on sensitivity of the model might be significant. The nominal values of all aerodynamic coefficients are known in a tabular form, for which an initial guess is based on previous free-flight experiments, results from the literature, semi-empirical codes, CFD simulations, etc. Each of the methods offers a different way to quantify the aerodynamic characteristics of a projectile, hence it can also be considered as a source of uncertainty over the initial guess of the values of the aerodynamic coefficients. Herein, an additional 5% of uncertainty is imposed. Secondly, as a test variable, an uncertainty of the projectile's mass  $m$  is imposed: the choice of mass as a parameter of interest is on one hand realistic, since some mass uncertainty is to be expected [15]; and on the other hand, mass uncertainty has only a small influence on the trajectory over a short-range firing. Therefore, it can be considered as an example of parameter which would be hard to identify using embedded sensors.

All the uncertainty intervals of the uncertain model parameters are summarized in Table 3.3. A uniform distribution is assumed on all the parameters.

Table 3.3: Uncertain projectile parameters

Parameter	Nominal value	Uncertainty	Unit
$m$	45	$\pm 0.25\%$	kg
$C_X$	tabular	$\pm 5\%$	—
$C_{N_\alpha}$	tabular	$\pm 5\%$	—

### 3.3.2 Setting up the sensitivity analysis

In the thesis, the Monte Carlo permutation-based method presented in 3.2.2 is used due to its simplicity, as it allows a direct computation of sensitivity indices. The authors take advantage of the non-rolling frame transformation in order to reduce the simulation time of each model run.

For the purpose of upcoming GSA, eight parameters from Tables 3.2 and 3.3 are considered as uncertain:  $\Omega = [u_0, q_0, r_0, \theta_0, \psi_0, m, C_X, C_{N_\alpha}]^T$ . Such a setting of uncertain parameters allows to evaluate their influence on the system dynamics, which in turn influences the accelerometer, gyroscope, and magnetometer measurements, as portrayed in Figure 3.2. Therefore, GSA can be used to answer which parameters, and to what extent, do influence the measurement sensor equations. Axial gyroscope  $G_x$  which directly measures  $p_0$  will not be considered in the analysis, as it can be predicted that it would be only sensitive to  $u_0$ . Moreover, the number of uncertain

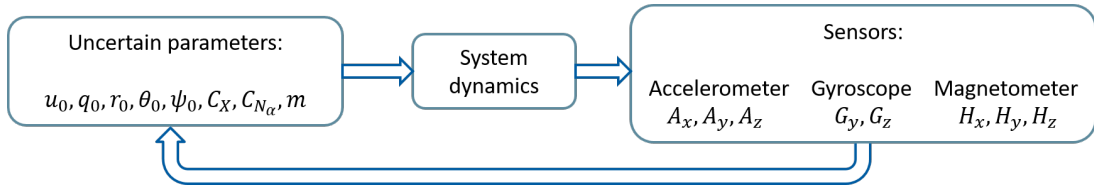


Figure 3.2: Diagram of the global sensitivity analysis.

parameters is equal to  $s = 8$ , whereas each simulation of a single trajectory of the quasi-LPV model lasts approximately three seconds [73]. Such a case further supports the selection of a variance-based methods as the basis of the global sensitivity assessment: for the cases when the number of parameters is lower than 20, and the CPU time per one run is lower than one minute, the choice of variance-based methods is suggested as a rule-of-a-thumb by De Rocquigny [95], as well as by Saltelli et al. [102].

### 3.3.3 Simulation results

Simulations for the purpose of GSA using Mara’s method have been performed based on the set of nominal conditions and their uncertainty intervals as summarized in Tables 3.2 and 3.3. The analysis has been performed in a time-varying approach—as information on sensitivity could be hidden at some periods of time, while being readily visible in the others [89]. The value of sensitivity indices is calculated every 2 ms, which is faster than the quasi-LPV model dynamics. Thus, an accurate representation of the time-varying behaviour of the model is possible.

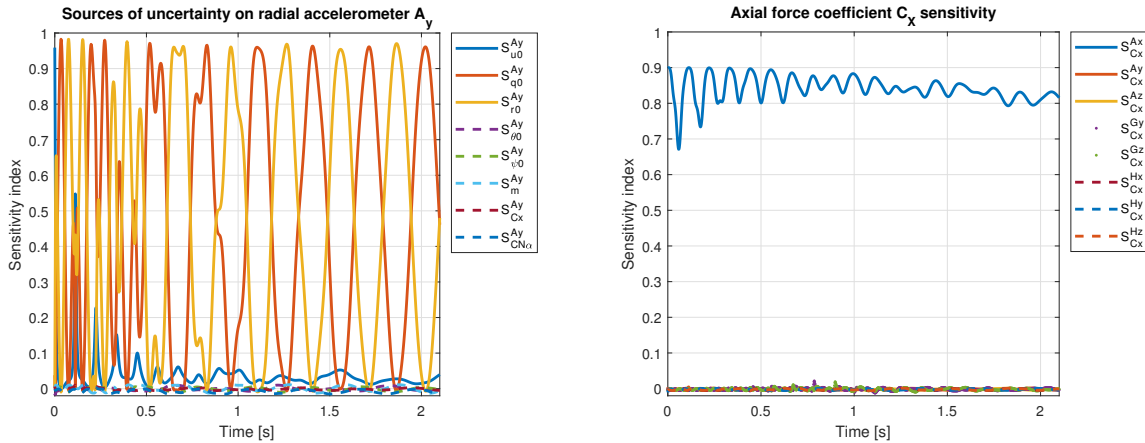
The procedure of obtaining the results that is used in the present analysis can be summarized as follows:

- Perform a sampling of the uncertain parameter space, using the uncertainty ranges as dictated by Tables 3.2 and 3.3, while assuming that the samples are uniformly distributed. The sampling size, for which convergent results have been obtained, equals to two samples  $\Omega^1$  and  $\Omega^2$ , each of the same size, with the total sample size of  $N = 40000$ .
- Simulate the model trajectory—i.e. the values of the time-varying output signals (1.19)-(1.22)—for each of the  $N$  samples over the distance of 1 km corresponding to the distance between the projectile launcher and the sandbay.

- Calculate the sensitivity indices  $S_i$ ,  $i = 1, 2, \dots, s$ , based on equation (3.13) for every time instant.

### Results interpretation for the full parameter vector

All the main sensitivity indices, calculated using Mara’s method, have been plotted for each time instant (see Figures 3.3 and 3.4). The figures show the evolution of sensitivity indices over the time of flight for the Scenario C. Therefore, results close to 1 indicate influential parameters, and these close to 0 indicate non-influential ones.



(a) Sensitivity indices of each uncertain parameter *w.r.t.*  $A_y$ . Influence of translational and angular velocities dominates over all the other parameters.

(b) Main sensitivity indices of the output sensors *w.r.t.*  $C_X$ . The influence of model uncertainties on sensors other than the axial accelerometer  $A_x$  is visibly low.

Figure 3.3: Exemplary results: an illustration of the domination of angular and translational velocities over all the other uncertain parameters.

Firstly, the initial translational and angular velocities are dominating the uncertainty of the output signals—with the influence of  $q_0$  and  $r_0$  oscillating due to projectile rotations—as shown in Fig. 3.3 (a) for the example of the radial accelerometer  $A_y$ . This result, although in-line with physical expectations, obscures the influence of other parameters on the output signals. That is especially visible for the case of the aerodynamic coefficients. For instance, as shown in Fig. 3.3 (b), it appears as if uncertainty around the nominal value of  $C_X$  does not visibly influence the measurement signals other than the axial accelerometer  $A_x$ . Such an effect would be worrying, as it could indicate non-identifiability of the aerodynamic coefficients by most of the sensors. However, this effect stems from the exponentially higher influence of initial velocities compared to other factors, rather than from the suspected lack of influence of the aerodynamic coefficients. Since  $u_0, q_0, r_0$  almost totally dominate, only a little effect is visible from the other parameters. Sensitivity indices are relative to each other, and hence neither can they be directly compared between outputs, nor will a clear influence of the uncertain parameter be visible if one of them logarithmically dominates. The uncertain translational and angular velocities influence the sensors uncertainty to such an extent, that the desired effects of Euler angles and aerodynamic coefficients uncertainty is invisible.

Another explanation would be to conclude that the influence of uncertain parameters is expressed

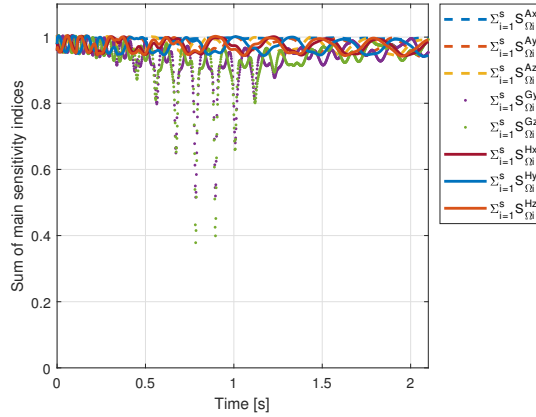


Figure 3.4: Sum of main sensitivity indices for each output signal. The results suggest the additive nature of the model.

through their interactions, and thus the total sensitivity indices would have to be calculated. However, such an assumption can be easily disproved, since  $\sum_{i=1}^s S_i^j > 0.9$  for almost all of the outputs  $j$  for the whole duration of the flight, which in accordance with Table 3.1 implies that the model is approximately additive (Fig. 3.4). Thus, the main indices  $S_i^j$  are equal to the total sensitivity indices  $S_{T_i}^j$ .

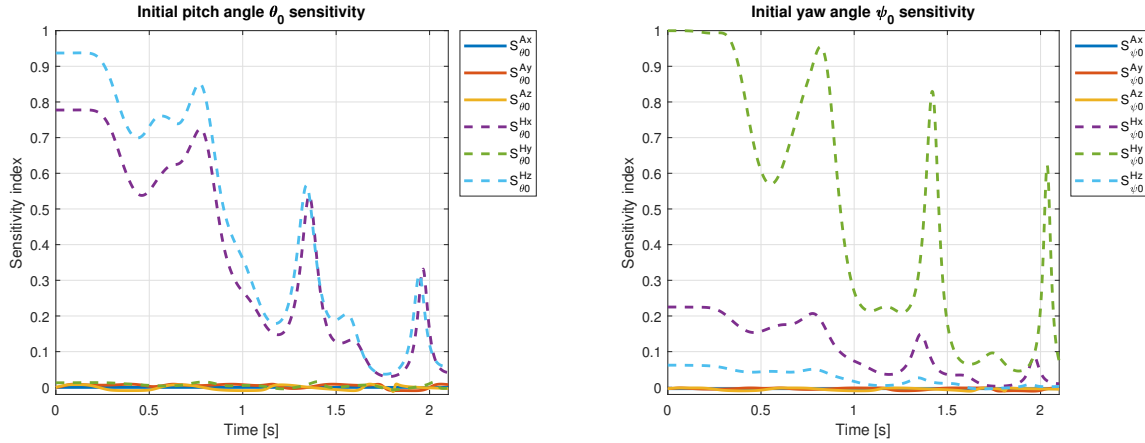
In order to be able to assess the influence of the uncertainty of the aerodynamic coefficients, as well as of the other less influential model parameters, it has been decided to repeat the analysis for a modified set of uncertain parameters, as explained below.

### Results interpretation for the reduced parameter vector

In the sequel, a modified set of parameters is examined. This time, the initial velocities are considered only at their nominal values, hence  $\Omega = [\theta_0, \psi_0, m, C_X, C_{N_\alpha}]^T$ , ( $s = 5$ ).

The results observed in such a setting—and shown again for Scenario C—as portrayed in Fig. 3.5 to 3.7 are more promising, as it is now visible that they confirm the predictions of the domain knowledge of ballistics and aerodynamics:

- The initial Euler angles  $\theta_0$  and  $\psi_0$  influence only the magnetometer measurements ( $H_x, H_z$  and  $H_y, H_z$  respectively, due to the angles acting in  $xz$  and  $yz$  planes), and their influence quickly diminishes over the time of flight. It is visible in Fig. 3.5 (a) and (b), on the example of magnetometer sensitivities (dotted line) and accelerometer sensitivities (solid lines): influence of Euler angles uncertainty on accelerometers is close to zero, suggesting their non-identifiability. In contrast, uncertainty of Euler angles explains most of magnetometers uncertainty initially, but the influence decreases to almost zero over just two seconds of flight.
- The effect of the uncertainty on axial force coefficient  $C_X$  is visible especially on  $A_x$  measurements: in Fig. 3.6 (a), its sensitivity (solid blue line) remains close to one during the whole flight. Moreover, radial accelerometers  $A_y, A_z$  (solid red and yellow lines) are influenced by  $C_X$  in the time instances, when they are not already strongly influenced by  $C_{N_\alpha}$ .



(a) The uncertainty of  $\theta_0$  influences only the magnetometer measurements  $H_x, H_z$ , especially in the beginning. Any attempt to identify it using accelerometers would be futile.

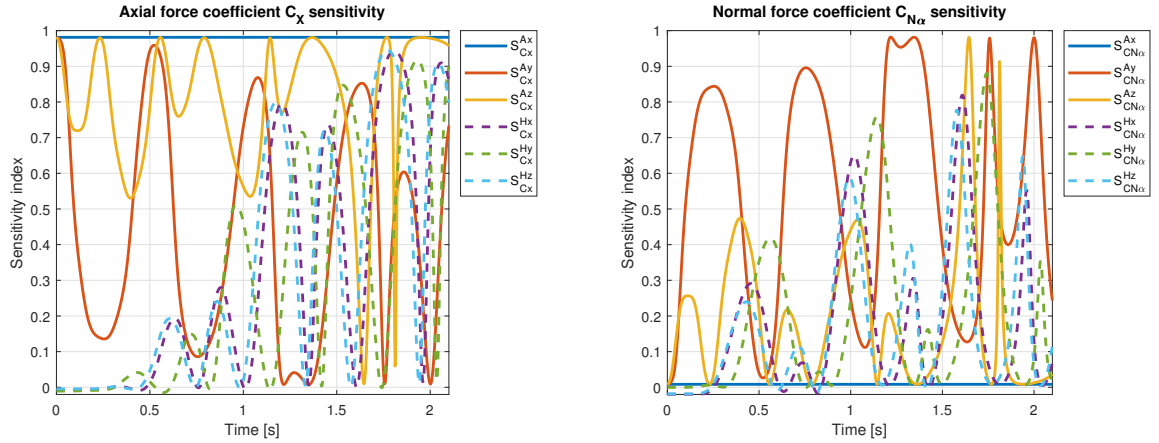
(b) The uncertainty of  $\phi_0$  influences the magnetometer measurements  $H_x, H_y$ , especially in the beginning. Any attempt to identify it using accelerometers would be futile.

Figure 3.5: Sensitivity indices *w.r.t.* the initial Euler angles.

Finally, by comparing Fig. 3.5 (b) and Fig. 3.6 (a), it can be concluded that the influence of Euler angles on magnetometers  $H_x, H_y, H_z$  is visible in the time instances when it is not dominated by  $C_X$  (dotted lines at both Figures).

- The effect of normal force coefficient  $C_{N\alpha}$  uncertainty is visible in the radial accelerometer measurements, but not in the axial one. It can be seen in Fig. 3.6 (b) that the axial accelerometer sensitivity  $S_{C_{N\alpha}}^{A_x}$  (solid blue line) remains close to zero. Such a result also suggests its non-identifiability when only axial accelerometer  $A_x$  data would be used. Radial accelerometer sensitivities  $S_{C_{N\alpha}}^{A_y}, S_{C_{N\alpha}}^{A_z}$  (red and yellow solid lines) significantly better explain  $C_{N\alpha}$  uncertainty.
- The mass influence on sensor measurements is negligible. This effect is visible in Fig. 3.7 (a), since all sensitivities remain close to zero. Such a result also suggests that mass would be effectively impossible to identify using only the embedded sensors. It additionally underlines the importance of precisely measuring the mass of the projectile before firing, as it would not be possible to identify it using the in-flight measurements.

The observed effects are especially interesting in the context of identification of unknown parameters. Knowing that non-influential parameters are non-identifiable [29], one can easily confirm that some of the model parameters might be identifiable using only some of the sensors, and only in some periods of time. For example, any attempt to identify initial Euler angles  $\theta_0$  and  $\psi_0$  using magnetometer measurements  $H_x, H_y, H_z$  after a few seconds of flight would be futile. Afterwards, the initial Euler angles—and all the other elements of  $\mathbf{x}_0$ —are overshadowed by the increasing influence of aerodynamic coefficients. Moreover, the conformity of the results with the domain knowledge combined with the previously described numerical accuracy of the quasi-LPV model [73], suggests that the quasi-LPV model has been correctly developed, and effectively preserves the real behaviour of a projectile. It can also be concluded that the model with reduced uncertain parameter vector becomes more additive, as can be seen in Fig. 3.7 (b) in comparison with Fig. 3.4. It is worth noting that the correctness of the obtained sensitivity indices evolution



(a)  $C_X$  influences especially the axial accelerometer  $A_x$ , as well as the radial measurements  $A_y, A_z$  in the instances of time when they are not influenced by  $C_{N\alpha}$ .

(b)  $C_{N\alpha}$  influences especially the radial accelerometer  $A_y, A_z$ , with an increasing over time influence on the magnetometers  $H_x, H_y, H_z$ .

Figure 3.6: Sensitivity indices *w.r.t.* the aerodynamic coefficients.

can be additionally tested by calculating the sensitivity indices for denser time-grids. For the studied model, results remain equivalent to those obtained for a lower density of time instances.

Overall tendencies of the sensitivity indices as obtained for all four scenarios have been summarised in Tables 3.4 and 3.5.

Table 3.4: Sensitivity of uncertain state variables.

	$A_x$	$A_y$	$A_z$	$H_x$	$H_y$	$H_z$	$G_y$	$G_z$
$\theta_0$	ni	ni	ni	ds	ni	ds	ni	ni
$\psi_0$	ni	ni	ni	ds	ds	ni	ni	ni
$m$	ni							

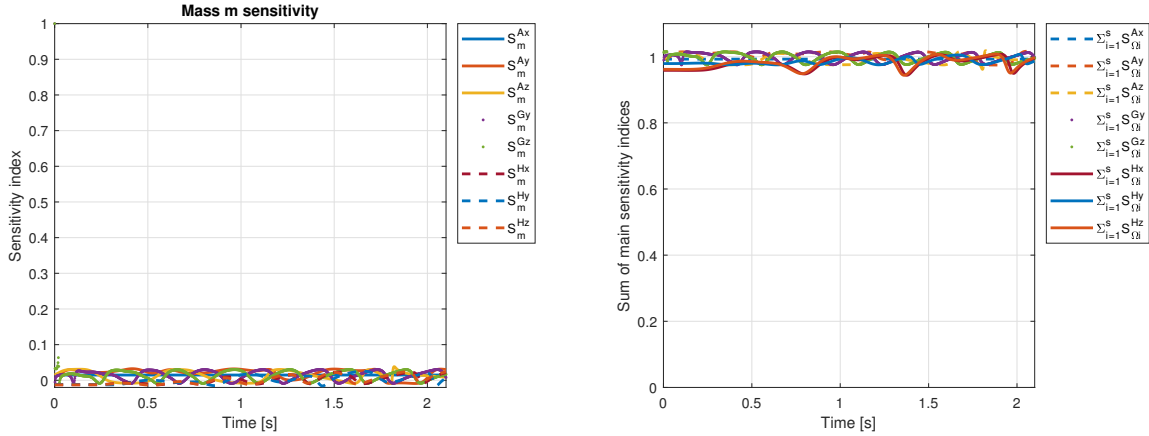
Legend: ni - parameter non-influential and non-identifiable, ds - sensitivity decreasing over time.

### Comparison to the standard Sobol' method from the literature

In order to assure the correctness of the obtained sensitivity indices evolution, two additional experiments were conducted.

The first one aimed to perform the analysis with two-times lower density of time instances at which the results are calculated. That way, it could be assessed if the results have converged *w.r.t.* time. Results are shown in Fig. 3.8 for the example of a radial gyroscope  $G_y$  on the initial yaw rate  $q_0$  for two sampling frequencies: normal corresponding to 2 ms, and sparse corresponding to every 4 ms. It can be seen that the twice as slow sampling does not significantly change the shape of the sensitivity index over time. Therefore, it can be concluded that the estimate of sensitivity indices has converged and does no longer depend on further increases on time sampling.

The second experiment aimed to assess if the results are coherent *w.r.t.* the classical method of



(a) Main sensitivity indices of the output sensors *w.r.t.*  $m$ . Mass uncertainty influences the sensors only slightly. An attempt to identify it using in-flight measurements would be difficult.

(b) Sum of main sensitivity indices. Results are approximately equal to one, indicating additive nature of the model.

Figure 3.7: Exemplary results: an illustration of the additive nature of the model and non-identifiability of the mass.

Table 3.5: Sensitivity of uncertain model parameters.

	$C_X$	$C_{N_\alpha}$
$A_x$	dominant	non-identifiable
$A_y$	sinusoidal decrease	sinusoidal increase
$A_z$	dominates, oscillatory	sinusoidal increase
$H_x$	average, oscillatory	sinusoidal increase
$H_y$	average, oscillatory	sinusoidal increase
$H_z$	average, oscillatory	sinusoidal increase
$G_y$	dominates, oscillatory	dominates, oscillatory
$G_z$	dominates, oscillatory	dominates, oscillatory

Sobol [117]. For that, the implementation available in SAFE toolbox for Matlab software [88] has been applied. The comparative analysis using SAFE toolbox has been performed on the same test case as for the Mara’s method, however with twice as many samples, *i.e.*  $N = 80000$ . As can be seen in Fig 3.9 (a), the standard approach allows to obtain the same shape of the evolution of sensitivity of  $G_y$  over time as the Mara’s method. However, due to lower convergence rate, it fails to accurately represent some of the parameters’ sensitivities, even though twice as many samples were applied. The latter is visible in Fig. 3.9(b) for the example of projectile’s mass—that is known to have negligible influence—which has Sobol’ main indices oscillating between 0.1 and 0.3, whereas the total indices reach the theoretically impossible negative values. In the same time, the proposed Mara’s method allows to calculate the mass influence which is approximately zero, as predicted based on the theoretical knowledge.

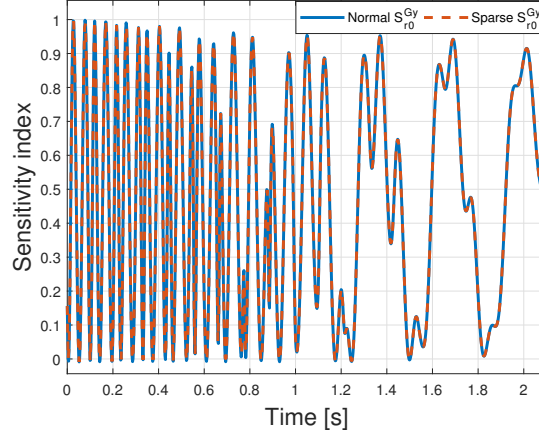


Figure 3.8: Sensitivity of  $G_y$  to  $r_0$  for normal and sparse sampling. The results suggest the selected sampling time is sufficiently high for the sensitivity estimation to converge.

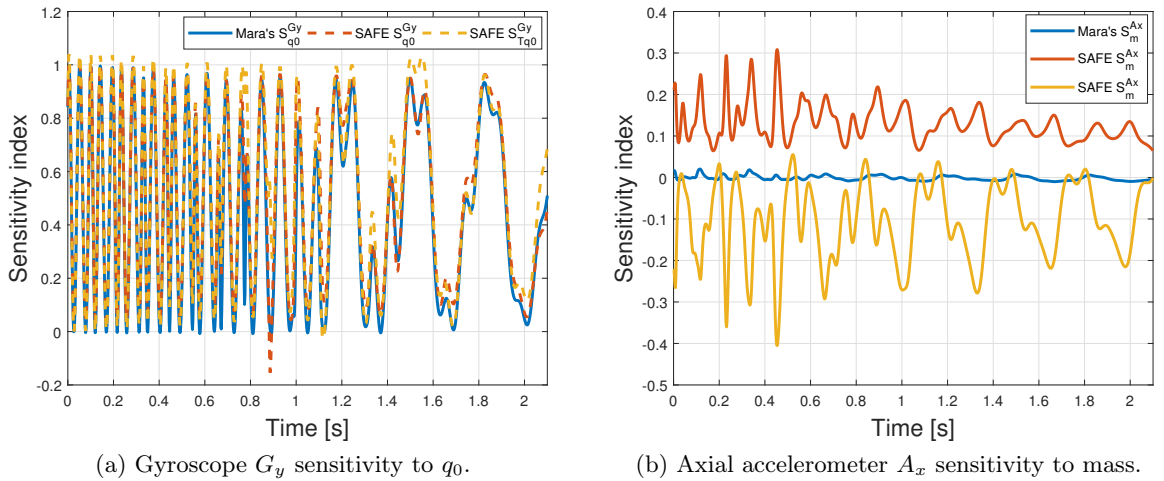


Figure 3.9: Comparison of sensitivity indices of Mara and standard Sobol methods. Sobol' method fails to detect the real influence of mass, that is close to zero; but allows to detect similar evolution of time-changing parameter influence, such as of the angular velocity.

### 3.4 Conclusions

This chapter deals with the application of global sensitivity analysis (GSA) methods to the case of free-flight projectile behaviour and interpretation of the results impact on the non-identifiability of model parameters.

The GSA has been performed on the quasi-LPV model proposed in Chapter 2. This model is much faster than the nonlinear one, due to the applied non-rolling reference frame. In effect, the duration of each simulation is shortened, which further motivates the use of quasi-LPV model rather than the nonlinear one. On top of that, a permutation-based sampling is used, in order

to reduce the total number of simulations.

Benefits of GSA are twofold. Firstly, it highlights the possible identifiability limitations. Since non-sensitive parameters are non-identifiable, the approach has allowed to determine which parameters of the model can be deemed non-identifiable, either during the whole flight (i.e. mass of the projectile), or during some periods of it (e.g. initial Euler angles after the first seconds of flight). This aspect of work can be considered as a practical approach to gain more insight into the parametric variations within the model.

Secondly, in the context of the present work, GSA is considered as a tool to analyse the behaviour of the model, which allows to confirm that the quasi-LPV model structure correctly represents the expected physical behaviour of a studied system.

Moreover, it is envisaged that applying GSA as a standardised tool for performing pre-experimentation procedure of different projectile architectures in the context of free-flight experiments conducted at the French-German Research Institute of Saint-Louis. As such, it will be used in tandem with uncertainty analysis that aim to evaluate the maximum dispersion of the impact points of the projectiles.

# Conclusions and future research prospects

The purpose of this thesis lies in investigating two concepts that could aid the preparation of free-flight experiments. The first one pertains to the prospects of representing projectile's flight dynamics in the framework of linear parameter-varying (LPV) models. The second one refers to the enhancement of the knowledge of how do the uncertain model parameters influence the measurement signals with the use of global sensitivity analysis (GSA).

The task of quasi-LPV modelling of a projectile in free-flight can be considered as a difficult one, due to specifics of the nonlinear model that needs to be transformed. Principally, it lacks the input signal and its state variables are mostly not directly measurable. Moreover, its dynamics evolve over a wide range of parametric variations—which on one hand necessitates simplifications—while on the other hand a strict accuracy constraints are imposed. As such, the modelling task has been tackled from the point of view of an approximations-free and simulation-oriented work. Firstly, the nonlinear model equations have undergone an analytic transformation that changed the projectile's reference frame into a non-rolling one. For a spin-stabilised projectile—such as the large-calibre artillery projectile considered in the thesis—the reference frame transformation results in a reduction of the computation time needed to calculate trajectory of all its state variables. Secondly, an algebraic function substitution approach that allows to preserve the nonlinear behaviour of the modelled projectile has been applied.

Both the nonlinear and the newly developed quasi-LPV models have been tested through simulations, with initial conditions corresponding to these of real-world long-range experiments. Their numerical accuracy has been studied, principally *w.r.t.* the selection of an ordinary differential equations solver. A numerical solution close to the exact one has been obtained by applying a fixed-step numerical solver with a high order and high sampling frequency. Such a method is computationally expensive but allows to obtain accurate results. Afterwards, the much faster variable step solvers have been applied. Their accuracy has been analyzed *w.r.t.* the fixed-step solver's solution, considered as a reference. It is shown that while it is possible to obtain a numerical solution for both representations, the quasi-LPV model in the non-rolling reference frames offers a solution with higher accuracy, better convergence properties, and shorter computation time. Therefore, the numerical accuracy and simplicity enables the use of the proposed model in simulations.

The second task tackled in the thesis consisted of investigating the influence of uncertain parameters on the model. Principally, the uncertainties are inherent due to the goal of applying the

model to describe dynamics of a projectile in a realistic scenario. For instance, during a real-world free-flight experiment, it must be assured that the projectile will land in a dedicated safe zone, even though some of the initial state variables are unknown, and that initial state vector will differ from its nominal value due to stochastic effects induced by interior ballistics. Similarly, the initial guess of the aerodynamic coefficients will likely be imprecise. These uncertainties influence the model dynamics, and thus are visible in the model output signals.

The influence that the uncertain model parameters have on the model output can be assessed by the means of sensitivity analysis that apportions the output uncertainty to its different sources. In the context of the aforementioned experimental and practical difficulties associated with free-flight experiments, GSA has been applied in order to investigate the possibilities of enhancing the traditional methods of executing the tests. Obtained benefits of GSA were twofold. Firstly, it highlighted the possible identifiability limitations. Since non-sensitive parameters are non-identifiable, the approach has allowed to determine which parameters of the model can be deemed non-identifiable—and when. For example, mass of the projectile is non-identifiable during the whole flight, whereas the initial Euler angles are non-identifiable during the last phase of flight. This aspect of work can be considered as a practical way to gain more insight into the parametric variations within the model, which could be used in future safety analysis preceding the flight tests.

The developments accomplished in the thesis can serve as an indication of several possible prospects in upcoming research projects.

Identification of uncertain model parameters can be envisaged as a natural future step of the analysis. Such a task would be difficult to achieve using real-world data, since not all of the scheduling signals of the quasi-LPV model can be considered as measurable in the context of free-flight experiments. Hence, this endeavour would require simultaneous estimation of the model parameters, but also the current value of unmeasured scheduling state variables. Perhaps nonlinear observers, such as an extended Kalman filter, would be capable of performing this task. However, their design would be directly dependent on a potential identifiability analysis.

Quasi-LPV model development has been based on a non-rolling reference frame transformation. In fact, it is not the only possible transformation, as similar reduction in computation time complexity can be achieved by applying a non-spinning transformation [142, 141]. Up to author's knowledge, such a transformation has not been applied in control nor identification applications, hence its suitability is not fully assessed. It could be especially interesting in the case of identifiability analysis, as a different model structure could result in different identifiability and observer design prospects.

The underlying assumption used in the process of quasi-LPV model development is that the projectile is spin-stabilised without the means of control. Should the projectile be stabilised by fins, or guided by actuators—the modelling process would need to be revisited. Such a setting would represent a more traditional task of quasi-LPV model design, due to presence of an input signal in the nonlinear model structure.

The aforementioned prospects could even further aid the long-term efforts of developing a quasi-LPV model that would be valid irrespective of a projectile's architecture, and that could be used for real-time identification.

# Appendix A

## Wind reference frame

The nonlinear model is often presented *w.r.t.* the wind reference frame. However, its representation in body reference frame is better adapted for the quasi-LPV modelling approach proposed in this thesis. For the sake of completeness, the model representation expressed *w.r.t.* the wind reference frame, is presented in the following using (1.5) and the force coefficients expressed in wind reference frame as the drag coefficient  $C_D$ , the lift coefficient  $C_L$  and the side force coefficient  $C_{Y_w}$  as:

$$\begin{aligned}
 C_D &= -C_X \cos \alpha \cos \beta - C_Y \sin \beta - C_Z \sin \alpha \cos \beta \\
 C_L &= C_X \sin \alpha - C_Z \cos \alpha \\
 C_{Y_w} &= -C_X \cos \alpha \sin \beta + C_Y \cos \beta - C_Z \sin \alpha \sin \beta
 \end{aligned} \tag{A.1}$$

Using (A.1), the force equations (1.4) and translational kinematic equations (1.18) will acquire the following form, where different colours have been used to mark **states of the system**, **constants**, and the **aerodynamic coefficients**.

*Force equations:*

$$\dot{V} = -\frac{\bar{q}S}{m}C_D + g(\cos \theta \cos \phi \sin \alpha \cos \beta + \cos \theta \sin \phi \sin \beta - \sin \theta \cos \alpha \cos \beta), \tag{A.2a}$$

$$\begin{aligned}
 \dot{\alpha} &= -\frac{\bar{q}S}{mV \cos \beta}C_L + \omega_y - \tan \beta(\omega_x \cos \alpha + \omega_z \sin \alpha) + \\
 &+ \frac{g}{V \cos \beta}(\cos \theta \cos \phi \cos \alpha + \sin \theta \sin \alpha),
 \end{aligned} \tag{A.2b}$$

$$\begin{aligned}
 \dot{\beta} &= \frac{\bar{q}S}{mV}C_{Y_w} + \omega_x \sin \alpha - \omega_z \cos \alpha + \\
 &+ \frac{g}{V}(\cos \theta \sin \phi \cos \beta + \sin \theta \cos \alpha \sin \beta - \cos \phi \cos \theta \sin \alpha \sin \beta).
 \end{aligned} \tag{A.2c}$$

*Translational kinematic equations:*

$$\begin{aligned}
 \dot{x}_E &= V \cos \alpha \cos \beta \cos \theta \cos \psi + V \sin \beta(\sin \phi \sin \theta \cos \psi - \cos \phi \sin \psi) + \\
 &+ V \sin \alpha \cos \beta(\cos \phi \sin \theta \cos \psi + \sin \phi \sin \psi),
 \end{aligned} \tag{A.3a}$$

$$\begin{aligned}
 \dot{y}_E &= V \cos \alpha \cos \beta \cos \theta \sin \psi + V \sin \beta(\sin \phi \sin \theta \sin \psi + \cos \phi \cos \psi) + \\
 &+ V \sin \alpha \cos \beta(\cos \phi \sin \theta \sin \psi - \sin \phi \cos \psi),
 \end{aligned} \tag{A.3b}$$

$$\dot{z}_E = -V \cos \alpha \cos \beta \sin \theta + V \sin \beta \sin \phi \cos \theta + V \sin \alpha \cos \beta \cos \phi \cos \theta. \tag{A.3c}$$

The dynamic moment equations and the rotational kinematic equations remain the same as in the case of body reference frame.

Such a form of the nonlinear model equations is often used, and can be found, for example, in [1]. However, the superabundance of trigonometric functions and interdependence of state variables render this representation difficult to linearise. For this reason, it is the description in body reference frame which is considered in Chapter 2.

## Appendix B

# Analytic equivalence of coordinate reference frames

An analytic equivalence between the trajectories of variable-roll and non-rolling models is claimed in Chapter 2. In order to support this claim, a full analytic derivation of the non-rolling model equations is presented.

The non-rolling reference frame is defined by a rotation around the  $x$  body axis by the roll angle  $\phi$ . It can be described using the following transformation equations [35, 142, 32]:

$$\begin{bmatrix} u \\ v \\ w \end{bmatrix} = \begin{bmatrix} 1 & 0 & 0 \\ 0 & \cos \phi & -\sin \phi \\ 0 & \sin \phi & \cos \phi \end{bmatrix} \begin{bmatrix} u_b \\ v_b \\ w_b \end{bmatrix} \quad (\text{B.1})$$

$$\begin{bmatrix} p \\ q \\ r \end{bmatrix} = \begin{bmatrix} 1 & 0 & 0 \\ 0 & \cos \phi & -\sin \phi \\ 0 & \sin \phi & \cos \phi \end{bmatrix} \begin{bmatrix} p_b \\ q_b \\ r_b \end{bmatrix} \quad (\text{B.2})$$

The reverse transformation is defined as follows:

$$\begin{bmatrix} u_b \\ v_b \\ w_b \end{bmatrix} = \begin{bmatrix} 1 & 0 & 0 \\ 0 & \cos \phi & \sin \phi \\ 0 & -\sin \phi & \cos \phi \end{bmatrix} \begin{bmatrix} u \\ v \\ w \end{bmatrix} \quad (\text{B.3})$$

$$\begin{bmatrix} p_b \\ q_b \\ r_b \end{bmatrix} = \begin{bmatrix} 1 & 0 & 0 \\ 0 & \cos \phi & \sin \phi \\ 0 & -\sin \phi & \cos \phi \end{bmatrix} \begin{bmatrix} p \\ q \\ r \end{bmatrix} \quad (\text{B.4})$$

### Transformation of the total velocity and total angle of attack

The aerodynamic forces and moments depend on the vehicle's total velocity and total angle of attack. The following development proves their equivalence in both reference frames.

$$\begin{aligned}
 V &= \sqrt{u^2 + v^2 + w^2} = \sqrt{u_b^2 + (v_b \cos \phi + w_b \sin \phi)^2 + (-v_b \sin \phi + w_b \cos \phi)^2} = \\
 &= \sqrt{u_b^2 + v_b^2 \cos^2 \phi + 2v_b w_b \sin \phi \cos \phi + w_b^2 \sin^2 \phi + v_b^2 \sin^2 \phi - 2v_b w_b \sin \phi \cos \phi + w_b^2 \cos^2 \phi} = \\
 &= \sqrt{u_b^2 + v_b^2 (\cos^2 \phi + \sin^2 \phi) + w_b^2 (\sin^2 \phi + \cos^2 \phi) + 2v_b w_b \sin \phi \cos \phi - 2v_b w_b \sin \phi \cos \phi} = \\
 &= \sqrt{u_b^2 + v_b^2 + w_b^2} = V_b
 \end{aligned} \tag{B.5}$$

The transformation of the total angle of attack is a bit more convoluted. Generally,  $\alpha_t$  is defined as follows:

$$\alpha_t^b = \arccos(\cos \alpha_b \cos \beta_b) \tag{B.6}$$

where:

$$\beta_b = \arcsin\left(\frac{v_b}{\sqrt{u_b^2 + v_b^2 + w_b^2}}\right) \quad \alpha_b = \arctan\left(\frac{w_b}{u_b}\right) \tag{B.7}$$

Firstly, the trigonometric identities:  $\cos(\arcsin(x)) = \sqrt{1 - x^2}$  and  $\cos(\arctan(x)) = \frac{1}{\sqrt{x^2 + 1}}$  have to be applied to (B.7), resulting in:

$$\cos \beta_b = \cos\left(\arcsin\left(\frac{v_b}{\sqrt{u_b^2 + v_b^2 + w_b^2}}\right)\right) = \sqrt{1 - \left(\frac{v_b}{\sqrt{u_b^2 + v_b^2 + w_b^2}}\right)^2} = \frac{\sqrt{u_b^2 + w_b^2}}{V_b} \tag{B.8}$$

$$\cos \alpha_b = \cos\left(\arctan\left(\frac{w_b}{u_b}\right)\right) = \frac{1}{\sqrt{\left(\frac{w_b}{u_b}\right)^2 + 1}} = \frac{u_b}{\sqrt{w_b^2 + u_b^2}} \tag{B.9}$$

Secondly, (B.9) and (B.8) can be applied to (B.6), leading to:

$$\alpha_t^b = \arccos(\cos \alpha_b \cos \beta_b) = \arccos\left(\frac{\sqrt{u_b^2 + w_b^2}}{V_b} \frac{u_b}{\sqrt{w_b^2 + u_b^2}}\right) = \arccos\left(\frac{u_b}{V_b}\right) \tag{B.10}$$

Finally, using (B.1) and (B.5) it can be proven that  $\alpha_t$  is the same in both frames:

$$\alpha_t^b = \arccos\left(\frac{u_b}{V_b}\right) = \arccos\left(\frac{u}{V}\right) = \alpha_t \tag{B.11}$$

Therefore, both the total velocity  $V$  and the total angle of attack  $\alpha_t$  remain the same, regardless of the reference frame selected.

Remark: if the  $u - v - w$  equations are used instead of  $V - \alpha - \beta$  equation, then  $\alpha_t$  may be equivalently defined as:

$$\alpha_t = \arctan\left(\frac{\sqrt{v^2 + w^2}}{u}\right) \tag{B.12}$$

---

## Transformation of attitude kinematics

The standard attitude equations in the variable-roll frame are as follows:

$$\dot{\phi} = p_b + \tan \theta (q_b \sin \phi + r_b \cos \phi) \quad (\text{B.13})$$

$$\dot{\theta} = q_b \cos \phi - r_b \sin \phi \quad (\text{B.14})$$

$$\dot{\psi} = \frac{1}{\cos \phi} (q_b \sin \phi + r_b \cos \phi) \quad (\text{B.15})$$

Equations (B.13)-(B.15) can be directly transformed into a non-rolling form, using transformation (B.4):

$$\begin{aligned} \dot{\phi} &= p + \tan \theta [(q \cos \phi + r \sin \phi) \sin \phi + (-q \sin \phi + r \cos \phi) \cos \phi] \\ &= p + \tan \theta [q \sin \phi \cos \phi + r \sin^2 \phi - q \sin \phi \cos \phi + r \cos^2 \phi] = \\ &= p + \tan \theta [r(\sin^2 \phi + \cos^2 \phi)] = p + r \tan \theta \end{aligned} \quad (\text{B.16})$$

$$\dot{\theta} = q_b \cos \phi - r_b \sin \phi = q \quad (\text{B.17})$$

$$\dot{\psi} = \frac{1}{\cos \phi} (q_b \sin \phi + r_b \cos \phi) = \frac{1}{\cos \phi} r \quad (\text{B.18})$$

## Transformation of linear velocities

The standard dynamic equation in the variable-roll frame for the  $u_b$  is as follows:

$$\dot{u}_b = (r_b v_b - q_b w_b) - g \sin \theta + \frac{\bar{q}S}{m} C_{x,aero}^b \quad (\text{B.19})$$

It can be transformed into non-rolling form using (B.3):

$$\begin{aligned} \dot{u}_b = \dot{u} &= (-q \sin \phi + r \cos \phi)(v \cos \phi + w \sin \phi) - \\ & (q \cos \phi + r \sin \phi)(-v \sin \phi + w \cos \phi) - g \sin \theta + \frac{\bar{q}S}{m} C_{x,aero}^b \\ &= -qv \sin \phi \cos \phi - qw \sin^2 \phi + rv \cos^2 \phi + rw \sin \phi \cos \phi \\ &+ qv \sin \phi \cos \phi - qw \cos^2 \phi + rv \sin^2 \phi - g \sin \theta + \frac{\bar{q}S}{m} C_{x,aero}^b = \\ &= -qw + rv - g \sin \theta + \frac{\bar{q}S}{m} C_{x,aero}^b \end{aligned} \quad (\text{B.20})$$

where

$$\begin{aligned} \frac{\bar{q}S}{m} C_{x,aero}^b &= \frac{\rho(z_E^b)S}{2m} V^{b2} (C_{X_0} + C_{X_a} \sin^2 \alpha_t) \\ &= \frac{\rho(z_E)S}{2m} V^2 (C_{X_0} + C_{X_a} (1 - \frac{u^2}{V^2})) = \frac{\bar{q}S}{m} C_{x,aero} \end{aligned} \quad (\text{B.21})$$

The standard dynamic equation for the  $v_b$  and  $w_b$  are as follows:

$$\dot{v}_b = (p_b w_b - r_b u_b) + g \sin \phi \cos \theta + \frac{1}{m} f_{y,aero}^b \quad (\text{B.22})$$

$$\dot{w}_b = (q_b u_b - p_b v_b) + g \cos \phi \cos \theta + \frac{1}{m} f_{z,aero}^b \quad (\text{B.23})$$

Here, they need to be transformed differently. Firstly, knowing that  $v = v_b \cos \phi - w_b \sin \phi$ , we can calculate derivative of  $v$ :

$$\begin{aligned}\dot{v} &= \dot{v}_b \cos \phi + v_b(-\sin \phi)\dot{\phi} - (\dot{w}_b \sin \phi + w_b \cos \phi \dot{\phi}) \\ &= \dot{v}_b \cos \phi - \dot{w}_b \sin \phi - \dot{\phi}(v_b \sin \phi + w_b \cos \phi) = \dot{v}_b \cos \phi - \dot{w}_b \sin \phi - \dot{\phi}w\end{aligned}\quad (\text{B.24})$$

Secondly, substituting  $\dot{v}_b$  and  $\dot{w}_b$  by (B.22) and (B.23), respectively, yields:

$$\begin{aligned}\dot{v} &= [(p_b w_b - r_b u_b) + g \sin \phi \cos \theta \\ &+ \frac{1}{m} f_{y,aero}^b] \cos \phi - [(q_b u_b - p_b v_b) + g \cos \phi \cos \theta + \frac{1}{m} f_{z,aero}^b] \dot{w}_b \sin \phi - \dot{\phi}w \\ &= p_b(w_b \cos \phi - v_b \sin \phi) - u_b(r_b \cos \phi + q_b \sin \phi) + \frac{1}{m} [f_{y,aero}^b \cos \phi + f_{z,aero}^b \sin \phi] - \dot{\phi}w \\ &= pw - ur - w(p + r \tan \theta) + \frac{1}{m} [f_{y,aero}^b \cos \phi + f_{z,aero}^b \sin \phi] \\ &= -ur - wr \tan \theta + \frac{1}{m} [f_{y,aero}^b \cos \phi + f_{z,aero}^b \sin \phi]\end{aligned}\quad (\text{B.25})$$

The same approach can be applied to  $w$ . Firstly, knowing that  $w = v_b \sin \phi + w_b \cos \phi$ :

$$\dot{w} = \dot{v}_b \sin \phi + v_b \cos \phi \dot{\phi} + \dot{w}_b \cos \phi + w_b(-\sin \phi)\dot{\phi} = \dot{v}_b \sin \phi + \dot{w}_b \cos \phi + v\dot{\phi}\quad (\text{B.26})$$

Secondly, substituting  $\dot{v}_b$  and  $\dot{w}_b$  by (B.22) and (B.23), respectively, yields:

$$\begin{aligned}\dot{w} &= [(p_b w_b - r_b u_b) + g \sin \phi \cos \theta + \frac{1}{m} f_{y,aero}^b] \sin \phi \\ &+ [(q_b u_b - p_b v_b) + g \cos \phi \cos \theta + \frac{1}{m} f_{z,aero}^b] \cos \phi + v\dot{\phi} \\ &= -p_b(v_b \cos \phi - w_b \sin \phi) + u_b(q_b \cos \phi - r_b \sin \phi) \\ &+ g \cos \theta(\sin \phi + \cos^2 \phi) + \frac{1}{m} (f_{y,aero}^b \sin \phi + f_{z,aero}^b \cos \phi) \\ &+ v(p + r \tan \theta) \\ &= uq + vr \tan \theta + g \cos \theta + \frac{1}{m} (f_{y,aero}^b \sin \phi + f_{z,aero}^b \cos \phi) + v\dot{\phi}\end{aligned}\quad (\text{B.27})$$

Additionally, it can be observed that the forces in a non-rolling frame have different values than forces in the variable-roll frame, but the equations for them remain the same—just the variables are expressed in a non-rolling frame:

$$\begin{aligned}f_{y,aero}^b \cos \phi - f_{z,aero}^b \sin \phi &= \bar{q}S [(-C_{yp\alpha} \frac{d}{2V} \frac{w_b}{V} p_b - C_{N\alpha} \frac{v_b}{V}) \cos \phi - (-C_{yp\alpha} \frac{d}{2V} \frac{v_b}{V} p_b - C_{N\alpha} \frac{w_b}{V}) \sin \phi] \\ &= \frac{1}{2} \rho(z_E) V^2 [(-C_{yp\alpha} \frac{d}{2V} \frac{w}{V} p - C_{N\alpha} \frac{v}{V})] = f_{y,aero}\end{aligned}\quad (\text{B.28})$$

$$f_{y,aero}^b \sin \phi + f_{z,aero}^b \cos \phi = \frac{1}{2} \rho(z_E) V^2 [(C_{yp\alpha} \frac{d}{2V} \frac{v}{V} p - C_{N\alpha} \frac{w}{V})] = f_{z,aero}\quad (\text{B.29})$$

Therefore, the dynamical equations in non-rolling frame for the linear velocities are as follows:

$$\dot{u} = -qw + rv - g \sin \theta + \frac{1}{m} f_{x,aero}\quad (\text{B.30})$$

$$\dot{v} = -ur - wr \tan \theta + \frac{1}{m} f_{y,aero}\quad (\text{B.31})$$

$$\dot{w} = uq + vr \tan \theta + g \cos \theta + \frac{1}{m} f_{z,aero}\quad (\text{B.32})$$

---

## Attitude dynamics

The standard dynamics equation in the variable-roll frame for  $p_b$  is as follows:

$$\dot{p}_b = -\frac{I_z - I_y}{I_x} q_b r_b + \frac{1}{I_x} \bar{q} S d C_{lp} p_b \quad (\text{B.33})$$

It can be transformed into non-rolling form using (B.4):

$$\begin{aligned} \dot{p} = \dot{p}_b &= -\frac{I_z - I_y}{I_x} (q \cos \phi + r \sin \phi) (-q \sin \phi + r \cos \phi) + \frac{1}{I_x} \bar{q} S d C_{lp} p \\ &= -\frac{I_z - I_y}{I_x} [\sin \phi \cos \phi (r^2 - q^2) + q r (\cos^2 \phi - \sin^2 \phi)] + \frac{1}{I_x} \bar{q} S d C_{lp} p \\ &\xrightarrow{I_y=I_z} \frac{1}{I_x} \bar{q} S d C_{lp} p \end{aligned} \quad (\text{B.34})$$

Equation (B.34) can be decoupled from the  $\phi$  angle if, and only if,  $I_y = I_z$ . Let us note it as  $I_t = I_y = I_z$ .

The standard dynamics equations for  $q_b$  and  $r_b$  are as follows:

$$\dot{q}_b = -\frac{I_x - I_t}{I_t} p_b r_b + \frac{1}{I_t} \bar{q} S d C_m^b \quad (\text{B.35})$$

$$\dot{r}_b = -\frac{I_t - I_x}{I_t} p_b q_b + \frac{1}{I_t} \bar{q} S d C_n^b \quad (\text{B.36})$$

Equations (B.35)-(B.36) can be transformed into the non-rolling frame, using the same mathematical trick as for the equations (B.22)-(B.23). Firstly, knowing that  $q = q_b \cos \phi - r_b \sin \phi$ :

$$\dot{q} = \dot{q}_b \cos \phi + q_b (-\sin \phi) \dot{\phi} - \dot{r}_b \sin \phi - r_b \cos \phi \dot{\phi} = \dot{q}_b \cos \phi - \dot{r}_b \sin \phi - r \dot{\phi} \quad (\text{B.37})$$

Secondly, substituting  $\dot{q}_b$  and  $\dot{r}_b$  by (B.35) and (B.36), respectively, yields:

$$\begin{aligned} \dot{q} &= \left[ -\frac{I_x - I_t}{I_t} p_b r_b + \frac{1}{I_t} \bar{q} S d C_m^b \right] \cos \phi - \left[ -\frac{I_t - I_x}{I_t} p_b q_b + \frac{1}{I_t} \bar{q} S d C_n^b \right] \sin \phi - r \dot{\phi} \\ &= \frac{I_t - I_x}{I_t} p_b (q_b \sin \phi + r_b \cos \phi) + \frac{\bar{q} S d}{I_t} (C_m^b \cos \phi - C_n^b \sin \phi) - r \dot{\phi} \\ &= \frac{I_t - I_x}{I_t} p r + \frac{\bar{q} S d}{I_t} (C_m^b \cos \phi - C_n^b \sin \phi) - p r - r^2 \tan \theta \\ &= \frac{I_t - I_x - I_t}{I_t} p r - r^2 \tan \theta + \frac{\bar{q} S d}{I_t} (C_m^b \cos \phi - C_n^b \sin \phi) = -\frac{I_x}{I_t} p r - r^2 \tan \theta + \frac{\bar{q} S d}{I_t} C_m \end{aligned} \quad (\text{B.38})$$

where:

$$\begin{aligned} C_m &= (C_m^b \cos \phi - C_n^b \sin \phi) \\ &= \left[ C_{m\alpha} \frac{w_b}{V} - C_{np\alpha} \frac{d}{2V} \frac{v_b}{V} p_b + C_{mq} \frac{d}{2V} q_b \right] \cos \phi - \left[ -C_{m\alpha} \frac{v_b}{V} - C_{np\alpha} \frac{d}{2V} \frac{w_b}{V} p_b + C_{mq} \frac{d}{2V} r_b \right] \sin \phi \\ &= C_{m\alpha} \frac{w}{V} - C_{np\alpha} \frac{d}{2V} \frac{v}{V} p + C_{mq} \frac{d}{2V} q \end{aligned} \quad (\text{B.39})$$

Similarly, knowing that  $r = q_b \sin \phi + r_b \cos \phi$ :

$$\dot{q} = \dot{q}_b \sin \phi + q_b \cos \phi \dot{\phi} + \dot{r}_b \cos \phi - r_b \sin \phi \dot{\phi} = \dot{q}_b \sin \phi + \dot{r}_b \cos \phi + q \dot{\phi} \quad (\text{B.40})$$

which can be further transformed by substituting  $\dot{q}_b$  and  $\dot{r}_b$  by (B.35) and (B.36), respectively:

$$\begin{aligned}\dot{q} &= \left[ -\frac{I_x - I_t}{I_t} p_b r_b + \frac{1}{I_t} \bar{q} S d C_m^b \right] \sin \phi + \left[ -\frac{I_t - I_x}{I_t} p_b q_b + \frac{1}{I_t} \bar{q} S d C_n^b \right] \cos \phi + q \dot{\phi} \\ &= -\frac{I_t - I_x}{I_t} p_b (q_b \cos \phi - r_b \sin \phi) + \frac{1}{I_t} \bar{q} S d (C_m^b \sin \phi + C_n^b \cos \phi) + q \dot{\phi} \\ &= \frac{I_x}{I_t} p q + q r \tan \theta + \frac{1}{I_t} \bar{q} S d C_n\end{aligned}\quad (\text{B.41})$$

where:

$$C_n = C_m^b \sin \phi + C_n^b \cos \phi = -C_{m\alpha} \frac{v}{V} - C_{n\beta} \frac{d}{2V} \frac{w}{V} p + C_{mq} \frac{d}{2V} r \quad (\text{B.42})$$

Therefore, the dynamical equations in non-rolling frame for the angular velocities are as follows:

$$\dot{p} = \frac{1}{I_x} \bar{q} S d C_{lp} p \quad (\text{B.43})$$

$$\dot{q} = -\frac{I_x}{I_t} p r - r^2 \tan \theta + \frac{\bar{q} S d}{I_t} C_m \quad (\text{B.44})$$

$$\dot{r} = \frac{I_x}{I_t} p q + q r \tan \theta + \frac{1}{I_t} \bar{q} S d C_n \quad (\text{B.45})$$

## Translational kinematics

In a standard non-rolling case, the differential equation describing translational kinematics of a projectile is developed using direction cosine matrix  $T^{EB}$ , which transforms the velocity vector from body-fixed to Earth reference frame:

$$T^{EB}(\phi, \theta, \psi) = \begin{bmatrix} \cos \theta \cos \psi & \sin \phi \sin \theta \cos \psi - \sin \psi \cos \phi & \cos \phi \sin \theta \cos \psi + \sin \phi \sin \psi \\ \cos \theta \sin \psi & \sin \phi \sin \theta \sin \psi + \cos \psi \cos \phi & \cos \phi \sin \theta \sin \psi - \sin \phi \cos \psi \\ -\sin \theta & \sin \phi \cos \theta & \cos \phi \cos \theta \end{bmatrix} \quad (\text{B.46})$$

In case of the non-rolling frame, we can observe that, e.g.  $z_E^b$  is equal to:

$$\begin{aligned}z_E^b &= -u_b \sin \theta + v_b \sin \phi \cos \theta + w_b \cos \phi \cos \theta = -u_b \sin \theta + \cos \theta (v_b \sin \phi + w_b \cos \phi) \\ &= -u \sin \theta + w \cos \theta = z_E\end{aligned}\quad (\text{B.47})$$

Derivation for  $x_E$  and  $y_E$  is equivalent. Consequently, the translational kinematics in the non-rolling frame have a following form:

$$\begin{bmatrix} \dot{x}_E \\ \dot{y}_E \\ \dot{z}_E \end{bmatrix} \begin{bmatrix} \cos \theta \cos \psi & -\sin \psi & \sin \theta \cos \psi \\ \cos \theta \sin \psi & \cos \psi & \sin \theta \sin \psi \\ -\sin \theta & 0 & \cos \theta \end{bmatrix} \begin{bmatrix} u \\ v \\ w \end{bmatrix} \quad (\text{B.48})$$

---

## Summary of the equations

The derivated equations are summed up in the following form:

*Translational dynamics*

$$\begin{bmatrix} \dot{u} \\ \dot{v} \\ \dot{w} \end{bmatrix} = \begin{bmatrix} 0 & -r & q \\ r & 0 & r \tan \theta \\ -q & -r \tan \theta & 0 \end{bmatrix} \begin{bmatrix} u \\ v \\ w \end{bmatrix} + g \begin{bmatrix} -\sin \theta \\ 0 \\ \cos \theta \end{bmatrix} + 1/m \begin{bmatrix} f_{x,aero} \\ f_{y,aero} \\ f_{z,aero} \end{bmatrix} \quad (\text{B.49})$$

*Attitude dynamics*

$$\begin{bmatrix} \dot{p} \\ \dot{q} \\ \dot{r} \end{bmatrix} = \begin{bmatrix} 0 \\ -\frac{I_x}{I_t} pr - r^2 \tan \theta \\ \frac{I_x}{I_t} pq + qr \tan \theta \end{bmatrix} + \begin{bmatrix} \frac{1}{I_x} m_{x,aero} \\ \frac{1}{I_y} m_{y,aero} \\ \frac{1}{I_z} m_{z,aero} \end{bmatrix} \quad (\text{B.50})$$

*Translational kinematics*

$$\begin{bmatrix} \dot{x}_E \\ \dot{y}_E \\ \dot{z}_E \end{bmatrix} = \begin{bmatrix} \cos \theta \cos \psi & -\sin \psi & \sin \theta \cos \psi \\ \cos \theta \sin \psi & \cos \psi & \sin \theta \sin \psi \\ -\sin \theta & 0 & \cos \theta \end{bmatrix} \begin{bmatrix} u \\ v \\ w \end{bmatrix} \quad (\text{B.51})$$

*Attitude kinematics*

$$\begin{bmatrix} \dot{\theta} \\ \dot{\psi} \end{bmatrix} = \begin{bmatrix} 1 & 0 \\ 0 & \frac{1}{\cos \theta} \end{bmatrix} \begin{bmatrix} q \\ r \end{bmatrix} \quad (\text{B.52})$$

The roll angle  $\dot{\phi}$  is decoupled from the rest of the state equations, and can be ignored. Should it be necessary, its value can be calculated *a posteriori* as:

$$\dot{\phi} = p + r \tan \theta \quad (\text{B.53})$$

*Aerodynamic forces and moments*

$$\begin{bmatrix} f_{x,aero} \\ f_{y,aero} \\ f_{z,aero} \end{bmatrix} = \bar{q} S \begin{bmatrix} C_{x,aero} \\ C_{y,aero} \\ C_{z,aero} \end{bmatrix} = \bar{q} S \begin{bmatrix} C_{X_0} + C_{X_a} \sin^2 \alpha_t \\ -C_{yp\alpha} \frac{d}{2V} \frac{w}{V} p - C_{N\alpha} \frac{v}{V} \\ -C_{yp\alpha} \frac{d}{2V} \frac{v}{V} p - C_{N\alpha} \frac{w}{V} \end{bmatrix} \quad (\text{B.54})$$

$$\begin{bmatrix} m_{x,aero} \\ m_{y,aero} \\ m_{z,aero} \end{bmatrix} = \bar{q} S d \begin{bmatrix} C_{l,aero} \\ C_{m,aero} \\ C_{n,aero} \end{bmatrix} = \bar{q} S d \begin{bmatrix} C_{lp} p \\ C_{m\alpha} \frac{w}{V} - C_{np\alpha} \frac{d}{2V} \frac{v}{V} p + C_{mq} \frac{d}{2V} q \\ -C_{m\alpha} \frac{v}{V} - C_{np\alpha} \frac{d}{2V} \frac{w}{V} p + C_{mq} \frac{d}{2V} r \end{bmatrix} \quad (\text{B.55})$$

The final form of the equations is similar to these presented in [141, 142], albeit based on a simpler derivation.



## Résumé en français

Le continuel développement des munitions d'artillerie a conduit à une plus grande précision de ces dernières, et un allongement de leur portée. Cela est particulièrement vrai pour les projectiles de gros calibre. L'architecture de 155 mm en est un excellent exemple: développée par Charles de Bange<sup>2</sup> comme un projectile d'artillerie polyvalent pour l'armée française en 1877 [39], elle a connu une amélioration continue jusqu'à nos jours. Ce qui a suivi, a été le changement de paradigmes dans les opérations d'artillerie. Des barrages intensifs couvrant de grandes surfaces de territoire, typiques de la Première et de la Seconde Guerre mondiale, l'accent s'est déplacé vers le ciblage d'objets uniques d'intérêt, réduisant efficacement les dommages collatéraux.

Cette tendance se reflète dans les exemples récents et classiques de munitions à longue portée (Figure 1), telles que les projectiles de type Excalibur, BONUS, Copperhead ou Krasnopol qui utilisent diverses techniques de guidage et de navigation pour assurer leur capacité de frapper même une petite cible ou une cible mobile [55, 11].

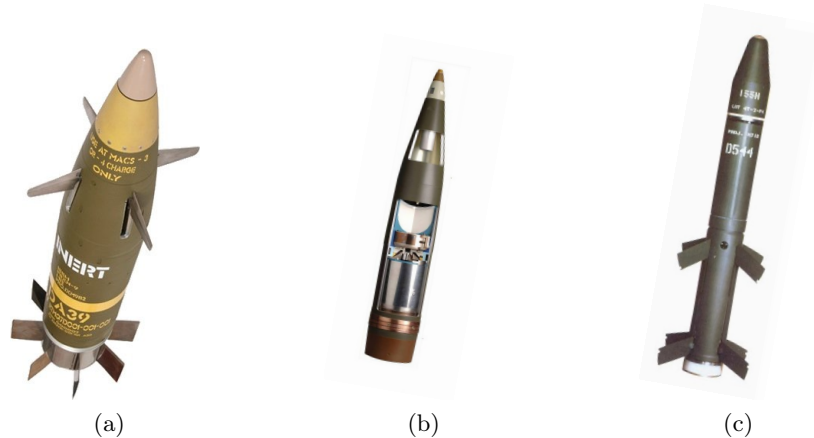


Figure 1: Architectures d'artillerie à longue portée exemplaires : (a) M982 Excalibur, (b) BONUS 155 mm, (c) M712 Copperhead

La mise en service d'une nouvelle pièce de munition d'artillerie est un processus long, dont une partie importante est l'évaluation du comportement en vol du projectile. En termes mathématiques, un tel comportement est décrit par les lois du mouvement de Newton-Euler et dépend d'un ensemble de coefficients aérodynamiques qui doivent être quantifiés pour chaque véhicule volant

---

<sup>2</sup>**Charles Ragon de Bange** (1833–1914) - Officier et ingénieur militaire français, responsable de la refonte des systèmes d'artillerie de haute précision pour l'armée française au lendemain de la guerre franco-prussienne.

[148]. Inversement, la connaissance des caractéristiques aérodynamiques permet de prédire la trajectoire et d'évaluer le comportement dynamique d'un projectile. En tant que tels, ils sont nécessaires à toute activité de guidage, de navigation ou de contrôle, et leurs recherches restent parmi les plus anciennes dans le domaine de l'aérospatiale. Les coefficients aérodynamiques peuvent être quantifiés à l'aide de plusieurs méthodes complémentaires, principalement divisées en l'utilisation de simulations de dynamique des fluides computationnelle [42], de codes semi-empiriques (PRODAS [13] et Missile DATCOM [42]), ou d'expériences en soufflerie (e.g. [31, 120]). Leurs résultats peuvent être traités comme une première estimation des coefficients aérodynamiques, qui sera confirmée plus tard par l'expérimentation du monde réel — en particulier sous la forme d'essais balistiques en vol libre. Dans ce contexte, le vol libre correspond à la situation dans laquelle le comportement en vol d'un projectile n'est influencé par aucun corps extérieur, tel que le canon d'un lanceur ou la surface de la cible.

L'expérimentation en vol libre susmentionnée peut être considérée comme une méthode réaliste de caractérisation aérodynamique, car le comportement en vol du projectile est observé — et capturé en direct grâce à des mesures — dans des conditions de vol réel. En utilisant les données obtenues, une procédure d'identification est appliquée, résultant en une meilleure estimation des coefficients aérodynamiques [4, 27, 134]. Rien qu'en Europe, il existe plusieurs installations balistiques dans lesquelles les expériences peuvent être effectuées. Les principaux exemples incluent l'installation des Techniques Terrestres de la DGA à Bourges en France [26], le Centre technique de la Bundeswehr pour les armes et les munitions à Meppen en Allemagne [33], et le site d'essai en plein air à Baldersheim en France, exploité par l'Institut de recherche franco-allemand de Saint-Louis (ISL) [1]. Le dernier est considéré comme une référence dans cette thèse, et les spécificités de la modélisation et de l'analyse présentées ci-après seront adaptées aux conditions et contraintes imposées par les conditions de vol et aux techniques de mesure disponibles sur le site de l'ISL.

La tâche de préparer des expériences de vol libre, d'identifier un modèle mathématique du projectile testé et de le préparer à être utilisé dans les activités de guidage et de navigation à venir pose une pléthore de difficultés techniques et scientifiques :

- **Réalisation des tests** n'est possible que si une estimation initiale des caractéristiques aérodynamiques est connue, de sorte que la trajectoire peut être prédite. De plus, il faut s'assurer que les résultats seront informatifs à des fins d'identification. Dans ce contexte, la connaissance du domaine permet de prédire si, par exemple les paramètres choisis seront identifiables à l'aide des techniques de mesure disponibles.
- **L'identification** des coefficients aérodynamiques doit être effectuée dans un large éventail de scénarios afin d'explorer suffisamment le comportement d'un projectile, y compris l'aérodynamique subsonique, transsonique et supersonique [4]. Les défis théoriques incluent la structure hautement non linéaire du modèle et le vecteur partiellement inconnu des variables d'état initial qui doit également être identifié [1]. La tâche d'identification est alors influencée par des contraintes pratiques, telles que les coûts élevés de réalisation d'expériences en vol libre.
- **Le guidage et la navigation** sont généralement effectués dans le cadre de techniques de modélisation spécialisées, telles que des structures quasi linéaires à paramètres variables (quasi-LPV) qui sont utiles pour la conception d'une boucle de contrôle pour projectiles [97, 108]. Le processus est plus difficile pour les modèles de structure générale non linéaire.

---

Par conséquent, si le modèle identifié a une structure non linéaire — comme c’est souvent le cas, en raison du modèle de premier principe utilisé — il doit être modifié.

Cette thèse propose une nouvelle approche pour une technique de modélisation quasi-LPV sans approximations et son utilisation ultérieure dans GSA. La méthode suggérée vise à :

- transformer analytiquement les équations du modèle non linéaire en changeant le cadre de référence du projectile en un cadre non roulant [142],
- appliquer une approche de substitution de fonction algébrique [87] qui permet de conserver le comportement non linéaire du projectile modélisé [130], tout en le représentant sous une forme quasi-LPV,
- utiliser le modèle quasi-LPV obtenu dans un ensemble de simulations de Monte Carlo afin de tester l’influence de paramètres de modèle incertains sur ses signaux de sortie à l’aide de GSA.

Le projectile analysé a une forme allongée avec un avant et un arrière fuselés, avec un diamètre de près de 155 mm et une longueur de 930 mm, comme détaillé dans la Figure 2. La partie intérieure a été initialement conçue comme un espace pour stocker une charge utile explosive. Le projectile est lancé à partir d’un canon rayé qui induit une vitesse de rotation initiale, ce qui lui permet d’être un véhicule stabilisé en rotation. On suppose que le projectile est symétrique d’axe avec le centre de masse situé le long de sa direction axiale. Le projectile est fait de matériaux non magnétiques, de sorte que les capteurs magnétiques peuvent être utilisés sans aucune perturbation.

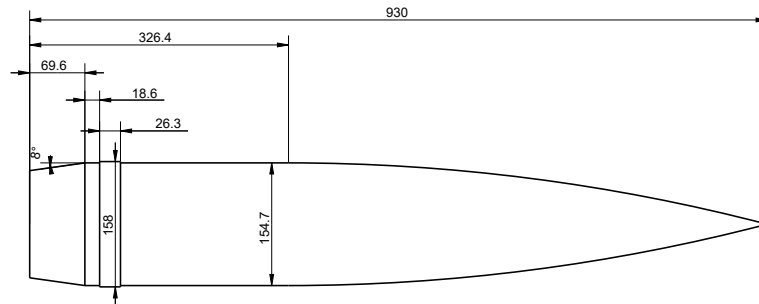


Figure 2: Architecture du projectile 155 mm.

Les développements sont adaptés aux contraintes imposées par le caractère expérimental des essais en vol libre. Le comportement du projectile est observé dans une large gamme de conditions initiales, la plupart des mesures sont indirectes et il n’y a pas de signal d’entrée de commande. Pour ces raisons, la linéarisation standard quasi-LPV est impossible, et l’approche sans approximations s’est avérée plus prometteuse. De plus, le large éventail de conditions expérimentales limite la quantité d’informations physiques pouvant être obtenues à l’aide d’une analyse de sensibilité locale, motivant ainsi l’utilisation de GSA.

De plus, pour un projectile gyrostabilisé, la transformation du référentiel entraîne une réduction du temps de calcul nécessaire pour calculer la trajectoire de toutes ses variables d’état.

Par conséquent, le modèle quasi-LPV obtenu pourrait être considéré comme aussi précis que le modèle non linéaire d'origine pour décrire le comportement du projectile en vol, mais il est également suffisamment simple sur le plan informatique pour être directement utilisé dans une GSA. Cette prémisse est ensuite étudiée: afin d'évaluer la précision de l'approche de modélisation proposée, le modèle quasi-LPV développé analytiquement a été implémenté dans Matlab et testé numériquement à travers une série de simulations correspondant aux trajectoires de vol libre d'un exemple de gros calibre projectile. Les trajectoires obtenues de toutes les variables d'état ont été comparées aux simulations du modèle non linéaire d'origine, montrant ainsi leur équivalence. De plus, le modèle quasi LPV s'est avéré moins sensible au choix d'un solveur numérique et plus rapide en termes de calcul, tous deux en raison de la dépendance à un référentiel non roulant.

Sur la base des difficultés connues dans les conditions expérimentales, plusieurs paramètres du modèle — tels que les valeurs initiales des variables d'état et les valeurs nominales des coefficients aérodynamiques — ont été considérés comme incertains dans les intervalles connus. Dans un tel contexte, GSA a permis de mieux comprendre le comportement physique du modèle quasi LPV et de valider son comportement comme équivalent au modèle non linéaire. De plus, comme les paramètres non sensibles ne sont pas identifiables, l'approche a permis de déterminer quels paramètres du modèle peuvent être considérés comme non identifiables, soit pendant tout le vol, soit pendant certaines périodes de celui-ci. Cet aspect du travail peut être considéré comme une approche pratique pour mieux comprendre les variations paramétriques au sein du modèle.

L'organisation de la thèse est la suivante.

Le chapitre 1 présente le modèle non linéaire d'un projectile et son cas d'utilisation. Ce chapitre présente les détails du site de test de l'ISL et les méthodes de mesure disponibles, les spécificités de l'architecture étudiée et du modèle non linéaire actuellement utilisé. Cette partie sera utilisée comme base pour les développements ultérieurs de la thèse.

Chapter 2 décrit l'approche de modélisation utilisée pour développer une représentation quasi-LPV d'un projectile en vol. Dans un premier temps, l'état de l'art de la modélisation LPV et quasi-LPV est présenté, y compris les méthodes les plus populaires et leurs avancées récentes. Ensuite, les spécificités du projectile de 155 mm stabilisé en rotation sont présentées dans le contexte des systèmes LPV et quasi-LPV — à savoir les implications de l'absence de signal d'entrée contrôlé, l'impossibilité d'une linéarisation ponctuelle et la nécessité de préserver le comportement non linéaire du système — afin de motiver le choix de la substitution de fonction analytique comme méthode appliquée dans la thèse. Le reste de ce chapitre est consacré au développement analytique d'un modèle quasi LPV dans le cadre de référence non glissant et à son évaluation de la précision numérique ultérieure.

Chapter 3 est dédié à la GSA du modèle quasi-LPV proposé au chapitre 2. Tout d'abord, la recherche bibliographique sur la GSA est présentée. Elle est suivie de la mise en place de l'analyse adaptée aux conditions expérimentales décrites au chapitre 1. Dans la suite, les résultats de la GSA et leur interprétation physique sont présentés.

Cette thèse a été menée en coopération avec l'Institut franco-allemand de recherche de Saint-Louis et le Centre de recherche automatique de Nancy (CRAN) de l'Université de Lorraine. Le financement nécessaire a été fourni par la Direction générale de l'armement (DGA) du ministère français des Forces armées. Le domaine de recherche couvert par cette thèse porte sur l'interconnexion des intérêts de ces trois organismes. La mission principale de l'ISL est de mener

---

des études de recherche et de pré-développement dans les domaines de la défense et de la sécurité. Le groupe Aerodynamics and eXterior Ballistics (ABX) de l'ISL, qui a lancé le projet, s'occupe de l'étude du comportement aérodynamique en vol de diverses architectures innovantes. Le CRAN se concentre sur la modélisation, l'identification et l'analyse de sensibilité de diverses structures de modèle dans leurs applications. Enfin, le domaine d'activité de la DGA réside dans le développement et la fourniture de nouveaux systèmes d'armes pour les forces armées françaises.

Les développements accomplis dans la thèse peuvent servir d'indication de plusieurs perspectives possibles dans les projets de recherche à venir.

L'identification des paramètres incertains du modèle peut être envisagée comme une étape future naturelle de l'analyse. Une telle tâche serait difficile à réaliser en utilisant des données du monde réel, car tous les signaux de programmation du modèle quasi-LPV ne peuvent pas être considérés comme mesurables dans le contexte d'expériences en vol libre. Par conséquent, cette entreprise nécessiterait une estimation simultanée des paramètres du modèle, mais également de la valeur actuelle des variables d'état d'ordonnement non mesurées. Peut-être que des observateurs non linéaires, comme un filtre de Kalman étendu, seraient capables d'effectuer cette tâche. Cependant, leur conception dépendrait directement d'une analyse potentielle d'identification.

Le développement du modèle Quasi-LPV a été basé sur une transformation de référentiel non glissant. En fait, ce n'est pas la seule transformation possible, car une réduction similaire de la complexité du temps de calcul peut être obtenue en appliquant une transformation sans rotation [142, 141]. À la connaissance de l'auteur, une telle transformation n'a pas été appliquée dans des applications de contrôle ou d'identification, donc sa pertinence n'est pas entièrement évaluée. Cela pourrait être particulièrement intéressant dans le cas de l'analyse de l'identifiabilité, car une structure de modèle différente pourrait entraîner des perspectives de conception de l'identifiabilité et des observateurs différentes.

L'hypothèse sous-jacente utilisée dans le processus de développement d'un modèle quasi-LPV est que le projectile est stabilisé en rotation sans moyens de contrôle. Si le projectile était stabilisé par des ailettes ou guidé par des actionneurs, le processus de modélisation devrait être revu. Un tel réglage représenterait une tâche plus traditionnelle de conception de modèle quasi-LPV, en raison de la présence d'un signal d'entrée dans la structure du modèle non linéaire.

Les perspectives susmentionnées pourraient même aider davantage les efforts à long terme de développement d'un modèle quasi-LPV qui serait valable quelle que soit l'architecture d'un projectile, et qui pourrait être utilisé pour une identification en temps réel.



# List of Figures

1	Exemplary long-range artillery architectures . . . . .	1
1.1	Architecture of the 155 mm projectile (dimensions in mm). . . . .	6
1.2	Example of experimental set-up on the ISL's test site. . . . .	7
1.3	Reference frames: Earth, wind and body axes . . . . .	8
1.4	Representation of state variables of a spin-stabilised projectile. . . . .	10
2.1	Evolution of exemplary state variables as calculated in both reference frames. . .	33
2.2	Evolution of the aerodynamic variables. . . . .	33
2.3	Evolution of the exemplary aerodynamic coefficients. . . . .	34
2.4	Comparison of exact and numerical solutions . . . . .	36
2.5	Convergence of a numerical solution for the nonlinear model on the example of the pitch rate $q$ . . . . .	37
2.6	The <i>rms</i> difference <i>w.r.t.</i> solution of the fifth-order solver with $20 \mu s$ . . . . .	38
2.7	Root mean square difference <i>w.r.t.</i> solution of the fifth-order solver with $300 \mu s$ .	38
2.8	Convergence of a numerical solution for the quasi-LPV model on the example of the pitch rate $q$ . . . . .	39
2.9	Consequences of poor selection of the <i>ODE</i> solvers: difference in $\alpha_t$ evolution for long-range trajectory . . . . .	42
2.10	Comparison of fixed-step solutions in both frames . . . . .	42
2.11	Comparison of variable-step solutions in both frames . . . . .	43
3.1	A framework selection tree for the sensitivity analysis . . . . .	48
3.2	Diagram of the global sensitivity analysis. . . . .	55
3.3	Exemplary results: an illustration of the domination of angular and translational velocities over all the other uncertain parameters. . . . .	56
3.4	Sum of main sensitivity indices for each output signal. The results suggest the additive nature of the model. . . . .	57
3.5	Sensitivity indices <i>w.r.t.</i> the initial Euler angles. . . . .	58
3.6	Sensitivity indices <i>w.r.t.</i> the aerodynamic coefficients. . . . .	59
3.7	Exemplary results: an illustration of the additive nature of the model and non- identifiability of the mass. . . . .	60
3.8	Sensitivity of $G_y$ to $r_0$ for normal and sparse sampling . . . . .	61
3.9	Comparison of sensitivity indices of Mara and standard Sobol methods. . . . .	61
1	Architectures d'artillerie à longue portée exemplaires . . . . .	75
2	Architecture du projectile 155 mm (dimensions en mm). . . . .	77



# List of Tables

1.1	Physical properties of the studied projectile. . . . .	6
1.2	Summary of state and output variables, and of the global aerodynamic coefficients. . . . .	14
2.1	Duration of a simulation for the non-rolling and variable-roll model structures. . . . .	39
2.2	Variable-roll reference frame: order of magnitude of the <i>rms</i> difference between the reference solution and variable-step simulations' results of the nonlinear model . . . . .	40
2.3	Non-rolling reference frame: order of magnitude of the <i>rms</i> difference between the reference solution and variable-step simulations' results of the quasi-LPV model . . . . .	40
2.4	Range of variation of state variables and the order of magnitude of the final-step difference <i>w.r.t.</i> the reference solution . . . . .	43
3.1	Rules for interpreting the obtained sensitivity indices. . . . .	49
3.2	Uncertain initial state variables . . . . .	54
3.3	Uncertain projectile parameters . . . . .	54
3.4	Sensitivity of uncertain state variables. . . . .	59
3.5	Sensitivity of uncertain model parameters. . . . .	60



# Bibliography

- [1] M. Albisser. “Identification of aerodynamic coefficients from free flight data”. PhD thesis. University of Lorraine, 2015.
- [2] M. Albisser and S. Dobre. “Sensitivity Analysis for Global Parameter Identification. Application to Aerodynamic Coefficients”. In: *IFAC-PapersOnLine* 51.15 (2018), pp. 963–968. ISSN: 24058963. DOI: 10.1016/j.ifacol.2018.09.069.
- [3] M. Albisser et al. “Aerodynamic Characterization of a New Concept of Long Range Projectiles from Free Flight Data”. In: *30th International Symposium on Ballistics*. Ed. by S. Chocron and J. Walker. Long Beach, CA, 2017.
- [4] M. Albisser et al. “Aerodynamic Coefficient Identification of a Space Vehicle from Multiple Free-Flight Tests”. In: *Journal of Spacecraft and Rockets* 54.2 (2017), pp. 426–435. ISSN: 0022-4650. DOI: 10.2514/1.A33587.
- [5] R. Ashino, M. Nagase, and R. Vaillancourt. “Behind and Beyond the MATLAB ODE Suite”. In: *Computers and mathematics with applications* 40 (2000), pp. 491–512. DOI: 10.1016/S0898-1221(00)00175-9.
- [6] S. P. Banks and S. K. Al-Jurani. “Pseudo-linear systems, Lie algebras, and stability”. In: *IMA Journal of Mathematical Control and Information* 13.4 (1996), pp. 385–401. ISSN: 1471-6887. DOI: 10.1093/imamci/13.4.385.
- [7] B. Barnett. *Trajectory equations for a six-degree-of-freedom missile*. Tech. rep. Dover, New Jersey: Picatinny Arsenal, 1962.
- [8] B. Barnett. *Trajectory equations for a six-degree-of-freedom missile using a fixed-plane coordinate system*. Tech. rep. Dover, New Jersey: Picatinny Arsenal, 1966.
- [9] G. Blatman and B. Sudret. “Efficient computation of global sensitivity indices using sparse polynomial chaos expansions”. In: *Reliability Engineering and System Safety* 95.11 (2010), pp. 1216–1229. ISSN: 09518320. DOI: 10.1016/j.ress.2010.06.015.
- [10] E. Borgonovo and E. Plischke. “Sensitivity analysis: A review of recent advances”. In: *European Journal of Operational Research* 248.3 (2016), pp. 869–887. ISSN: 03772217. DOI: 10.1016/j.ejor.2015.06.032.
- [11] C. Brustlein. “Maîtriser la puissance de feu: un défi pour les forces terrestres”. In: *Focus stratégique*, 61 (2015).
- [12] F. Bruzelius, S. Pettersson, and C. Breitholtz. “Linear parameter-varying descriptions of nonlinear systems”. In: *Proceeding of the American Control Conference*. 2004, pp. 1374–1379. ISBN: 0-7803-8335-4.
- [13] J. Bryson et al. “Approach for Understanding Range Extension of Gliding Indirect Fire Munitions”. In: *2018 AIAA Atmospheric Flight Mechanics Conference*. 2018, pp. 1–20. DOI: 10.2514/6.2018-3158.

- [14] J. D. Caigny, J. Camino, and J. Swevers. “Identification of MIMO LPV models based on interpolation”. In: *Proceedings of the International Conference on Noise and Vibration Engineering*. 2008, pp. 2631–2644. ISBN: 9781615671915.
- [15] D. E. Carlucci and S. S. Jacobson. *Ballistics: Theory and Design of Guns and Ammunition*. 3rd ed. Boca Raton, Miami, Florida, USA: Taylor & Francis Group, 2018. ISBN: 978-1-138-05531-5.
- [16] S. Changey, E. Pecheur, and T. Brunner. “Attitude Estimation of a projectile using Magnetometers and Accelerometers: Experimental Validation”. In: *IEEE/ION PLANS Symposium 2014* (2014), pp. 1168–1173. DOI: 10.1109/PLANS.2014.6851488.
- [17] H. Chaofan et al. “Linear parameter-varying attitude controller design for a reusable launch vehicle during reentry”. In: *IEEE CGNCC 2014*. 2014. ISBN: 9781479946990. DOI: 10.1109/CGNCC.2014.7007596.
- [18] G.-Y. Chung. “An Analytical Approach to Real-Time Linearization of a Gas Turbine Engine Model”. PhD thesis. Georgia Institute of Technology, 2013.
- [19] R. Colgren. *Method and System for Estimation and Correction of the Angle of Attack and Sideslip Angle from Acceleration Measurements*. 1999.
- [20] M. Cook. *Flight Dynamics Principles: A Linear Systems Approach to Aircraft Stability and Control*. 2nd ed. Burlington, MA: Elsevier Butterworth-Heinemann, 2007. ISBN: 978-0-7506-6927-6.
- [21] M. Costello and A. Peterson. *Linear Theory of a Dual-Spin Projectile in Atmospheric Flight*. Tech. rep. Army Research Laboratory, 2000.
- [22] R. I. Cukier, H. B. Levine, and K. E. Shuler. “Nonlinear Sensitivity Analysis of Multiparameter Model Systems”. In: *Journal of Computational Physics* 26.1 (1978), pp. 1–42.
- [23] R. I. Cukier, J. H. Schaibly, and K. E. Shuler. “Study of the sensitivity of coupled reaction systems to uncertainties in rate coefficients. III. Analysis of the approximations”. In: *Journal of Chemical Physics* 63.3 (1975), pp. 1140–1149.
- [24] R. I. Cukier et al. “Study of the sensitivity of coupled reaction systems to uncertainties in rate coefficients. I Theory”. In: *Journal of Chemical Physics* 59.8 (1973), pp. 3873–3878. ISSN: 10897690. DOI: 10.1063/1.1680571.
- [25] J. Dannenhoffer and R. Haimes. “Design Sensitivity Calculations Directly on CAD-based Geometry”. In: *AIAA Scitech 2015 Forum*. 2015, pp. 1–25. DOI: 10.2514/6.2015-1370.
- [26] H. Demailly. “Identification des coefficients aérodynamiques d’un projectile à partir de mesures prises en vol”. PhD thesis. Université d’Orléans, 2011.
- [27] H. Demailly et al. “Identification inverse des coefficients aérodynamiques d’un engin hypersonique à partir de données issues de vol”. In: *20ème Congrès Français de Mécanique*. 2011.
- [28] S. Dobre et al. “Identification of the Aerodynamic Coefficients of a 155mm Artillery Shell Based on Free Flight Data”. In: *29th International Symposium on Ballistics*. 2016.
- [29] S. Dobre et al. “Limits of variance-based sensitivity analysis for non-identifiability testing in high dimensional dynamic models”. In: *Automatica* 48.11 (2012), pp. 2740–2749. DOI: 10.1016/j.automatica.2012.05.004.

- 
- [30] F. Donida et al. “Integrated modelling and parameter estimation: an LFT-Modelica approach”. In: *Joint 48th IEEE Conference on Decision and Control and 28th Chinese Control Conference*. 2009, pp. 8357–8362.
- [31] A. Dupuis and C. Berner. “Wind Tunnel Tests of a Long Range Artillery Shell Concept”. In: *AIAA Atmospheric Flight Mechanics Conference and Exhibit*. 2002, pp. 1–9.
- [32] M. Fischer and W. Hathaway. *Aeroballistic Research Facility Data Analysis System*. Tech. rep. Eglin Air Force Base, USA, 1988.
- [33] V. Fleck, E. Sommer, and M. Brökelmann. “Study of real-time filtering for an Inertial Measurement Unit (IMU) with magnetometer in a 155mm projectile”. In: *IEEE/ION Position, Location, And Navigation Symposium*. 2006, pp. 803–807. ISBN: 0-7803-9454-2. DOI: 10.1109/PLANS.2006.1650676.
- [34] S. Fleischmann et al. “A Systematic LPV/LFR Modelling Approach Optimized for Linearised Gain Scheduling Control Synthesis”. In: *AIAA Modeling and Simulation Technologies Conference (2016)*. DOI: 10.2514/6.2016-1921.
- [35] G. Frost and M. Costello. “Linear Theory of a Projectile With a Rotating Internal Part in Atmospheric Flight”. In: *Journal of Guidance Control and Dynamics* 27.5 (2004), pp. 898–906. DOI: 10.2514/1.1115.
- [36] A. Fujimori. “Descriptor Polytopic Model of Aircraft and Gain Scheduling State Feedback Control”. In: *Transactions of the Japan Society for Aeronautical and Space Sciences* 47.156 (2004), pp. 138–145.
- [37] A. Fujimori and L. Ljung. “Model identification of linear parameter varying aircraft systems”. In: *Proceedings of the Institution of Mechanical Engineers, Aerospace Engineering Journal* 220 Part G (2007).
- [38] A. S. Ghersin and R. S. Sanchez Pena. “LPV control of a 6-DOF vehicle”. In: *IEEE Transactions on Control Systems Technology* 10.6 (2002), pp. 883–887. ISSN: 10636536. DOI: 10.1109/TCST.2002.804123.
- [39] B. Gudmundsson. “The French Artillery in the First World War”. In: *King of Battle: Artillery in World War I*. Ed. by S. Marble. Brill Academic Pub, 2016. Chap. 3. ISBN: 978-9004305243.
- [40] L. E. Hale, M. Patil, and C. J. Roy. “Sensitivity Analysis Methods for Systems with Epistemic Uncertainties”. In: *AIAA Scitech 2015 Forum*. 2015, pp. 1–8. DOI: 10.2514/6.2015-1818.
- [41] D. M. Hamby. “A review of techniques for parameter sensitivity analysis of environmental models”. In: *Environmental Monitoring and Assessment* 32.2 (1994), pp. 135–154. ISSN: 01676369. DOI: 10.1007/BF00547132.
- [42] N. Hamel and E. Gagnon. “CFD and Parametric Study on a 155 mm Artillery Shell Equipped with a Roll-Decoupled Course Correction Fuze”. In: *29th AIAA Applied Aerodynamics Conference*. 2011, pp. 1–10.
- [43] D. Henrion et al. *Linearization and Identification of Aircraft Turbofan Engine Models*. Tech. rep. 2004.
- [44] C. Hoffmann and H. Werner. “A survey of linear parameter-varying control applications validated by experiments or high-fidelity simulations”. In: *IEEE Transactions on Control Systems Technology* 23.2 (2015), pp. 416–433.

- [45] R. Holsapple, R. Iyer, and D. Doman. “Variable Step-size Selection Methods for Implicit Integration Schemes for ODES”. In: *International Journal of Numerical Analysis and Modeling* 4.2 (2007), pp. 210–240. ISSN: 17055105. DOI: 10.1109/ACC.2006.1657179.
- [46] T. Homma and A. Saltelli. “Importance measures in global sensitivity analysis of nonlinear models”. In: *Reliability Engineering & System Safety* 52 (1996), pp. 1–17. ISSN: 09518320. DOI: 10.1016/0951-8320(96)00002-6.
- [47] X. Huan et al. “Global Sensitivity Analysis and Estimation of Model Error, Toward Uncertainty Quantification in Scramjet Computations”. In: *AIAA Journal* 56.3 (2018), pp. 1170–1184. DOI: 10.2514/1.J056278.
- [48] T. E. Hull et al. “Comparing Numerical Methods for Ordinary Differential Equations”. In: *SIAM Journal on Numerical Analysis* 9.4 (1974), pp. 603–637. DOI: 10.1137/0711054.
- [49] R. L. Iman and S. C. Hora. “A Robust Measure of Uncertainty Importance for Use in Fault Tree System Analysis”. In: *Risk Analysis* 10.3 (1990), pp. 401–406. ISSN: 15396924. DOI: 10.1111/j.1539-6924.1990.tb00523.x.
- [50] B. Iooss and P. Lemaître. “A Review on Global Sensitivity Analysis Methods”. In: *Uncertainty Management in Simulation-Optimization of Complex Systems*. Ed. by G. Dellino and C. Meloni. Vol. 59. Springer US, 2015. Chap. 5, pp. 101–122. ISBN: 978-1-4899-7546-1. DOI: 10.1007/978-1-4899-7547-8.
- [51] Z. Jiang, W. Chen, and B. J. German. “Multidisciplinary Statistical Sensitivity Analysis Considering Both Aleatory and Epistemic Uncertainties”. In: *AIAA Journal* 54.4 (2016), pp. 1326–1338. ISSN: 0001-1452. DOI: 10.2514/1.J054464.
- [52] A. Al-jiboory et al. “LPV Model Development for a Flexible Wing Aircraft”. In: *58th AIAA/ASCE/AHS/ASC Structures, Structural Dynamics, and Materials Conference*. Grapevine, TX, 2017. DOI: 10.2514/6.2017-1817.
- [53] T. A. Johansen et al. “Off-equilibrium linearisation and design of gain-scheduled control with application to vehicle speed control”. In: *Control Engineering Practice* 6.2 (1998), pp. 167–180. ISSN: 09670661. DOI: 10.1016/S0967-0661(98)00015-X.
- [54] A. V. Kamalapur, M. Yilmaz, and S. Adediran. “Linear Parameter Varying Modeling and Control of a Nonlinear Power Plant”. In: *Seventh Annual IEEE Green Technologies Conference*. 2015. ISBN: 978-1-4799-8884-6. DOI: 10.1109/GREENTECH.2015.11.
- [55] G. S. Kinne, J. A. Tanzi, and J. W. Yaeger. “FA PGMs: Revolutionizing Fires for the Ground Force Commander”. In: *Field Artillery, May-June* (2006), pp. 16–21.
- [56] J. P. Kleijnen and J. C. Helton. “Statistical analyses of scatterplots to identify important factors in large-scale simulations, 1: Review and comparison of techniques”. In: *Reliability Engineering and System Safety* 65.2 (1999), pp. 147–185. ISSN: 0951-8320. DOI: 10.1016/S0951-8320(98)00091-X.
- [57] J. P. Kleijnen and J. C. Helton. “Statistical analyses of scatterplots to identify important factors in large-scale simulations, 2: Robustness of techniques”. In: *Reliability Engineering and System Safety* 65.2 (1999), pp. 187–197. ISSN: 09518320. DOI: 10.1016/S0951-8320(98)00090-8.
- [58] M. E. Knapp et al. “Development of a Full Flight Envelope F-16 VISTA Simulation Model from Closed-loop Flight Data”. In: *AIAA Atmospheric Flight Mechanics Conference*. 2018. DOI: 10.2514/6.2018-0525.

- 
- [59] A. Kwiatkowski, M.-T. Boll, and H. Werner. “Automated Generation and Assessment of Affine LPV Models”. In: *Proceedings of the 45th IEEE Conference on Decision and Control*. 2. 2006, pp. 6690–6695. ISBN: 1-4244-0171-2. DOI: 10.1109/CDC.2006.377768.
- [60] E. V. D. Laan, F. Veldpaus, and M. Steinbuch. “LPV Modeling of Vehicle Occupants”. In: *Proceedings of the 9th International Symposium on Advanced Vehicle Control*. 2008, pp. 620–625.
- [61] W. E. Larimore. “ADAPT-lpv software for identification of nonlinear parameter-varying systems”. In: *IFAC Proceedings Volumes*. Vol. 45. 16. 2012, pp. 1820–1825. ISBN: 9783902823069. DOI: 10.3182/20120711-3-BE-2027.00418.
- [62] L. H. Lee. “Identification and robust control of linear parameter-varying systems”. PhD thesis. University of California at Berkeley, 1997.
- [63] M. Leitão, F. Peter, and F. Holzapfel. “Adaptive Augmentation of a Fighter Aircraft Autopilot Using a Nonlinear Reference Model”. In: *Proc. of the EuroGNC 2013*. 2013, pp. 1464–1483.
- [64] D. J. Leith and W. E. Leithead. “Appropriate Realisation of MIMO Gain-Scheduled Controllers”. In: *International Journal of Control* 70.1 (1998). DOI: 10.1080/002071798222442.
- [65] D. J. Leith and W. E. Leithead. “Gain-scheduled controller design: An analytic framework directly incorporating non-equilibrium plant dynamics”. In: *International Journal of Control* 70 (1998), pp. 249–269. ISSN: 0020-7179. DOI: 10.1080/002071798222398.
- [66] D. J. Leith and W. E. Leithead. “Survey of Gain-Scheduling Analysis & Design”. In: *International Journal of Control* 73.11 (2000), pp. 1001–1025. DOI: 10.1080/002071700411304.
- [67] D. J. Leith et al. “Application of velocity-based gain-scheduling to lateral auto-pilot design for an agile missile”. In: *Control Engineering Practice* 9 (2001), pp. 1079–1093. DOI: 10.1016/S0967-0661(01)00077-6.
- [68] D. J. Leith et al. “Comments on gain scheduling dynamic linear controllers for a non linear plant”. In: *Automatica* 34.8 (1998), pp. 1041–1043.
- [69] D. Machala et al. “Global Sensitivity Analysis for Modeling the Free-Flight Behavior of an Artillery Projectile”. In: *AIAA Journal (submitted)* (2019), pp. 1–21.
- [70] D. Machala et al. “Global Sensitivity Analysis of ballistic free-flight experiments: does the model preserve the behaviour of the system”. In: *Ninth International Conference on Sensitivity Analysis of Model Output, SAMO 2019*. Barcelona, Spain, 2019.
- [71] D. Machala et al. “LPV Modelling of the Atmospheric Re-Entry Vehicle in Free Flight”. In: *20th IFAC World Congress*. Toulouse, France, 2017.
- [72] D. Machala et al. “Quasi-LPV modelling of a projectile’s behaviour in flight”. In: *18th IFAC Symposium on System Identification, SYSID2018*. Elsevier B.V., 2018, pp. 1080–1085. DOI: 10.1016/j.ifacol.2018.09.050.
- [73] D. Machala et al. “The Analysis of Vehicle’s In-Flight Behaviour Using Quasi-LPV and Nonlinear Models”. In: *AIAA Scitech 2019 Forum*. San Diego, CA, 2019, pp. 1–12. DOI: 10.2514/6.2019-1321.
- [74] D. Makhija and P. S. Beran. “Spiral: A General Framework For Parameter Sensitivity Analysis”. In: *AIAA Scitech 2017 Forum*. 2017, pp. 1–16. DOI: 10.2514/6.2017-1306.

- [75] T. A. Mara and O. Rakoto. “Comparison of some efficient methods to evaluate the main effect of computer model factors”. In: *Journal of Statistical Computation and Simulation* 78.2 (2008), pp. 167–178. ISSN: 0094-9655. DOI: 10.1080/10629360600964454.
- [76] T. A. Mara and S. Tarantola. “Variance-based sensitivity indices for models with dependent inputs”. In: *Reliability Engineering and System Safety* 107 (2012), pp. 115–121. ISSN: 09518320. DOI: 10.1016/j.ress.2011.08.008.
- [77] A. E. Marcos and G. J. Balas. “Development of Linear Parameter Varying Models for Aircraft”. In: *Journal of Guidance Control and Dynamics* 27.2 (2004), pp. 218–228.
- [78] A. E. Marcos and G. J. Balas. “Linear parameter varying modeling of the Boeing 747-100/200 longitudinal motion”. In: *AIAA GNC Conference*. 2001, pp. 1–11. ISBN: 9781563479786.
- [79] A. Marcos et al. “Application of LPV modeling, design and analysis methods to a re-entry vehicle”. In: *AIAA GNC Conference*. 2010. ISBN: 9781600869624 (ISBN). DOI: 10.2514/6.2010-8192.
- [80] MathWorks. *Control System Toolbox: LPV System block documentation (R2014a)*. 2014.
- [81] B. N. McMaster et al. *Historical Overview of the Nike Missile System*. Tech. rep. Aberdeen Proving Ground, USA: U.S. Army Toxic and Hazardous Materials Agency, 1983.
- [82] M. D. Morris. “Factorial plans for preliminary computational experiments”. In: *Technometrics* 33.2 (1991), pp. 161–174.
- [83] R. Murray-smith, T. A. Johansen, and R. Shorten. “On Transient Dynamics, Off-Equilibrium Behaviour and Identification In Blended Multiple Model Structures”. In: *European Control Conference*. September. 1999, pp. 3569–3574.
- [84] F. C. Paddison. “Talos Control System.” In: *Johns Hopkins APL Technical Digest (Applied Physics Laboratory)* 3.2 (1982), pp. 154–156. ISSN: 02705214.
- [85] F. Peter, M. Leitão, and F. Holzapfel. “Adaptive Augmentation of a New Baseline Control Architecture for Tail-Controlled Missiles Using a Nonlinear Reference Model”. In: *AIAA GNC Conference*. 2012. ISBN: 978-1-60086-938-9. DOI: 10.2514/6.2012-5037.
- [86] H. Pfifer. “LPV / LFT Modeling and its Application in Aerospace”. In: June (2013).
- [87] H. Pfifer. “Quasi-LPV Model of a NDI-Controlled Missile Based on Function Substitution”. In: *AIAA GNC Conference*. 2012, pp. 1–12. ISBN: 978-1-60086-938-9. DOI: 10.2514/6.2012-4970.
- [88] F. Pianosi, F. Sarrazin, and T. Wagener. “A Matlab toolbox for Global Sensitivity Analysis”. In: *Environmental Modelling and Software* 70 (2015), pp. 80–85. DOI: 10.1016/j.envsoft.2015.04.009.
- [89] F. Pianosi and T. Wagener. “Understanding the time-varying importance of different uncertainty sources in hydrological modelling using global sensitivity analysis”. In: *Hydrological Processes* 30.22 (2016), pp. 3991–4003. ISSN: 10991085. DOI: 10.1002/hyp.10968.
- [90] E. Plischke, E. Borgonovo, and C. L. Smith. “Global sensitivity measures from given data”. In: *European Journal of Operational Research* 226.3 (2013), pp. 536–550. ISSN: 03772217. DOI: 10.1016/j.ejor.2012.11.047.
- [91] S. Portier. *3D position and attitude determination of a vehicle in free flight based on 3D high-speed videos*. Tech. rep. French-German Research Institute of Saint-Louis, 2014.

- [92] W. Qin et al. “Robust parameter dependent receding horizon H-infinity control of flexible air-breathing hypersonic vehicles with input constraints”. In: *Asian Journal of Control* 17.2 (2015), pp. 508–522. ISSN: 19346093. DOI: 10.1002/asjc.1084.
- [93] M. Ratto, A. Pagano, and P. C. Young. “Non-parametric estimation of conditional moments for sensitivity analysis”. In: *Reliability Engineering and System Safety* 94 (2009), pp. 237–243. DOI: 10.1016/j.ress.2008.02.023.
- [94] L. Reberga et al. “LPV modeling of a turbofan engine”. In: *Proceedings of the International Federation of Automatic Control* 16 (2005), pp. 526–531. ISSN: 14746670. DOI: 10.3182/20050703-6-CZ-1902.00488.
- [95] E. de Rocquigny, N. Devictor, and S. Tarantola. “Chapter 18. Sensitivity analysis methods”. In: *Uncertainty in Industrial Practice*. Wiley and Sons, 2008, pp. 259–284. ISBN: 978-0-470-99447-4.
- [96] W. J. Rugh. “Analytical Framework for Gain Scheduling”. In: *1990 American Control Conference*. San Diego, CA, 1990, pp. 1688–1694. DOI: 10.23919/ACC.1990.4791022.
- [97] W. J. Rugh and J. S. Shamma. “Research on gain scheduling”. In: *Automatica* 36.10 (2000), pp. 1401–1425. DOI: 10.1016/S0005-1098(00)00058-3.
- [98] A. Saltelli. “Making best use of model evaluations to compute sensitivity indices”. In: *Computer Physics Communications* 145 (2002), pp. 280–297.
- [99] A. Saltelli, S. Tarantola, and K. P. Chan. “A Quantitative Model-Independent Method for Global Sensitivity Analysis of Model Output”. In: *Technometrics* 41.1 (1999), pp. 39–56.
- [100] A. Saltelli et al. *Global Sensitivity Analysis. The Primer*. Wiley and Sons, 2007, pp. 237–275. ISBN: 9780470725184. DOI: 10.1002/9780470725184.
- [101] A. Saltelli et al. “Sensitivity analysis for chemical models”. In: *Chemical Reviews* 105.7 (2005), pp. 2811–2827. ISSN: 00092665. DOI: 10.1021/cr040659d.
- [102] A. Saltelli et al. *Sensitivity analysis in practice*. John Wiley & Sons Ltd., 2004. ISBN: 0-470-87093-1.
- [103] A. Saltelli et al. “Variance based sensitivity analysis of model output. Design and estimator for the total sensitivity index”. In: *Computer Physics Communications* 181.2 (2010), pp. 259–270. ISSN: 00104655. DOI: 10.1016/j.cpc.2009.09.018.
- [104] A. Saltelli et al. “Why So Many Published Sensitivity Analyses Are False. A Systematic Review of Sensitivity Analysis Practices”. In: *Environmental Modelling and Software* 114 (2019), pp. 29–39. DOI: 10.1016/j.envsoft.2019.01.012.
- [105] P. L. dos Santos et al. *Linear Parameter-Varying System Identification New Developments and Trends*. 1st. Vol. 14. World Scientific, 2011. ISBN: 978-981-4355-44-5.
- [106] J. H. Schaibly and K. E. Shuler. “Study of the sensitivity of coupled reaction systems to uncertainties in rate coefficients. II Applications”. In: *Journal of Chemical Physics* 59.8 (1973), pp. 3879–3888. ISSN: 10897690. DOI: 10.1063/1.1680572.
- [107] W. Schoutens. *Stochastic Processes and Orthogonal Polynomials*. Springer-Verlag New York, Inc., 2000. ISBN: 9783642124648. DOI: 10.1007/978-1-4612-5056-2.
- [108] F. Sève and S. Theodoulis. “Design of an H-infinity Gain-Scheduled Guidance Scheme for a Guided Projectile”. In: *AIAA Scitech 2019 Forum*. 2019, pp. 1–23. ISBN: 978-1-62410-578-4. DOI: 10.2514/6.2019-2345.

- [109] F. Sève et al. “Pitch/Yaw Channels Control Design for a 155mm Projectile with Rotating Canards, using a H-infinity Loop-Shaping Design Procedure”. In: *AIAA GNC Conference*. 2014, pp. 1–24. ISBN: 9781600869624. DOI: 10.2514/6.2014-1474.
- [110] J. S. Shamma and M. Athans. “Analysis of Gain Scheduled Control for Nonlinear Plants”. In: *IEEE Transactions on Automatic Control* 35.8 (1990), pp. 898–907. ISSN: 15582523. DOI: 10.1109/9.58498.
- [111] J. S. Shamma and J. R. Cloutier. “Gain-scheduled missile autopilot design using linear parameter varying transformations”. In: *Journal of Guidance, Control, and Dynamics* 16.2 (1993), pp. 256–263. ISSN: 0731-5090. DOI: 10.2514/3.20997.
- [112] L. F. Shampine and M. W. Reichelt. “The MATLAB ODE Suite”. In: *SIAM Journal on Scientific Computing* 18.1 (1997), pp. 1–22. ISSN: 1064-8275. DOI: 10.1137/S1064827594276424.
- [113] J. Y. Shin. *Quasi-Linear Parameter Varying Representation of General Aircraft Dynamics Over Non-Trim Region*. Tech. rep. USA: National Institute of Aerospace, 2005.
- [114] J. Y. Shin, G. J. Balas, and A. M. Kaya. “Blending Approach Of Linear Parameter Varying Control Synthesis For F-16 Aircraft”. In: *Journal of Guidance Control and Dynamics* 25.6 (2002).
- [115] J.-Y. Shin. “Worst-case analysis and linear parameter-varying gain-scheduled control of aerospace systems”. PhD thesis. University of Minnesota, 2000.
- [116] R. Shorten et al. “On the interpretation of local models in blended multiple model structures”. In: *International Journal of Control* 72.7-8 (1999), p. 620. DOI: 10.1080/002071799220812.
- [117] I. M. Sobol. “Sensitivity estimates for nonlinear mathematical models”. In: *Mathematical modelling and computational experiments* 1.4 (1993), pp. 407–414.
- [118] K. Srinivasarengan. “State and parameter estimation, and identifiability of quasi-LPV models”. PhD thesis. Université de Lorraine, 2018.
- [119] R. F. Stengel. *Flight Dynamics*. Princeton University Press, 2004. ISBN: 9780691114071.
- [120] G. Strub. “Modeling, Identification and Control of a Guided Projectile in a Wind Tunnel”. PhD thesis. Université de Haute-Alsace, 2016.
- [121] B. Sudret. “Global sensitivity analysis using polynomial chaos expansions”. In: *Reliability Engineering and System Safety* 93.7 (2008), pp. 964–979. ISSN: 09518320. DOI: 10.1016/j.ress.2007.04.002.
- [122] I. Szász, P. Gáspár, and J. Bokor. “Nonlinear Active Suspension Modelling Using Linear Parameter Varying Approach”. In: *10th Mediterranean Conference on Control and Automation*. 2002.
- [123] I. Szász et al. “Linear Parameter-Varying Detection Filter Design for a Boeing 747-100/200 Aircraft”. In: *Journal of Guidance Control and Dynamics* 28.3 (2005), pp. 461–470. ISSN: 07315090. DOI: 10.2514/1.6689.
- [124] W. Tan. *Application of linear parameter-varying control theory*. Master’s thesis. 1997.
- [125] W. Tan, A. K. Packard, and G. J. Balas. “Quasi-LPV Modeling and LPV Control of a Generic Missile”. In: *Proceeding of the American Control Conference*. 2000, pp. 3692–3696.

- 
- [126] S. Tarantola and T. A. Mara. “Variance-Based Sensitivity Indices of Computer Models With Dependent Inputs: the Fourier Amplitude Sensitivity Test”. In: *International Journal for Uncertainty Quantification* 7.6 (2017), pp. 511–523. ISSN: 2152-5080. DOI: 10.1615/int.j.uncertaintyquantification.2017020291.
- [127] S. Theodoulis et al. “LPV modeling of guided projectiles for terminal guidance”. In: *18th Mediterranean Conference on Control and Automation, MED’10 - Conference Proceedings* (2010), pp. 1455–1460. DOI: 10.1109/MED.2010.5547843.
- [128] W. Toledo et al. “Aeroballistics Diagnostics Fuze (DFuze) Analysis of a 120 mm Mortar Munition”. In: *AIAA Infotech at Aerospace Conference*. Seattle, USA: American Institute of Aeronautics and Astronautics, 2009. DOI: 10.2514/6.2009-2022.
- [129] S. Torres. “Trajectory Accuracy Sensitivity to Modeling Factors”. In: *15th AIAA Aviation Technology, Integration, and Operations Conference AIAA*. June. Dallas, TX, 2015, pp. 1–19. DOI: 10.2514/6.2015-2599.
- [130] R. Tóth. *Modeling and Identification of Linear Parameter-Varying Systems*. Vol. 403. Springer, 2010. ISBN: 978-3-642-13811-9. DOI: 10.1007/978-3-642-13812-6.
- [131] R. Tóth. “Modeling and Identification of Linear Parameter-Varying Systems an Orthonormal Basis Function Approach”. PhD thesis. Delft University of Technology, 2008, p. 382. ISBN: 9789090237428.
- [132] R. Tóth et al. “Discrete time LPV I/O and state space representations, differences of behavior and pitfalls of interpolation”. In: *Proc. of the European Control Conference* 0.4 (2007), pp. 5418–5425.
- [133] V. Verdult, M. Lovera, and M. Verhaegen. “Identification of linear parameter-varying state-space models with application to helicopter rotor dynamics”. In: *International Journal of Control* 77.13 (2004), pp. 1149–1159. DOI: 10.1080/0020717042000274527.
- [134] A. Vitale and F. Corraro. “Identification from flight data of the italian unmanned space vehicle”. In: *16th IFAC Symposium on System Identification*. Vol. 45. 16. IFAC, 2012, pp. 1419–1424. ISBN: 9783902823069. DOI: 10.3182/20120711-3-BE-2027.00336.
- [135] D. Vizer, G. Mercère, and E. Laroche. “Gray-box LPV model identification of a 2-DoF surgical robotic manipulator by using an H-infinity norm-based local approach”. In: *Proceedings of the International Federation of Automatic Control Workshop on Linear Parameter Varying Systems* April 2016 (2015), pp. 79–84. ISSN: 24058963. DOI: 10.1016/j.ifacol.2015.11.117.
- [136] H. M. Wagner. “Global Sensitivity Analysis Software”. In: *Operations Research* 43.6 (1995), pp. 948–969. DOI: 10.1287/opre.43.6.948.
- [137] L. Wang et al. “Sensitivity Analysis of Multidisciplinary Rotorcraft Simulations”. In: *AIAA Scitech 2017 Forum*. 2017, pp. 1–14. DOI: 10.2514/6.2017-1670.
- [138] M. Warwel et al. “Real-time thermal monitoring of power semiconductors in power electronics using linear parameter-varying models for variable coolant flow situations”. In: *IEEE 15th Workshop on Control and Modeling for Power Electronics, COMPEL 2014* (2014), pp. 1–6. DOI: 10.1109/COMPEL.2014.6877142.
- [139] P. Wei, Z. Lu, and J. Song. “Extended Monte Carlo Simulation for Parametric Global Sensitivity Analysis and Optimization”. In: *AIAA Journal* 52.4 (2014), pp. 867–878. ISSN: 0001-1452. DOI: 10.2514/1.j052726.

- [140] P. Wernert. *Simulation de trajectoires de projectiles à 6 degrés de liberté dans le cadre de la mécanique du vol avion. Partie 1 : Mise en équation et résolution par la méthode des quaternions*. Tech. rep. Saint-Louis, France: French-German Research Institute of Saint-Louis (ISL), 2004.
- [141] P. Wernert. *Simulations de trajectoires de projectiles à 6 degrés de liberté dans le cadre de la mécanique du vol avion. Partie 3 : Utilisation de repères non liés au projectile*. Tech. rep. Saint-Louis, France: French-German Research Institute of Saint-Louis (ISL), 2007.
- [142] P. Wernert, S. Theodoulis, and Y. Morel. “Flight Dynamics Properties of 155 mm Spin-Stabilized Projectiles Analyzed in Different Body Frames”. In: *AIAA AFM Conference*. 2010, pp. 1–17. ISBN: 978-1-62410-151-9. DOI: 10.2514/6.2010-7640.
- [143] B. A. White, L. Bruyere, and A. Tsourdos. “Missile autopilot design using quasi-LPV polynomial eigenstructure assignment”. In: *IEEE Transactions on Aerospace and Electronic Systems* 43.4 (2007), pp. 1470–1483. ISSN: 00189251. DOI: 10.1109/TAES.2007.4441752.
- [144] R. H. Whyte and W. H. Hathaway. *Aeroballistic Range Data Reduction Technique Using Numerical Integration*. Tech. rep. 1974.
- [145] M. J. Wilson. *Attitude Determination With Magnetometers for Gun-Launched Munitions*. Tech. rep. ARL-TR-3209. Aberdeen Proving Ground, USA: Army Research Laboratory, 2004.
- [146] C. Xu and G. Z. Gertner. “Uncertainty and sensitivity analysis for models with correlated parameters”. In: *Reliability Engineering and System Safety* 93.10 (2008), pp. 1563–1573. ISSN: 09518320. DOI: 10.1016/j.ress.2007.06.003.
- [147] M. A. York et al. “Efficient Aircraft Multidisciplinary Design Optimization and Sensitivity Analysis via Signomial Programming”. In: *AIAA Journal* 56.11 (2018), pp. 4546–4561. ISSN: 0001-1452. DOI: 10.2514/1.j057020.
- [148] P. H. Zipfel. *Modeling and Simulation of Aerospace Vehicle Dynamics*. 2nd ed. Blacksburg VA: AIAA Inc., 2007, p. 607. ISBN: 978-1-56347-875-8.



Free-flight experiments can be considered as a realistic source of aerodynamic data-based knowledge, since the behaviour of a projectile is observed under real flight conditions. However, the experimental framework introduces several sources of uncertainty: the initial flight conditions are unknown, and only an initial guess of aerodynamics of the projectile is available. Additionally, the nonlinear model structure used in identification of aerodynamic behaviour is different from the structures typically used in guidance and navigation activities, which necessitates switching between model structures---depending on the task at hand.

Such a setting lays the groundwork for the following main contributions developed in the thesis:

- A novel model structure is proposed: the nonlinear model equations are transformed into a quasi-LPV structure in a non rolling reference frame. The new structure resembles the ones used in guidance and navigation activities, while preserving the projectile's nonlinear behaviour. It is also much faster in computation time for the case of spin-stabilised projectiles, making it more efficient for simulations.
- Influence of the aforementioned uncertainties on the quasi-LPV model was assessed using global sensitivity analysis: it has allowed to determine which parameters of the model can be deemed non-identifiable, and to gain further insight into the physical behaviour of the quasi-LPV model..

These developments could be used in future safety analysis preceding the flight tests.

**Keywords:** *global sensitivity analysis, LPV modelling, aerodynamics*

Les essais en vol libre peuvent être considérés comme une référence pour l'étude du comportement d'un projectile en vol, puisque la caractérisation aérodynamique se base sur des données mesurées dans des conditions de vol réelles. Néanmoins, cette détermination est entièrement conditionnée par le cadre expérimental qui peut introduire plusieurs sources d'incertitude telles que les conditions initiales de vol ainsi que les coefficients aérodynamiques partiellement connus. Par ailleurs, la structure non linéaire du modèle, bien qu'adaptée pour la description et l'identification du comportement aérodynamique, est différente de celle utilisée généralement pour la conception des boucles de pilotage. Ainsi, l'intérêt repose sur le développement d'un modèle commun et exploitable quel que soit l'objectif de l'étude.

Dans ce contexte, deux contributions principales sont apportées dans cette thèse.

- Une nouvelle structure de modèle a été suggérée. Les équations non linéaires ont été transformées en forme quasi-LPV dans un repère non-tournant, similaire aux structures utilisées dans les études GNC. Cette méthode, réduisant le temps de calcul pour des projectiles gyrostabilisés tout en conservant la description complète du comportement d'un projectile en vol, s'avère ainsi adaptée.
- L'influence des incertitudes sur le modèle quasi-LPV a été examinée à travers l'analyse de sensibilité globale du modèle, en déterminant ses paramètres influents et non-identifiables. Cette analyse a permis de mieux comprendre son comportement physique et de guider les études de sauvegarde effectuées en amont des essais en vol.

**Mots-clés :** *analyse de sensibilité globale, modélisation LPV, aérodynamique*

